BRNO UNIVERSITY OF TECHNOLOGY
VYSOKÉ UČENÍ TECHNICKÉ V BRNĚ

FACULTY OF MECHANICAL ENGINEERING
FAKULTA STROJNÍHO INŽENÝRSTVÍ

INSTITUTE OF AEROSPACE ENGINEERING
LETECKÝ ÚSTAV

AERODYNAMIC ANALYSIS OF ANTI-SURGE MODIFICATIONS ON TURBOPROP ENGINE
AERODYNAMICKÁ ANALÝZA PROTIPUMPÁŽNÍCH ÚPRAV TURBOVRTULOVÉHO MOTORU

MASTER'S THESIS
DIPLOMOVÁ PRÁCE

AUTHOR — **Bc. Ondřej Novák**
AUTOR PRÁCE

SUPERVISOR — **Ing. Robert Popela, Ph.D.**
VEDOUCÍ PRÁCE

BRNO 2021

BRNO UNIVERSITY OF TECHNOLOGY
FACULTY OF MECHANICAL ENGINEERING

Assignment Master's Thesis

Institut:	Institute of Aerospace Engineering
Student:	**Bc. Ondřej Novák**
Degree programm:	Mechanical Engineering
Branch:	Aircraft Design
Supervisor:	**Ing. Robert Popela, Ph.D.**
Academic year:	2020/21

As provided for by the Act No. 111/98 Coll. on higher education institutions and the BUT Study and Examination Regulations, the director of the Institute hereby assigns the following topic of Master's Thesis:

Aerodynamic analysis of anti–surge modifications on turboprop engine

Brief Description:

Compressor surge is very dangerous regime and there are applied during design process all possible technical devices to eliminate possible occurrence of such a regime.
Nevertheless if there is not possible to eliminate this regime modification of engine to exit this regime is applied, including special valves and flow return channels.

Master's Thesis goals:

The goal of thesis lies in design of return channel for interconnection of a anti–surge valve and IGV area to eliminate surge regime by bringing energy back to flow and to direct flow on vanes and blades to eliminate compressor stall.

Recommended bibliography:

SOEMARWOTO, B., I., BOELENS, O.,J., KANAKIS, T., Aerodynamic design of gas turbine engine intake duct, Aircraft Engineering and Aerospace Technology, ISSN: 0002-2667, September 2016.

SEDDON, J., GOLDSMITH, E., Intake Aerodynamics (AIAA Education Series), American Institute of Aeronautics and Astronautics, ISBN-10 : 1563473615, 1999.

Deadline for submission Master's Thesis is given by the Schedule of the Academic year 2020/21

In Brno,

L. S.

doc. Ing. Jaroslav Juračka, Ph.D. Director of the Institute	doc. Ing. Jaroslav Katolický, Ph.D. FME dean

Abstract

This thesis is focused on aerodynamic analysis of principles of increasing surge margin. The first chapter introduces aerospace compressors and sets up baseline knowledge of compressor characteristics and anti-surge devices. The second chapter provides detailed description of CFD model, settings, mesh dependence study and correlation with experimental data. The third chapter contains data from baseline configuration and identifies problematic areas of 1st stage compressor. The fourth chapter contains information obtained from CFD of each anti-surge device and subsequent process of optimalization. The thesis is concluded with comparission of the best version of each device using two objective criteria.

Keywords

CFD, CFX, surge, anti-surge device, compressor, jetflap

Abstract

Tahle práce se zaměřila na aerodynamickou analýzu principů zvyšování pumpážních záloh. V první kapitole jsou popsány kompresory leteckých motorů a zavedeny potřebné znalosti kompresorových charakteristik a proti-pumpážních zařízení. V druhé kapitole se nachází detailní popis CFD modelu, jeho nastavení, citlivostní analýzy sítě a korelace výsledků s experimentálním měřením. V třetí kapitole jsou popsány data neupraveného kompresoru a jsou zde popsány problematická místa první stupně kompresoru z pohledu proti-pumpážních zařízení. Ve čtvrté kaptiole jsou popsány CFD výsledky z analýz jednotlivých proti-pumpážních zařízení a také popis jejich optimalizace. Práce je zakončena srovnáním jednotlivých zařízení pomocí dvou objektivních kritérií.

Klíčová slova

CFD, CFX, pumpáž, protipumpážní zařízení, kompresor, jetflap

Rozšířený abstrakt

Jako každé jiné zařízení, tak i turbovrtulový motor se skládá z více částí. Jedna z nejdůležitějších a nejvlivnějších je kompresor. Jeho úkolem je stlačovat vzduch a posunout ho do spalovací části motoru. To je velmi důležitý úkol, protože narušení těchto dvou atributů může vést k závažnému snížení výkonových parametrů motoru s možnými i katastrofickými následky pro letoun. Protože turbovrtulový motor pracuje v širokém rozsahu atmosférických podmínek, musí tak činit i kompresor. To může vést k riziku práce kompresoru v oblasti nestabilní práce, tzv. pumpáže, nebo v oblasti termodynamického ucpání kompresoru. Tato práce se zaměřila na oblast nestabilní práce a její prevenci.

Často se v provozu letounu stává, že letoun stojí na ranveji a čeká. Protože rychlost letounu je malá nebo nulová, do kompresoru vtéká menší množství vduchu. To způsobuje zvýšení úhlů náběhu na lopatkách kompresoru. Tento jev ještě umocňuje nízká teplota nasávaného vzduchu. Vysoké úhly náběhu můžou vést k odtržení proudu vzduchu na hřbetu rotorových lopatek prvních stupňů kompresoru a vzniku nestabilit, které mohou vést až k pumpáži kompresoru. Aby se zbránilo tomuto nepříznivému jevu instalují se do kompresoru protipumpážní zařízení. Protipumpážní zařízení má za úkol snížit nepříznivý úhel náběhu proudu vzduchu na lopatky kompresoru. Z tohoto důvodu byl hlavním kritériem pro posouzení účinnosti protipumpážního zařízení vybrán průběh úhlu náběhu na rotorovou mříž prvního stupně kompresoru. V principu protipumpážní zařízení umožní zvětšit šířku otáčkové větve v charakteristice kompresoru směrem doleva k nižším hmotnostním průtokům a tím zvýšit vzdálenost mezi pracovní čarou motoru a pumpážní čarou. Tento posun můžeme považovat za další kritérium při posuzování miry stabilní práce kompresoru. Toto jsou závěry vyvozené z první kapitoly, která definovala a vysvětlila nestabilní práci kompresoru. Dále také popsala princip činnosti vybraných protipumpážních zařízení.

Druhá kapitola detailně popisuje použitý CFD model. Úkolem CFD modelu je především predikce rozložení úhlu náběhu před rotorem, celkového a statického tlaku a teploty a hmotnostního průtoku kompresorem. Model musel tyto parametry predikovat spolehlivě pro všechna protipumpážní zařízení. Dále muselo být možné pro všechna protipumpážní zařízení tyto výstupy vzájemě srovnat. To vedlo k tomu, že model je poměrně složitý a atypický pro danou úlohu, především vstupním zařízením. Protože nebylo možné model porovnat s odpovídajícím experimentem, byly volené paremetry výpočtu aplikovány na NASA Rotor 37. Tato úloha prokázala dobrou shodu v požadovaných parametrech. Správnosti výsledků se také z části věnuje třetí kapitola.

Třetí kapitola se zabývá detailním post-processingem neupraveného kompresoru bez protipumpážních zařízení. V této kapitole jsou analyzovány výsledky na základě úhlu náběhu a jeho změny při výpočtech na různých bodech otáčkových větví. Dále byla vytvořena kompresorová mapa a prověřeny isentropické účinnosti. U všech zmíněných výsledků proběhla kontrola, zda hodnoty dosahují očekávaných předpokladů a zda se mění s očekávanou logikou (konzultace s pracovníky GE). Všechny požadavky výpočet splnil a proto byl vybrán jeden základní režim pro který byla simulována jednotlivá protipumpážní zařízení. Tímto vybraným režimem se stal volnoběžný režim, který je na nestabilní práci kompresoru velmi citlivý. Dále byly identifikovány dva důležité jevy, které mají vliv na kvalitu proudění v prvním stupni kompresoru a zároveň

podstatně ovlivňují kvalitu práce protipumpážního zařízení. Prvním je vír, který se generuje na špičce rotorové lopatky a podporuje odtržení na rotorové lopatce. Druhým je radiální vstup vzduchu do axiálního kompresoru, který urychluje proud vzduchu před špičkou rotorových lopatek prvního stupně kompresoru, což neguje efekty některých protipumpážních zařízení. Tato zjištění měla značný vliv na účinnost jednotlivých protipumpážních zařízení.

Čtvrtá kapitola popisuje průběh optimalizace a výsledky z výpočtů jednotlivých protipumpážních zařízení. Prvním zařízením je předehřev vzduchu před vstupem do kompresoru. U toho bylo uvažováno využití vzduchu z protipumpážního ventilu. Výsledky nicméně ukazují že teplota recyklovaného vzduchu je příliš malá a zvýšení pumpážních záloh je samo o sobě nedostatečné. Druhým zařízením je využití protipumpážního ventilu či protipumpážních pasů. Ten ukázal výbornou účinnost pro zvyšování pumpážních záloh. Jeho nevýhodou je plýtvání už stlačeným vzduchem, ale nabízí rovnoměrné snížení úhlu náběhu. Bohužel jeho efektivitu je možné srovnávat pouze za použití prvního kritéria, tj. úhel náběhu, protože druhé kritérium neukáže jeho plný efekt. Odpouštěcí ventil totiž zvyšuje pumpážní zálohy nejenom posunem pumpážní čáry do leva v charakteristice kompresoru, ale i zároveň posunem pracovní čáry motoru v charakteristice kompresoru do prava. Tento efekt zvýší vzdálenost mezi pracovní a pumpážní čarou v charakteristice kompresoru, což je princip zvýšení stabilní práce motoru (kompresoru). Další zařízení pro zvýšení stabilní práce kompresoru bylo instalování předstatoru do vstupního kanálu. Princip práce tohoto zařízení je generovat rozvíření před první stupeň kompresoru. Pro toto zařízení bylo simulováno několik variant úhlu nastavení předstatoru a jeho polohy. I přesto, že bylo dosaženo velkého zlepšení oproti první variantě, zařízení nepřekonalo odpouštěcí ventil. Posledním zařízením pro zvýšení stabilní práce kompresoru byla instalace jetflapu. Postupnou optimalizací zařízení byla nakonec vytvořena finální varianta, která využívá vhodných hmotnostních průtoků jednotlivých trysek a především ofukování špičky rotoru pomocí slotu. U této kombinace došlo k značnému snížení úhlu náběhu i zvýšení pumpážních záloh v charakteristice kompresoru.

Na závěr této práce lze konstatovat, že předehřev vzduchu před vstupem do kompresoru zvyšuje pumpážní zálohy, ale aby byl dostatečně účinný musel by být vzduch předehřán několikanásobně více než je možné dosáhnout jenom recyklací vzduchu z odpouštěcího ventilu. Předstator se ukázal jako relativně neúčinný vzhledem k nákladům na zástavbu tohoto zařízení a ukázal se jako nevhodný pro toto konstrukční provedení tohoto kompresoru. Odpouštěcí ventil se ukázal jako velmi účinný, ale energeticky nejméně šetrný. Jediné zařízení, které ve svém výsledku překoná odpouštěcí ventil je jetflap v kombinaci se slotem. Jetlfap & slot v kostrukční konfiguraci, která byla použita pro tuto analýzu prokázal, že ze všech protipumpážních zařízení dokáže nejvíce snížit úhel náběhu na rotorových lopatkách kompresoru a tím zvýšit pumpážní zálohu kompresoru. Toto tvrzení bylo potvrzeno i přes porovnání druhým kritériem pro zvýšení pumpážních záloh (posun pumpážní čáry do leva v charakteristice kompresoru). Na základě těchto zjištění tedy má tato konfigurace potenciál překonat aktuálně používaný odpouštěcí ventil.

NOVÁK, Ondřej. Aerodynamic analysis of anti-surge modifications on turboprop engine. Brno, 2021. Available at: https://www.vutbr.cz/studenti/zav-prace/detail/132427. Master's Thesis. Brno University of Technology, Faculty of Mechanical Engineering, Institute of Aerospace Engineering. Advised by Ing. Robert Popela, Ph.D.

Declaration

I hereby declare that I have authored this thesis independently, that I have not used other than the declared sources, and that I have explicitly marked all material which has been quoted either literally or by content from the used sources

Brno, May 21st 2021 Ondřej Novák

Acknowledgement

I would like to thank Ing. Robert Popela, Ph.D., for being my university advisor at Brno University of Technology, through my work on this thesis.

I am very grateful to Ing. Pavel Hečl, my supervisor at General Electric Aviation Czech, for his patient guidance, knowledge and time.

Lastly I am grateful to General Electric Aviation Czech for the opportunity to cooperate on this thesis.

Contents

1. Introduction

Just like any other device, turboprop engine comprises of several parts. One of the most important and influential one is compressor. Its task is to compress the air and deliver it to the combustion side of the engine. This is extremely important task, because disruption of air delivery or decrease in compression ratio could lead to decrease in engine performance or engine malfunction with severe, potentialy catastrophic consequences. And because compressor consumes considerable part of engine power, compression and air delivery efficiency is really essential. That is why compressor R&D is huge part of engine development.

Because turboprop engine operates at a wide range of atmospheric conditions, so has to do compressor. This can lead to the risk of compressor unstable work (surge) or thermodynamic choking. This thesis focuses on unstable work and its prevention. For the reasons that are explained in the following chapters, compressor unstable work must not occur. Because we want to use a compressor at wide range of atmospheric conditions, various altitudes, and aircraft velocities, we have to use anti-surge devices. These devices are active mostly in low compressor revolution regimes. Because these devices are working as prevention, they must be active before there is a risk that compressor can enter the area of unstable work. And just like any engineering solution, anti-surge devices are a compromise, in this case between efficient usage of shaft power and smooth engine operation on one hand, and engine power characteristics (engine shaft power and fuel consumption) on another.

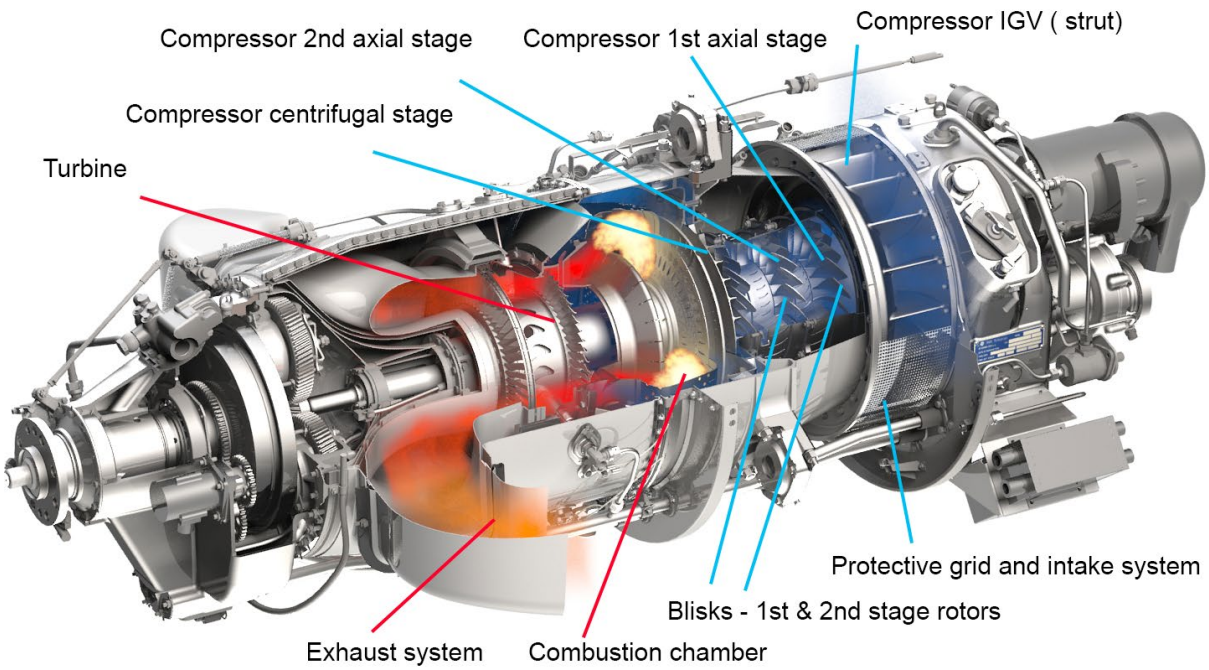

Fig. 1.1: Ge H80 turboprop engine [5]

General Electric H-Series is based on the proven M601 Walter design, therefore it is still two-shaft and reverse flow design just like its predecessor. However, it was improved by a new compressor, which lead to an increase in performance. Even though these improvements raised the engine performance, it is still considered

a less expansive model with low or medium level shaft power. Because of its comparatively simple construction, its price is modest and one of its selling points. That being said, GE H-series is still a very advanced, complicated and expansive piece of engineering.

GE H-Series is well established in the aviation industry and is being operated reliably for some time. It is obvious that these engines must be fitted with anti-surge device. In this case, anti-surge valve was placed aft the second axial compressor stage. It is reliable and proven solution, but there are other possible solutions, possibly better ones. Before significant funds are invested in developing a new device, it is necessary to perform a preliminary analysis to assess which one of these methods has the most potential and whether it is worth investing in these new solutions in the first place.

All anti-surge modifications were applied to GE H-series compressor with appropriate input values. The aim of this thesis is to preliminarily analyze these different approaches and compare them to anti-surge valve. The thesis was divided into 4 main sections. The first one provides necessary theoretical knowledge of unstable work and axial compressor anti-surge devices. The second one describes CFD methods and how they were applied to compressor analysis. The third one presents CFD results of H-series compressor without any anti-surge modification. The fourth describes CFD analysis of several anti-surge modifications and draws a conclusion about their effectiveness. The thesis was written under the supervision of GEAC development engineer Ing. Pavel Hečl.

Tab. 1.1: GE H-series technical data [6]

Dimensions (L×W×H)	1 670 × 560 × 580 mm		
Dry weight	180 kg		
Compressor	1st and 2nd stage axial & 3rd stage centrifugal		
Combustor	Annular with fuel slinger		
Turbine	1-stage axial gas. gen & 1-stage axial power		
Fuel	Jet-A/A1		
Shaft power	751 hp (560 kW)	800 hp (597 kW)	850 hp (634 kW)
Eq. shaft power	795 hp (593 kW)	845 hp (630 kW)	898 hp (670 kW)
Power-to-weight ratio	1,93	2,05	2,18
Gas gen. RPM	35 524	35 854	36 183
Shaft RPM	2 080		
Mass flow rate	3,66 kg/s	3,73 kg/s	3,79 kg/s
TBO	4,000h		
Overall pressure ratio	6,8	7,0	7,2

2. Aerospace compressor theory

2.1. Turboprop engine

Turboprop engine uses energy from the fuel, which is extracted from fuel inside can type or annular type combustion chambers. That energy is converted by the turbine to mechanical energy, which is used to power propeller and compressor. Propeller generates thrust and compressor feeds the engine with necessary mass of air with given compression. Turboprop engines follow the Ericsson-Brayton thermodynamic cycle. Low and medium power engines use most often combined compressors, that means one or two axial compressors combined with one or two radial compressors.

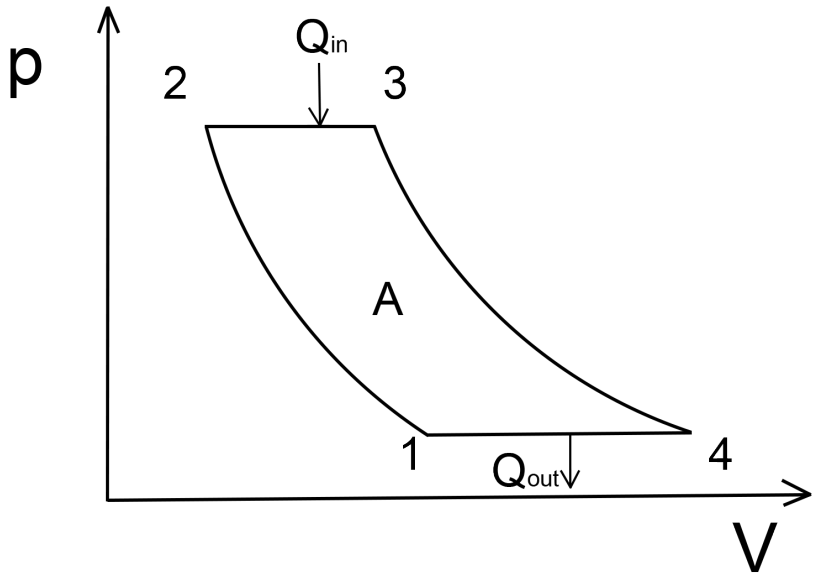

Fig. 2.1: Ericsson-Brayton thermodynamic cycle

Ericsson-Brayton thermodynamic cycle comprises of two isentropes and two isobars (Fig. 2.1).

2.2. Static and total properties

In order to describe fluid moving through the engine static, stagnation and total properties are used. They describe pressure and temperature changes when changing velocity. It is also beneficial to use them when measuring the temperature and pressure of a moving fluid.

Equation 2.2.1 describes the stagnation (in this case also total) pressure and static pressure. Stagnation pressure is the sum of static and dynamic pressure. Static pressure corresponds to pressure measured when the measuring device is moving with the same velocity and direction as the fluid, or the fluid and the measuring device are being both stationary. Stagnation pressure in theory equals to the static value we would get if the fluid was adiabatically slowed down to a complete stop. Equation 2.2.2 defines the total temperature. Equation 2.2.3 defines Mach number that represents the compressibility in equations. For purpose of this thesis, stagnation and total properites are the same thing, because hydrostatic pressure is negligible.

Total pressure $$p_T = p \cdot (1 + \frac{(\kappa - 1)}{2} \cdot M^2)^{\frac{\kappa}{\kappa - 1}} \quad (2.2.1)$$

Total temperature $$T_T = T \cdot (1 + \frac{(\kappa - 1)}{2} \cdot M^2) \quad (2.2.2)$$

Mach number $$M = \sqrt{\kappa \cdot R \cdot T} \quad (2.2.3)$$

2.1. Velocity triangles

In order to effectively work with rotating parts containing blades, simplification is necessary. The goal of this simplification is the creation of blade cross section of the compressor row, which will allow us to work with the profiles in similar fashion to the aircraft wing profile to a certain extent.

Blade cross section row is formed from the perpendicular cross section on the mean diameter of axial compressor, containing IGV, rotor, and stator (Fig. 2.2).

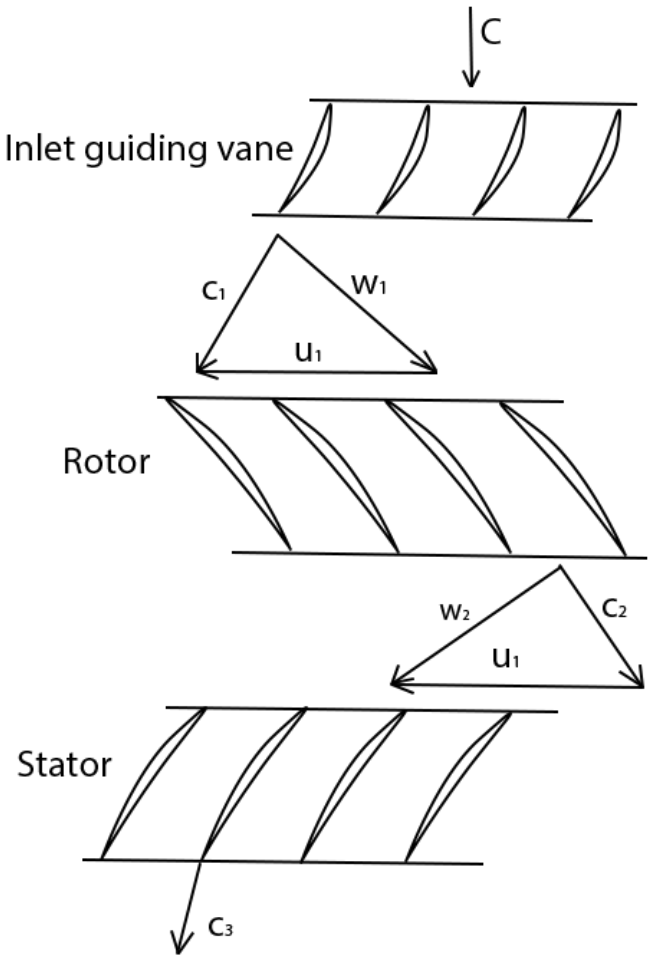

Fig. 2.2: Velocity triangles – axial compressor [7]

In the Fig. 2.2, there are components of the flow velocity triangle. Relative speed is marked as $\vec{w}$. Relative speed is equivalent of infinite speed $\overrightarrow{v_\infty}$ for wing, this means

we can also to a certain degree use incidence angle i in the same manner as we would use angle of attack during aircraft wing design. This assumption can be done because there is tangential blade speed $u = \omega \cdot r$. Its purpose is to remove the effect of rotation. It is necessary to add that angle of attack is defined relative to the chord line and incidence angle is defined relative to the camber line, and therefore these parameters are not the same thing. However, these parameters can be used in a similar way to certain degree in most cases. The last velocity component is absolute velocity $\vec{c}$, which is defined as resultant of the sum of relative and tangential blade speed. Tangential blade speed is zero for the stator and IGV, because these parts are stationary.

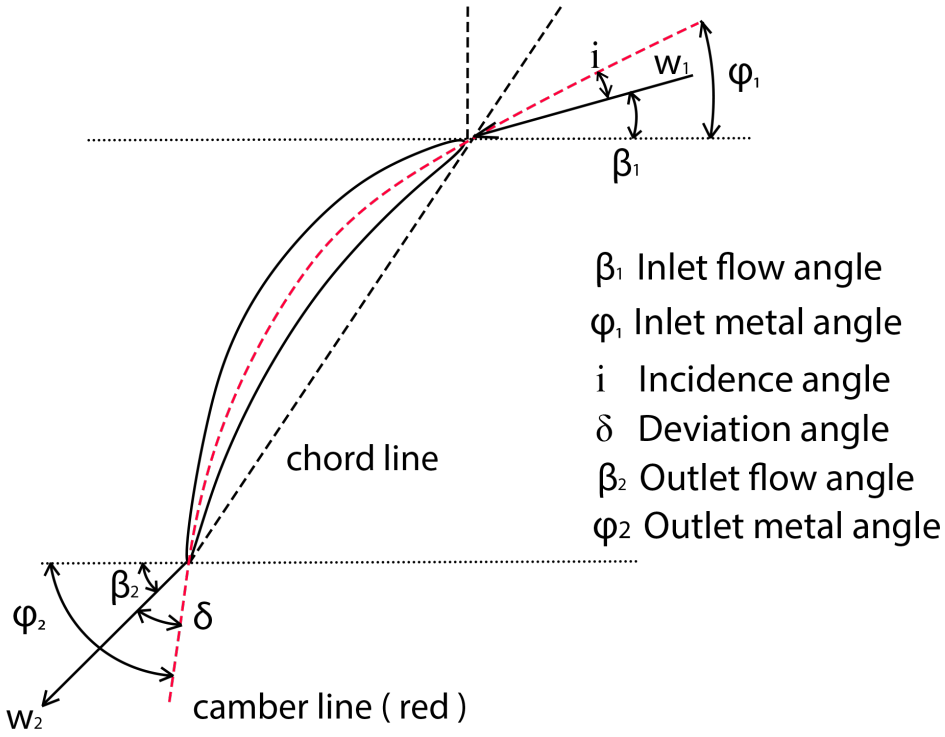

Fig. 2.3: Incidence angle definition

Other important parameters are defined in Fig. 2.3, the most important of which is incidence angle.

2.2. Compressor

2.2.1 Axial compressor

Main parts of axial compressor are

1) Inlet guiding vane (IGV)
2) Rotor
3) Stator

IGV is not always necessary, only in cases where a swirl in front of the first stage rotor is necessary. Reasons for that might be necessity to lower Mach number on the tip of rotor blade or when adjusting the compressor surge margin. The goal of IGV is to change the direction of flow in front of the first rotor, giving it necessary angle of attack. Its function is described in the following picture.

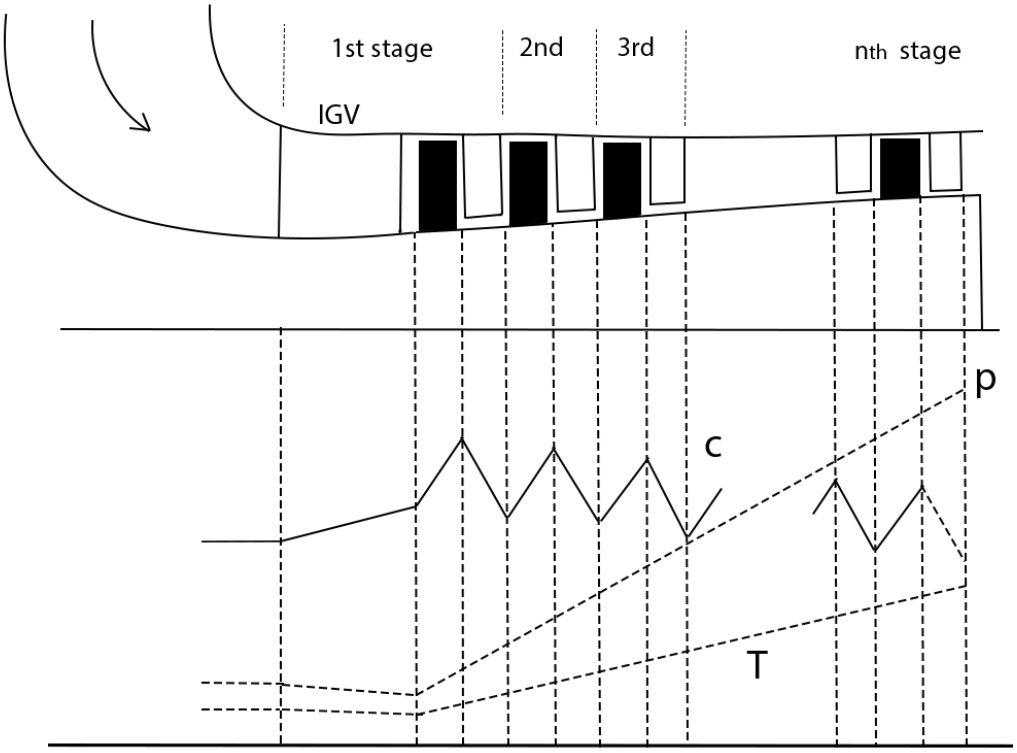

Fig. 2.4: Axial compressor – properties profile

The diagram (Fig. 2.4) shows how each part of compressor changes the absolute velocity „c“, static pressure and temperature. Steady increase in static pressure can be seen in the compressor, the further the air travels. This is in fact the main task of the compressor. There is also an increase in temperature due to the air being compressed. The task of the rotor is to increase the absolute velocity of air that is then processed by stator. Stator works as a diffusor, transforming velocity (dynamic pressure) to static pressure. Static pressure increase is seen in the rotor as well as stator. This is due to the fact that both rotor and stator have a diffusor like shaped channel.

2.2.2 Centrifugal compressor

Centrifugal compressors are mainly used in turboprop engines with low or medium power (less than 1000 – 1500 kW shaft power). Usually they are combined with an axial compressor as axial-centrifugal combined compressor. Centrifugal compressors were used long before axial because there were used as turbochargers in piston engines.

Centrifugal compressor consists of an inlet system that feeds the centrifugal impeller, often called rotor. The impeller rotates and as the centrifugal and other forces act on the air, it is being sped up to high velocity, compressed and heated up significantly. In the next part called diffusor, the air slows down while increasing static pressure. Diffusor has 2 parts. The first one is diffusor without blades. Its task is to calm the disturbed air from impeller and lower the absolute velocity, preferably to subsonic

speed if possible. The second diffusor contains blades. Its task is to transform very high dynamic pressure to static pressure with as high as possible efficiency. Sometimes the diffusor with blades is replaced by a channel with shape of diffusor without blades, but because this approach is not very efficient, its rarely used in aviation. The last part is the outlet system that guides the air to the combustion chamber.

As seen in Fig. 2.5 on the left, centrifugal compressor consists of a rotor (cut 1-2), that consists of an impeller and shaft. Next is diffusor, consisting of diffusor without blades (cut 2- 3) and diffusor with blades (cut 3-4). The last part is the outlet system (cut 4-5).

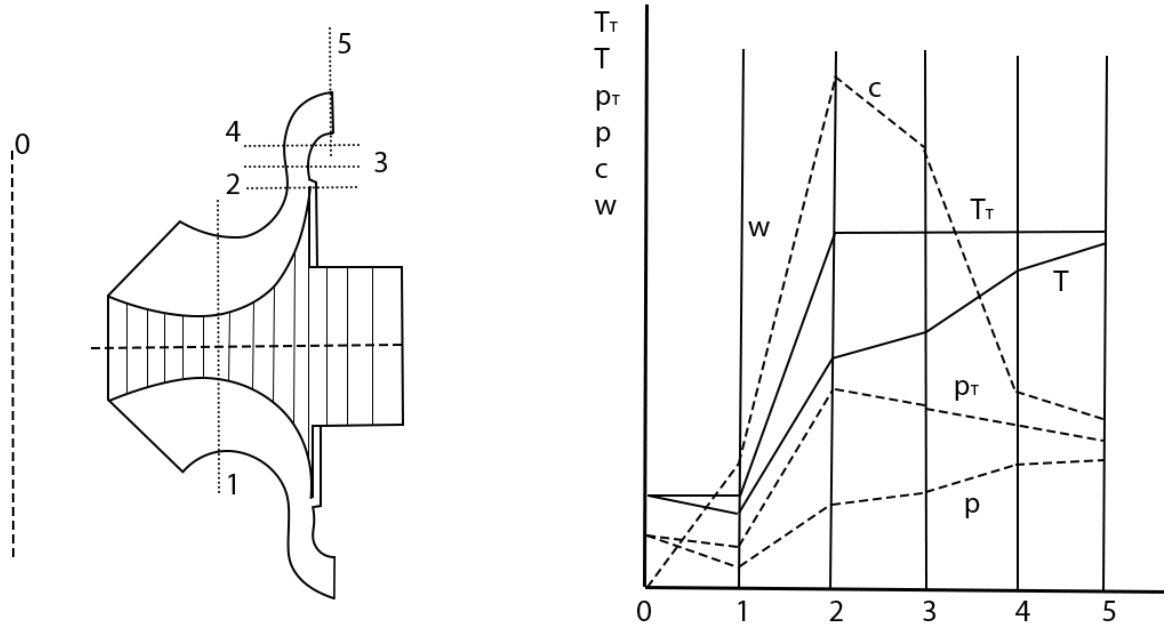

Fig. 2.5: Centrifugal compressor – properties profile

As seen in Fig. 2.5, on the right there is a course of parameters inside the compressor in each cross section that match the left side of picture.

2.3. Compressor characteristic

Before compressor characteristics is created, several symbols must be defined.

Tab. 2.1: Index explanation

p_{1T}	Total pressure at the inlet bubble
p_{2T}	Total pressure at the first stage stator outlet
p_2	Static pressure at the first stage stator outlet
T_{1T}	Total temperature at the inlet bubble
T_{2T}	Total temperature at the first stage stator outlet

Compression ratio

$$\pi = \frac{p_{2T}}{p_{1T}} = \frac{p_{2T}}{p_{atm}} \tag{2.3.1}$$

Isentropic efficiency

$$\eta = \frac{T_{1T} \cdot (\pi^{\frac{\kappa-1}{\kappa}} - 1)}{T_{2T} - T_{1T}} \tag{2.3.2}$$

Just like any other device, axial and centrifugal compressors have a range of design regimes. We tend to optimize these devices so that they have maximum efficiency and service life at these design points. Aircraft engine has to operate at a wide range of conditions. Parameters like altitude, atmospheric conditions, (air temperature and pressure), aircraft velocity, engine revolutions, and many other, all have an effect. Physical properties of air, like viscosity, thermal conductivity, isentropic expansion factor, and specific heat capacity change during flight change very little but also have an effect. Geometric parameters of compressors can have an effect and can also change under the right circumstances. All of this affects the compressor efficiency and compression ratio. If we create the dependence of mass flow rate, compression ratio, and isentropic compressor efficiency on compressor revolutions, we get compressor map with absolute values (Fig. 2.6).

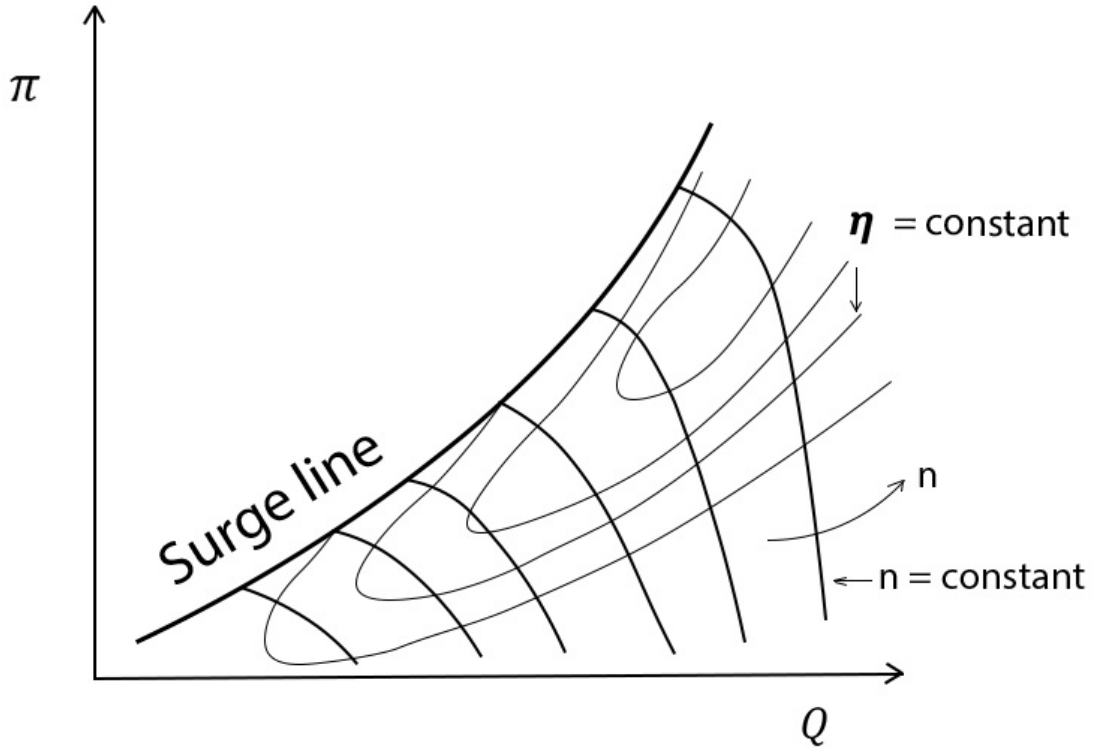

Fig. 2.6: Compressor map with absolute values

Applicability of this characteristics is limited. Changing atmospheric conditions, altitude, and flight conditions will change its shape. That is why characteristics that won't be affected by these parameters is needed. That is why the general compressor map is used.

However, before a general compressor map is created, the following criteria of similarity must be fulfilled. The first one is geometrical similarity. Engines don't usually change their dimensions and because our engine does not have adjustable parts, this condition can be considered fulfilled. Next, the similarity of velocity, pressure, and temperature fields is assumed to be fulfilled (similarity of velocity triangles). Because steady-state airflow is assumed, Strouhal number can be omitted. Because it can be assumed that the physical properties of air won't change, Prandtl number can be omitted as well. Because compressors work at high Reynolds numbers (Re>10^5), friction losses change only very little and changes in Reynolds number can be omitted as well. Adiabatic factor and gas constant for air are assumed to be constant as well. Because air is compressible, the constant Mach number must be assumed as well.

Assuming all previously mentioned conditions are fulfilled, general compressor map can be created by plotting on horizontal axis parameter of corrected mass flow rate defined by $Q_m = \frac{Q \cdot \sqrt{T_{1T}}}{p_{1T}}$ and on vertical axis total compression ratio $\pi = \frac{p_{2T}}{p_{1T}}$. This compressor map is not dependent on atmospheric conditions, altitude or flight velocity. Both previously plotted parameters depend on revolutions parameter defined by $\frac{n}{\sqrt{T_{1T}}}$. These parameters, however, tend to have very different values from real revolutions and mass flow rate. That is why we further modify plotted parameters. This means that measured values we get are modified so that they correspond to values of ISA at *0 m* altitude. Equations describing modifications are 2.3.3 and 2.3.4.

Standardised revolutions

$$n_r = n \cdot \sqrt{\frac{288{,}15}{T_{1T}}} \tag{2.3.3}$$

Standardised corrected mass flow rate

$$Q_{mr} = Q \cdot \sqrt{\frac{T_{1T}}{288{,}15}} \cdot \frac{101325}{p_{1T}} \tag{2.3.4}$$

General compressor map takes into account atmospheric conditions, altitude, and flight velocity and should not change in the entire range of values.

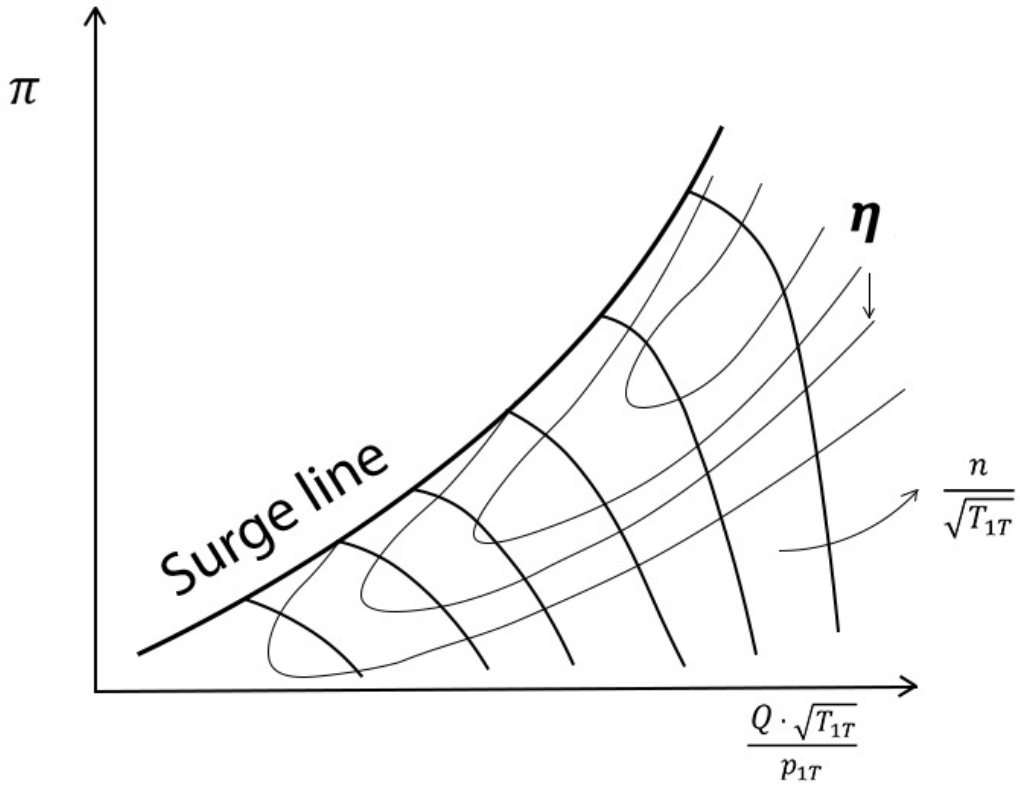

Fig. 2.7: General compressor map

2.4. Compressor unstable operation

Just like any other device, compressors, turbines, and pumps have limitations. In case of compressor, the limitation is the unstable work. Unstable work occurs when compressor operating point moves along the speed line left, far too close to or even past the surge line. The further left along the speed line we force the compressor to operate, the lower the mass flow rate gets. This causes a decrease in incidence angle, eventually leading to flow separation on the suction side of blade. As the separation grows, so do losses. Eventually, the compressor characteristics collapses. This will lead to dramatic, potentially catastrophic consequences for the entire engine.

The boundary between stable work and unstable work is called the surge line (Fig. 2.7). On the right side of the surge line is an area of stable compressor work. However, if we operate the compressor close to the surge line, compressor loses power, temperature in turbine stage rises, excessive noise and vibration occur and all of this might damage compressor and the entire engine.

That is why we define the compressor surge margin, which is an area that is some distance from the surge line. It is difficult to accurately predict where unstable work occurs. Surge margin functions as a safety margin against unstable work and surging. It allows the engine to operate reliably in various conditions such as high altitude, acceleration, deceleration, and low revolution regimes. If the surge margin is not big enough, instability might occur and cause engine malfunctions.

2.5.1 Rotating stall

Unstable work is caused by the decreasing mass flow rate while maintaining the same revolutions. This will lower the absolute speed and because the tangential blade speed remains constant, incidence angle will increase until flow separation occurs. Increase in mass flow rate will on the other hand decrease incidence angle until it reaches a negative value causing flow separation on the pressure side of blade causing aerodynamic choking.

Less severe type of unstable work is rotating stall. In most cases, it is precursor to hard surging. This type of instability causes noise and vibrations (in the range of hundreds of Hz). Working in this regime for extended periods of time would lead to metal fatigue with consequent mechanical damage to engine.

Rotating stall is caused by air stall blocking one or more channels because of the high incidence angle. This flow structure rotates periodically around the axis of a given part. In case of rotor, the direction of rotation is opposite to the rotor rotation and its speed is in relation to rotor revolutions.

Rotating stall is described by Fig. 2.8. If due to, for example, manufacturing error and consequent higher incidence angle the flow separates on suction side of blade no. 3, the channel B gets blocked. This will change incidence angle in neighbouring channels. incidence angle will increase in channel A and decrease in channel C. This will shift the separation onto blade no. 2 and block channel A. Meanwhile, the airflow in channel B gets stabilized. This way the rotating stall rotates in the opposite direction of rotor. This phenomenon can occur on stationary parts as well.

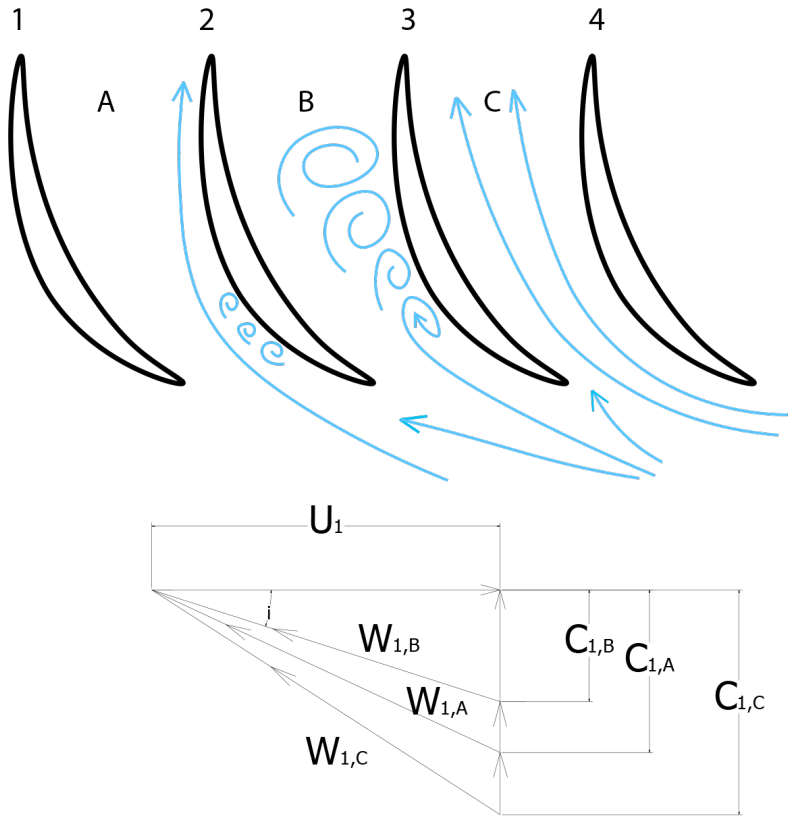

Fig. 2.8: Axial compressor blade row – rotating stall

2.5.2 Compressor surge

Compressor surge (collapse of compressor characteristics) can stem from rotating stall or start directly from the stable mode due to very fast shift of the operating point to unstable work due to quick engine acceleration. It manifests it-self as low frequency vibrations (less than 10 Hz), loud and deep noises, and in extreme cases flow reversal. Flow reversal will cause flames coming out of the engine intake.

Fig 2.9 describes the formation of surge. Surge is sometimes a cyclic phenomenon, that is affected by downstream components. These components cause throttling and back pressure. In this description of events, constant revolutions are assumed. Events begin at operating point V. As we decrease the mass flow rate (points V,M), we arrive at point P. Point P lies on the compressor surge line. As per Fig 2.9, there is increase in pressure due to the decrease in mass flow rate. At this point, compressor flow characteristics breakdown leading to unstable work. At this point, the pressure behind compressor is lower than in the combustion chamber. This causes a pressure drop in compressor (from point P to point 2). As we reach point 2, the mass flow between compressor and combustion chamber reaches equilibrium. Pressure behind the compressor is higher than the combustion chamber pressure, causing an increase in mass flow rate until pressures reaches equilibrium (point 3). Assuming the throttling conditions won't change, this cycle will repeat it-self until pressure conditions reach equilibrium. If not, the cycle amplitude will increase during each cycle (point 4) untill flow reversal, deep surge and subsequent complete destruction of engine occur.

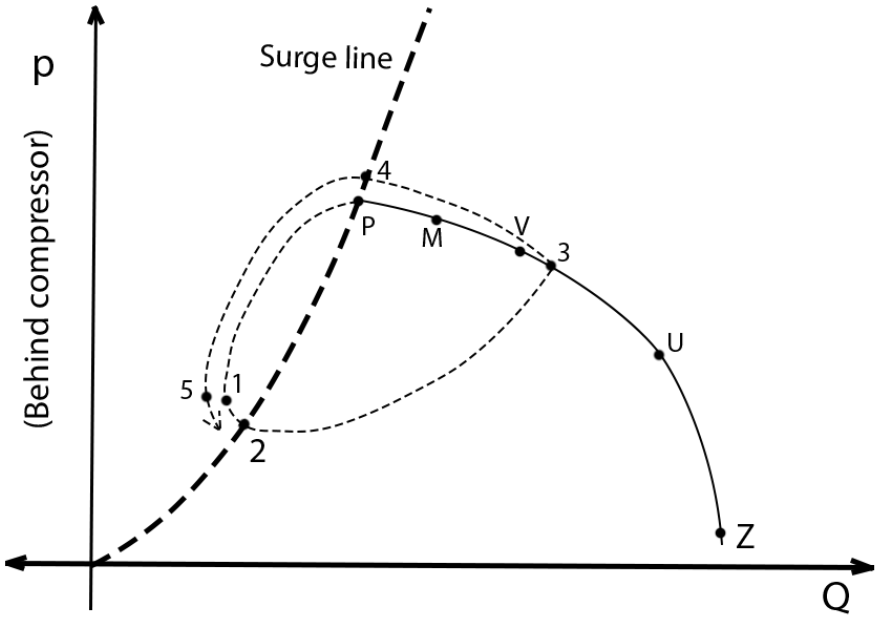

Fig. 2.9: Compressor surge in compressor characteristics [7]

It is clear that surge during normal engine operation must not occur. That is why the compressor surge margin is defined (Fig. 2.10). This margin must be big enough so that during any standard operating regime at a given altitude and flight velocity unstable work won't occur. However, to exploit regimes with good isentropic efficiency of the compressor, an engine can not be operated too far from the surge line either. So that both previously mentioned conditions are fulfilled, anti-surge devices are used

to delay the surging and push the surge line further left, increasing the surge margin in process.

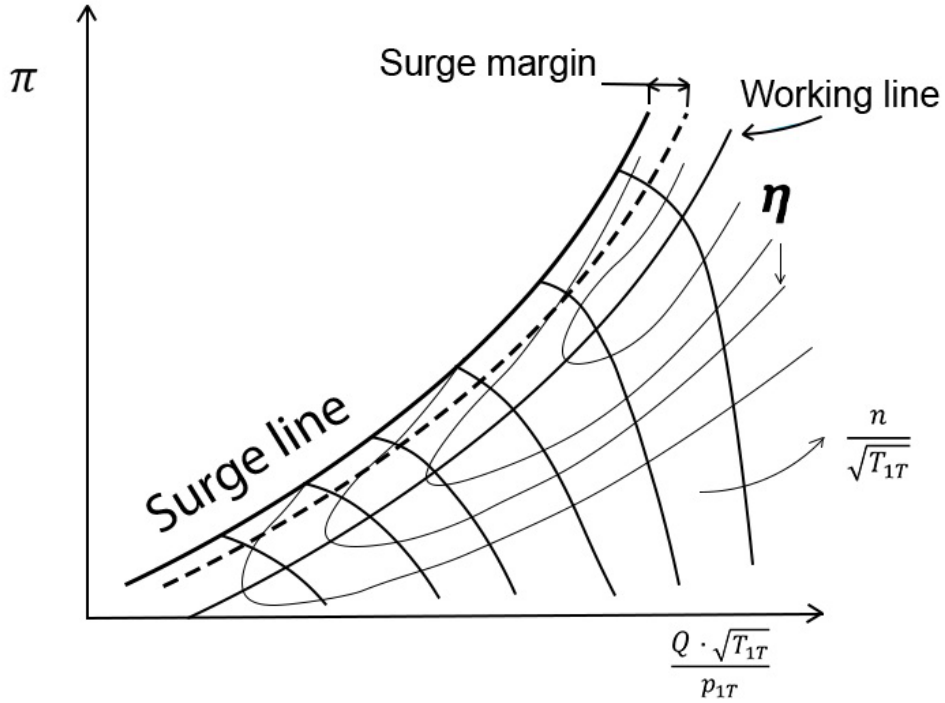

Fig. 2.10: Compressor surge margin

2.5. Anti-surge devices

There are several devices that can increase the area of stable work. Their purpose is to increase the surge margin in regimes where the compressor might operate close to the surge line. The main principle is lowering the airflow incidence angle on blades. This will prevent the flow from separating and therefore prevent unstable work. Each device will be described and simulated based on their physical principle. Real life applicability of each solution will be taken into account.

It is necessary to mention that the goal of this thesis is to analyze the principle of work of each solution using CFD, not to evaluate specific design solution.

It is important to state that it was assumed that compressor can only stall, but not surge [4]. Surging is a far more complicated process that would require a model with several devices in order to analyze the problem. However, the goal of this thesis is finding prevention rather than cure. This means that prediction of stalling can be a bit tricky in terms of precision of prediction. That is why effectiveness of devices will be judged based on how much each device can change the incidence angle. This incidence angle based approach was therefore used in theory for each device.

2.5.3 Anti-surge valve

The simplest way and also the cheapest is adding anti-surge valve (Fig. 2.11). In operation modes where there is not big enough compressor surge margin (usually idle revolutions) for stable work to continue, the valve will open. The easiest way is to

use pressure valve. It is located downstream of troublesome compressor stages, in this case aft 2nd axial stage. Valve will let out some air out of compressor, in our case Q_{m0} as per equation no. 2.5.1 and Fig. 2.11. Opening the valve will stop throttling of mass flow in the compressor, causing increase in mass flow rate at compressor inlet. Increase in mass flow rate will cause increase in $\boldsymbol{c_1}$ leading to decrease in incidence angle on the first compressor stage.

This system is easy, reliable, and cheap but it does come with downsides. The most prominent is that the first stages of compressor have already put some work into compressing, speeding up, and heating up the air that is now being blown out from engine into atmosphere. Lost work will manifest it-self as increase in fuel consumption.

$$Q_{m1} = Q_{m0} + Q_{mk} \tag{2.5.1}$$

$$c_1 \cdot \rho \cdot A_1 = Q_{m0} + c_k \cdot \rho \cdot A_k \tag{2.5.2}$$

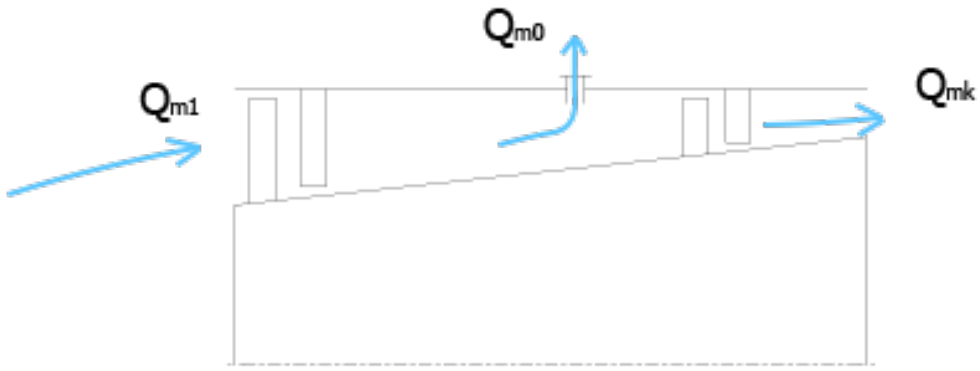

Fig. 2.11: Flow diagram – anti-surge vave

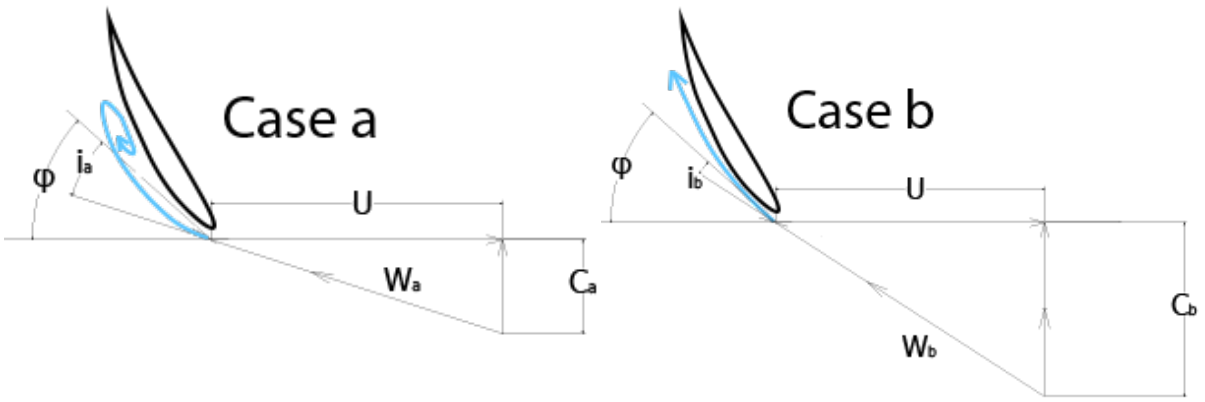

Fig. 2.12: Anti-surge valve – blade cross section row (rotor)

Fig. 2.12 describes how anti-surge valve works. „Case a“ shows partially stable airflow state when anti-surge valve is not active. Opening the valve will cause increase in inlet mass flow causing increase in c_a. Because we assume constant revolutions,

the tangential blade speed U remains the same in both cases. This means that increase in c_a will cause increase in W_a and decrease in i_a, thus lowering incidence angle and preventing separation.

This way of increasing the surge margin will also cause changes in the shape of surge line and working line. Leaving the valve open at high revolutions will cause opposite effect on downstream compressor stages, causing flow separation and decreasing the surge margin as well as a massive decrease in performance. Fig. 2.13 shows how anti-surge valve changes surge line.

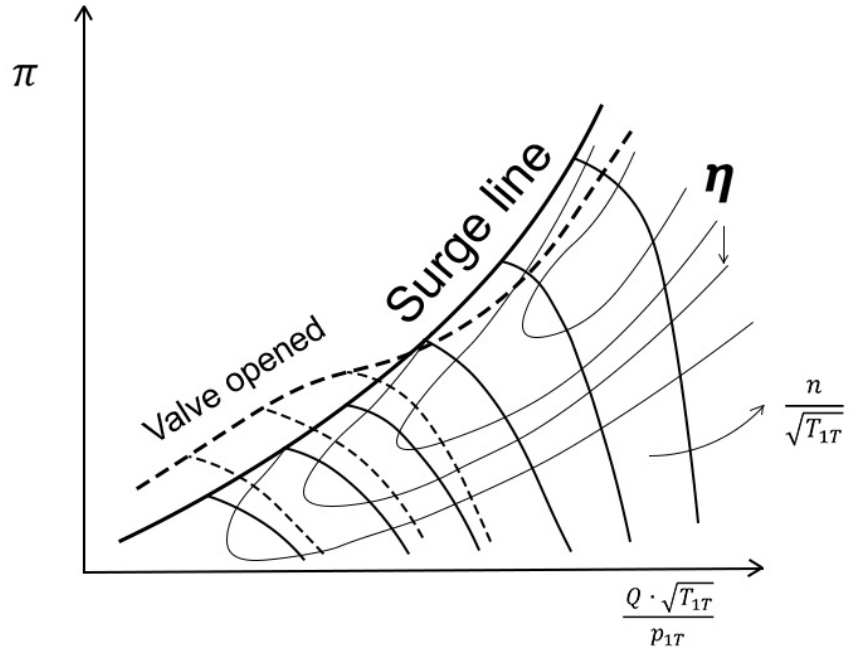

Fig. 2.13 Surgle line – anti-surge valve [7]

2.5.4 Inlet guiding vane

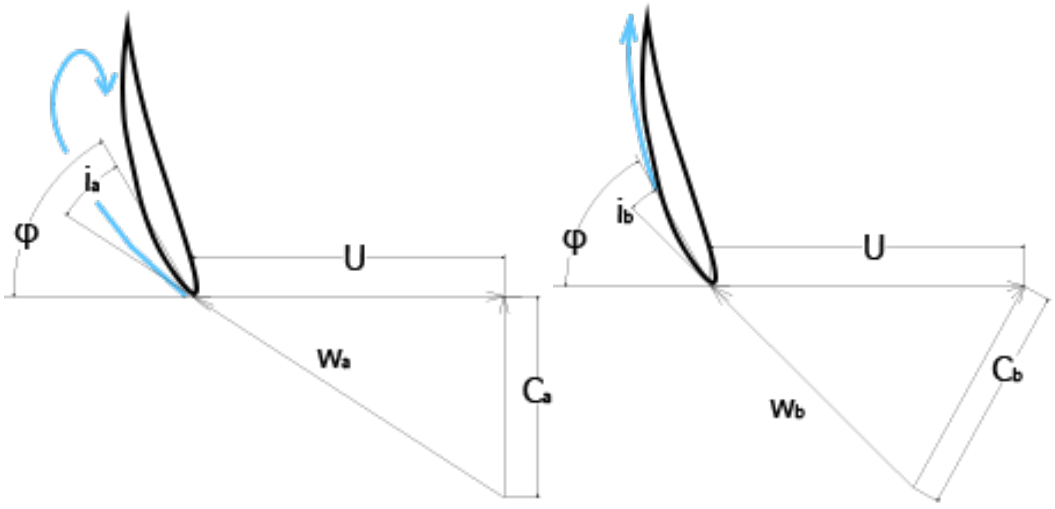

Fig. 2.14: Pre-swirl (IGV)

This solution requires inlet guiding vane (IGV) installed in front of the first compressor stage. If there is need to stabilize flow on second stage, the first stage stator must be adjustable as well. IGV prevents unstable work by creating swirl in front of compressor stage. Fig. 2.14 (left side) explains what happens when there is no IGV and flow

separation occurs. Fig. 2.14 (right side) explains how IGV creates swirl in front of rotor. Direction of absolute velocity c_b is changed by IGV. This caused change in direction of relative velocity w_b and leading to decrease in incidence angle i_b.

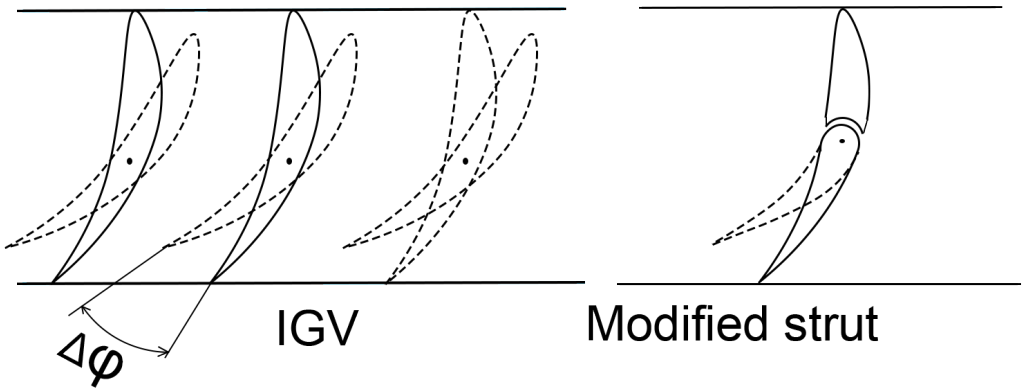

Fig. 2.15 IGV types [7]

There are two ways to create IGV (Fig. 2.15). The first is by adding another blade (Fig. 2.15 left). However, if there are struts in the engine, it is possible to use them and make part of the strut around trailing edge adjustable, as seen in Fig. 2.15 on the right side.

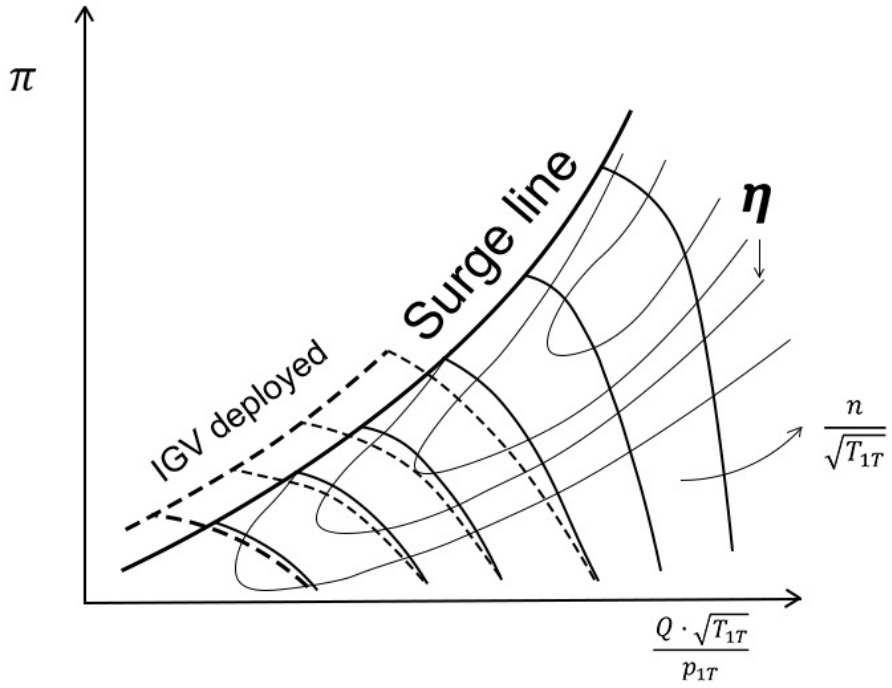

Fig. 2.16 Surge line – IGV [7]

Using IGV will cause a change in surge as seen in Fig. 2.16. IGV is an effective way to prevent unstable work, but its relatively complex system. Increased system complexity leads to an increase in maintenance and manufacturing costs and can affect reliability. Adding another set of blades will also increase the pressure losses and therefore decrease the efficiency and compression ratio.

2.5.5 Air preheating

Another way of preventing unstable work is feeding the compressor with air of higher temperature. Hotter air will increase the mass flow causing an increase in inlet flow

velocity magnitude. Common cause of surge is ingesting cold air into the compressor combined with aircraft being stationary or moving very slowly. Low air density will further lower the mass flow rate Q as seen in equations no. 2.5.3 and no. 2.5.4.

$$c_{1,cool} \cdot \rho_{cool} \cdot A_1 = Q \quad \textbf{(2.5.3)}$$

$$c_{1,hot} \cdot \rho_{hot} \cdot A_1 = Q \quad \textbf{(2.5.4)}$$

Ways of increasing inlet air temperature:

1) Heating up the air
2) Bleeding hot air from the combustion part of engine
3) Recycling air from anti-surge valve

Heating up the air is difficult and costly, because it would require a heat exchanger. This would not only cause pressure losses, but will more importantly significantly increase complexity, and manufacturing costs leading to a significant increase in price. Another issue is finding a suitable source of heat. We can either use an external heat source or recuperate heat from the exhaust flow. Both options require complicated, heavy and expansive parts to be added to engine. It is possible that the potential benefit would not outweighs costs.

The next option is to bleed the hot air from hot parts of the engine into compressor. It can be achieved with a series of ducts and small channels. Feeding the engine with hot air will lead to a decrease in engine performance. This is, however, not a big issue, because anti-surge devices are only active in operation modes close to the surge line. This option will increase engine complexity and drive up manufacturing costs, but is easier to achieve than heating up air.

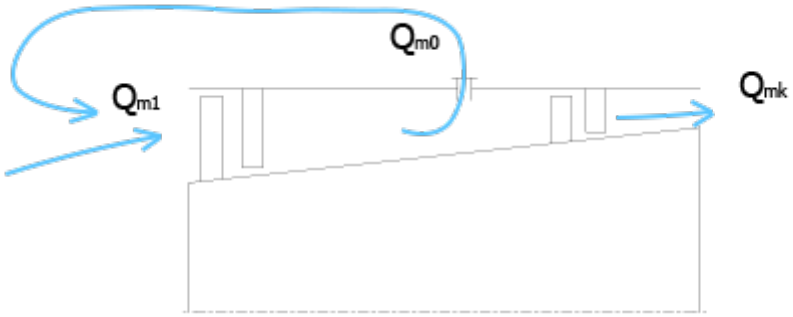

Fig. 2.17: Air recuperation diagram

The last option is to capture air from anti-surge valve and feed it back to compressor. It would require a small duct that starts in anti-surge valve and exits somewhere in the struts area. In this case, the location of duct exit can be strategically positioned to get the maximum benefit, depending on the flow separation location. First of all, it will be assumed that the duct exit will not have a specific location and hot air will be added freely to air inlet, then complexity of system will be ramped up. Advantages of this approach are that benefit of pressure and heat energy recuperation can be seen in isolation. The principle of this system is explained by equation no. 2.5.3 and no. 2.5.4. Increase in air density causes an increase in mass flow which leads to a decrease in incidence angle which prevents separation. The price for all of this are pressure losses in ducts, increased engine complexity, and increased manufacturing costs.

2.5.6 Jetflap

Jetflap utilizes all previously mentioned principles of preventing unstable work. The first is the recycling of air and the benefits that come with it. It also makes use of struts to create necessary changes to inlet flow direction. This is achieved by small jets that alter the flow direction. Another benefit is that we can put these small jets in places where they can effectively prevent separation. It can be placed to struts or hub if necessary.

The main issue that needs to be solved is where air with necessary pressure can be found. First option is anti-surge valve. The problem is that the air leaving valve might not have necessary pressure and temperature to make an impact. Next option is bleeding air from the combustion chamber or any suitable location around combustion chambers. Air in these areas has high pressure and temperature, but its bleeding might decrease efficiency of combustion side of engine.

Disadvantage of this system also lies in the increased complexity, as well as research, development, and manufacturing costs. Moreover, a system that can make sure that the duct will not be clogged up must be devised. The main question is, how effective this system will be and whether the benefit will justify extra costs.

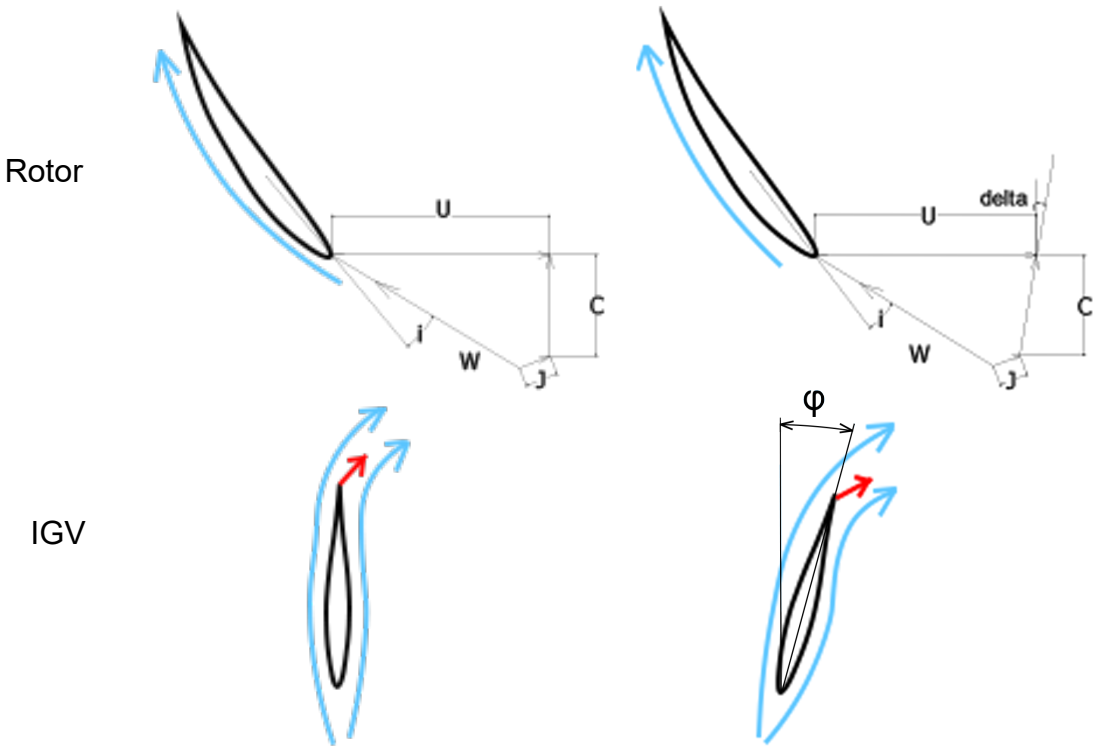

Fig. 2.18: Jet flap and jet flap & IGV combination

As per Fig. 2.18, the jetflap can be used to lower the incidence angle on rotor. It changes direction of tangential speed w_1. It can be combined with IGV to achieve greater reduction of incidence angle. If this system is combined with anti-surge valve, it will lower incidence angle only when the valve opens. Once the engine reaches higher revolutions, anti-surge valve will close and deactivate the Jetflap in process.

3. Methodology

In the previous chapter, technical challenge and possible solutions were described. Once that is done it is necessary to choose correct tools for detailed analysis. There are several ways to do it. Full scale prototype can be built. However, this is extremely costly and time consuming. Another option is to create simplified small scale prototype to test ideas more quickly. This would still require large investments. In recent decades, computing power has become relatively cheap which led to the development of powerful computing software like CFX and Fluent. They allow trained and experienced engineers to simulate their ideas very quickly and cheaply. Even to this day, it is tricky to use these tools without experimental data, but when combined with real life testing they can provide more insight than testing on its own.

Probably the most important step is the problem definition. It is of paramount importance to define what are the expected results from CFD. This will guide the simulation setup, so that time is not wasted on capturing unnecessary details while leaving out important flow features. The goal of CFD in this thesis is to simulate different ideas and evaluate its potential in preventing flow separation by increasing the incidence angle.

3.1. CFD theory

This chapter describes necessary mathematical apparatus used in a solving turbomachinery numerical task using CFD. The first attempt to skip testing in turbomachinery was made by Wu with the introduction of blade-to-blade (S1) and hub-to-tip (S2) stream surfaces [10]. Through flow calculations were introduced and became an important part of turbomachinery design. They, however, had significant drawback, and that was the inability to predict recirculating flows. Later, three-dimensional calculations were introduced allowing recirculating flows to improve accuracy. However, because of the boundary layer calculations, Navier-Stokes (N-S) Equations are now used. At first, the computing domain must be discretized (mesh generation). Once that is done, N-S Equations are applied to smaller volumes using Control Volume Method.

2.5.7 Governing Equations

There are three main basic principles that help user to define the necessary equations, that are then applied to mesh. That allows user to calculate all the necessary quantities like velocity, temperature, and pressure. These equations describe different laws of conservation.

3.1.1.1. Conservation of Mass

First assumption is that mass can not be created nor destroyed. For relative and absolute frames, the equation is formally identical.

$$\frac{\partial \rho}{\partial t} + \frac{\partial (\rho u)}{\partial x} + \frac{\partial (\rho v)}{\partial y} + \frac{\partial (\rho w)}{\partial z} = 0 \qquad (3.1.1)$$

3.1.1.2. Conservation of Momentum & Energy

Relevant equations were not subject of thesis. It is necessary to mention that thay are fundamental part of CFD and it is important to understand that they do exist and how they affect solution. However it is not necessary to copy them from source material and full version can be found in CFX theory guide [2].

2.5.8 Turbulence modeling

Due to the high speed of airflow inside the compressor, CFD has to deal with turbulence in some way. One way is simulating the movement of each individual molecule. Even if this was possible, the number of molecules would be immense rendering the simulation impractical due to high computing costs. That is why air is simulated as a continuum, meaning that turbulence must be modelled in some other way. Up until now, several ways were devised.

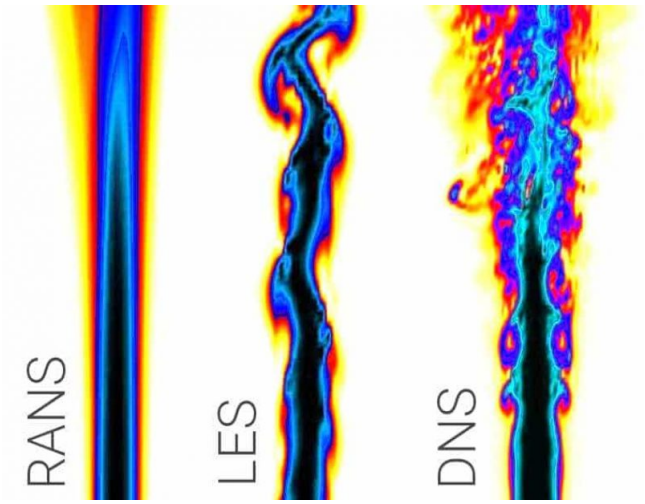

Fig. 3.1: RANS vs LES vs DNS [9]

Direct numerical simulation (DNS) is the most precise. This approach solves N-S equations without any turbulence model. Its advantage in accuracy is obvious, because eddies from the smallest ones to largest ones are resolved. Disadvantages are erroneous computional power requirements, rendering this approach unsuitable.

Large eddy simulation (LES) filters the smallest eddies, causing a decrease in computational power requirements which are, however, still too high.

Reynolds-averaged Navier-Stokes (RANS) approach approximates turbulence by averaging values over time. This approach greatly reduces computational costs while maintaining sufficient precision. It is however necessary to provide turbulence model that will predict turbulence without resolving all turbulent fluctuations.

2.5.9 Turbulence model $k-\omega$

The model selected for this thesis is Shear Stress Transport (SST). It is two-equations model. The first one determines the energy in turbulence and it is called turbulent kinetic energy k. Second one ω gives specific dissipation. Its purpose is to determine the scale of turbulence. Its advantage is in the treatment of all parts of the boundary layer, especially the viscous sub-layer, meaning that it can be used as Low-Re turbulence model even without additional damping functions. SST also solves known problem of simple $k-\omega$ by switching to $k-\varepsilon$ in free-stream, thus preventing increased model sensitivity to inlet free-stream turbulence properties. The main reason why this model was chosen is its performance in areas of adverse pressure gradient where flow separation occurs or could occur.

Turbulent eddy viscosity $k-\omega$ [2]

$$\mu_T = \frac{\rho \cdot k}{\omega} \tag{3.1.2}$$

2.5.10 Boundary layer treatment

Due to the fluid viscosity, fluid ”sticks“ to solid surfaces causing the fluid velocity to slow down near walls, creating a boundary layer. This generates viscous forces and losses. This phenomenon is also very important part of flow separation. That is why it needs to be modelled in CFD as well.

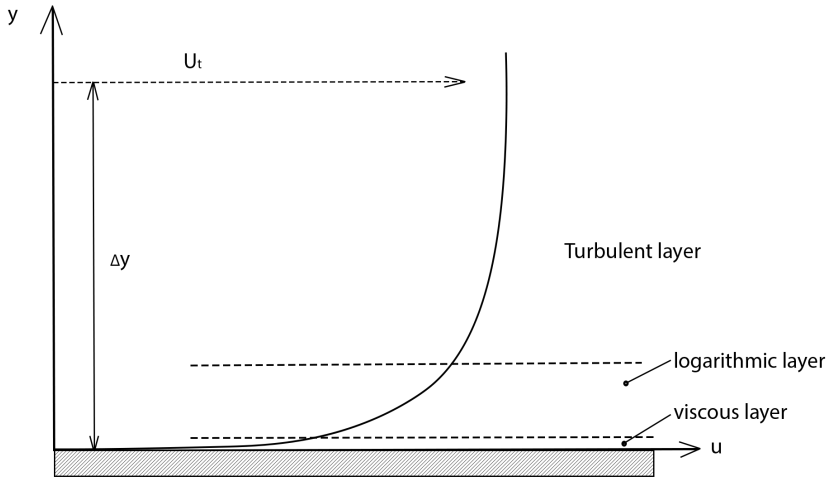

Fig. 3.2: Boundary layer division

Near wall region can be divided into two layers. The first one is the viscous layer. Flow tends to be almost laminar and viscous forces dominate this region. Much thicker part is the logarithmic layer where mixing processes dominate the region. If we plot velocity along the surface, we get the boundary layer velocity profile. These phenomenons have profound effects on CFD results. That is why we usually add thin prismatic layers of cells onto No-slip walls to improve accuracy of boundary layer prediction. The issue is, how thick these cells should be (whether they are prismatic or not is beside the point). That is why we define y^+ to help us determine correct thickness.

The non-dimensional wall distance

$$y^+ = \frac{\rho \cdot \Delta y \cdot u_\tau}{\mu} \tag{3.1.3}$$

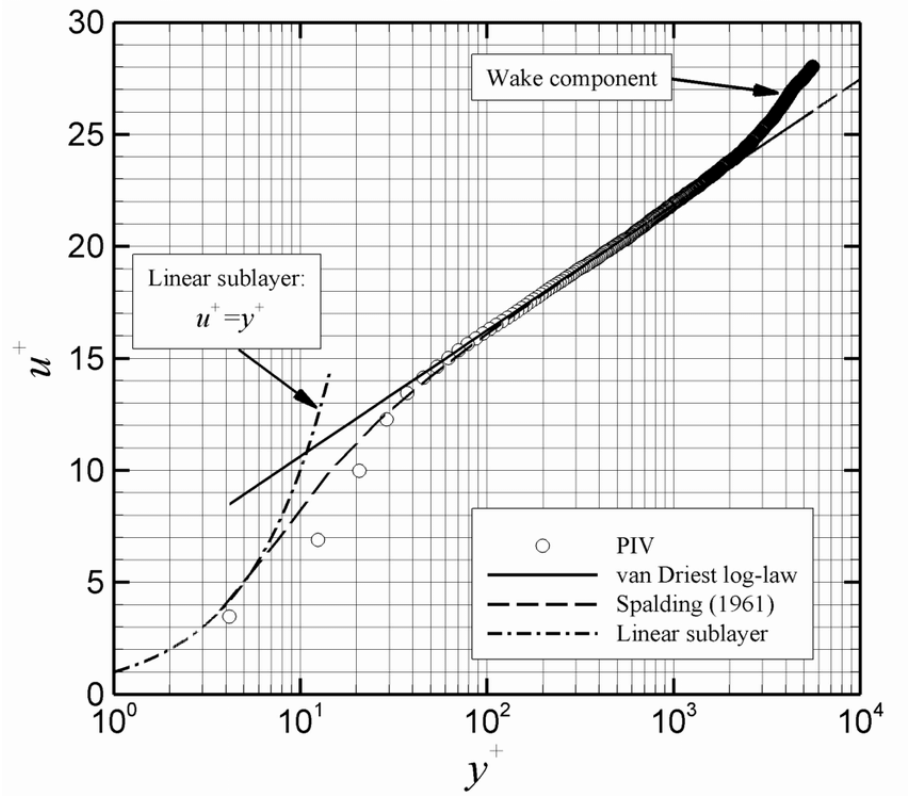

Fig. 3.3: Law of Wall [3]

Fig. 3.3 represents the measured data in wind tunnel around a flat plate. It can be seen that in the viscous sublayer the behaviour is actually linear (the horizontal axis is logarithmic). That is why in this region following approach is used.

The non-dimensional velocity – viscous sublayer

$$U^+ = y^+ \tag{3.1.4}$$

However, this approach would be inaccurate in log-law region, that is why the following is applied.

The non-dimensional velocity – log law

$$u^+ = \frac{U_t}{u_\tau} = \frac{1}{\kappa} \cdot \ln(y^+) + C^+ \tag{3.1.5}$$

Shear velocity

$$u_\tau = \sqrt{\frac{\tau_\omega}{\rho}} \tag{3.1.6}$$

Where Δy is distance to the wall of tangent velocity U_t, τ_ω is wall shear stress, κ is von Karman constant and C^+ is the log-layer constant, that depends on wall roughness.

We can see that y^+ is function of distance to the wall. This means that thickness of the first layer of cells will affect y^+ value on surface. Depending on the turbulence model, there are recommended values of y^+ in which model operates correctly with appropriate accuracy. CFX gives the user only ”Automatic near wall treatment“ option when using SST turbulence model.

This in reality for CFX user means that $if\ y^+ < 11{,}05$, than constant (viscouss) treatment is applied. And $if\ y^+ > 11{,}05$ than log law is applied. Switching between functions is done automatically by solver, hence ”automatic“ setting. The most important conclusion from this theory (Fig. 3.3), is that there is a buffer layer. In this region, there is visible disagreement between either constant or log law and if the mesh is done in such a way that y^+ is at buffer layer values, large errors can be produced. One can argue why not use function, that will approximate boundary layer correctly no matter the y^+. There is such function called Spalding’s wall function. However, it is currently not implemented in CFX, so it could not be used. The second conclusion is, that to accurately predict the separation and therefore viscus sublayer, y^+ should be lower than 11,05, ideally around 1 [1].

2.5.11 Finite volume method

Once the domain is discretized, the previously mentioned equations can be applied. Finite volume method is the most commonly used method for CFD. It is called Finite volume method, because it works with the control volume, not with the intersection points of grid. This means that any type of grid, whether it is structured or unstructured, can be used. Previously mentioned conservation equations are integrated over each control volume. Gauss’s Divergence Theorem is also used to evaluate cell centered values at the cell faces.

CFX as well as Fluent have several numerical schemes. For the purpose of this thesis high resolution was used. This means that the 2nd (and higher) order schemes were applied to increase accuracy. This means values were averaged from values from two adjacent cell centers (the first order would use only 1 adjacent cell center). High resolution also prevents undesired behaviour, such as smearing due to numerical diffusion, or false oscillations. This can be especially important, because numerical diffusion can diffuse supersonic shock wave.

3.2. CFD methodology & feasibility study

It is clear that using CFD is the best way and given circumstances the only way to properly analyze the issue at hand. CFD in this thesis was used to simulate the airflow in an engine compressor in conditions during which the first flow separations happen. Once this was achieved, anti-surge modifications to the compressor were added to the model and their effect analyzed. First separations were most likely to occur on the first stage rotor or stator.

It meant that the following parts were simplified and included in model:

1) Compressor intake system
2) Strut section
3) 1st axial stage rotor
4) 1st axial stage stator

Full simulation of the engine intake system and the 1st stage of compressor would require a very large mesh. Intake system can be easily simplified. Parts containing the blades can be simplified using the rotational periodic boundary condition and therefore only 1 blade per part has to be used. This kind of simulation is possible in CFX or Fluent. Fluent is a very capable software and is able to analyze many types of engineering problems. It offers many tools for incialization and solution steering. This is where CFX falls short. However where CFX excels is turbomachinery because of its implemented turbo mode. Turbo mode simplifies simulation pre-processing as well as post-processing. However probably the most important is that Fluent requires twice the amount of RAM as CFX for the same turbomachinery mesh. However, it is still possible to analyze the problem with both softwares.

There are 3 commonly used approaches:

1) Frozen rotor
2) Mixing plane
3) Sliding mesh

Sliding mesh is certainly the most accurate way. However, because it requires transient simulation setup, its computational costs are significant and for the purpose of this thesis are unnecessary. Frozen rotor and mixing plane are very similar in setup and computational requirements. However, the results however differ. Frozen rotor fixes the blades in their relative positions. This means that their relative positions are very important for final results. That is why it is often used as an initial guess for sliding mesh approach. Mixing plane is much more user friendly in this regard. And since the mixing plane tends to be easier to use and provides better results given the task in hand, the mixing plane was chosen.

Once the basic simulation run is accurate enough, anti-surge modifications can be implemented. Mass flow rate as well as temperature and inlet flow direction can be adjusted easily. There are, however, several ways to implement the jet flap.

1) Full resolution (CFX & Fluent)
    a. Conformal mesh
    b. Non-conformal mesh
2) Injection regions (CFX only)
3) Boundary condition (CFX & Fluent)
4) Source terms (CFX only)

Full resolution is probably the most accurate, especially when using a conformal interface. It is, however, time consuming to prepare when many solution iterations are simulated. It would also increase the number of elements in simulation, but the increase is negligible. Mesh preparation times make it inappropriate for preliminary aerodynamic analysis. Using non-conformal mesh will deminish some of its precision

advantages, but thanks to clever tools in CFX and Fluent, it is much faster to use. Big advantage is that the local phenomenons around the hole edges are resolved as well as correct flow vector profile is determined by the geometry and flow it-self.

Injection regions are a great option. It is very simple to prepare and modify the simulation using CCL file. It is also accurate. However, since it is relatively new option in CFX, only the mass flow condition can be assigned. That could be a significant disadvantage, because sometimes pressure is the only parameter we know. Injection regions require user to specify the flow vector, making prediction of the mixing of main flow and jet less accurate.

Creating a jetflap 2D zone and assigning the boundary condition is a good option. However, when compared to non-conformal full resolution, it struggles because it requires mesh modification, whereas non-conformal mesh can be imported directly to CFX or Fluent and connected using interface.

Source terms is the least accurate option that also comes with all the disadvantages of injection regions, rendering this approach rather obsolete.

Considering the mentioned advantages and disadvantages, injection regions appear to be the best option for jetflap and following method were used. In the end non-confomal full resolution was implemented to anti-surge valve and injection regions were used for jetflap. Slot was modeled by 2D zone and assigning boundary condtion.

3.3. Geometry & boundary conditions

The computational model is made up of 3 main parts.The first one is the inlet device. The inlet device contains bubble, to which inlet boundary condition is applied. Its shape was made so that ISA conditions can be applied, especially so that the dynamic pressure was as close as possible to the stationary air. The bubble was connected to the inlet device channel. Channel and bubble are connected with 70mm radius so that the air was not separating in the connection region around edges. This separation would increase the mesh size requirement in the region and worsens residuals in area. In the channel there are two NACA 0009 jets. Both of them were cut in half creating a new surface to which inlet boundary condition is applied, simulating returning air from anti-surge valve. In cases when returning air or pre-heating was not used, all surfaces of NACA 0009 jet were free slip walls. Length of the channel and number of jets are related. These parameters were determined so that the hot and cold air from the jet and atmosphere are already mixed and as uniform as possible when hitting the struts, removing any local effects. Local effects of jets (jetflap) were also simulated, but modifications were applied in the 1st stage axial compressor stage (red and metal parts – Fig. 3.4). This region is made up from 3 sub-parts. First one is strut section, the second one is rotor section and the third one is stator section.

The last part is the outlet device. Its purpose is solely to increase numerical stability by allowing separations and shock waves to dissipate before hitting the outlet boundary condition. These effects would not affect significantly the pressure outlet condition, but would cause the simulation to crash when using the outlet mass flow rate condition.

The lenght of this region is 600mm. It might be considered excessive, but 400mm section was tested unsuccessfully, producing „fatal overflow in linear solver“ error. The walls in the inlet device and outlet device were set to „free slip condition“. Meaning that no viscous losses were calculated on these walls as well as no boundary layer. That meant that the mesh did not require prism layers, lowering the total number of cells.

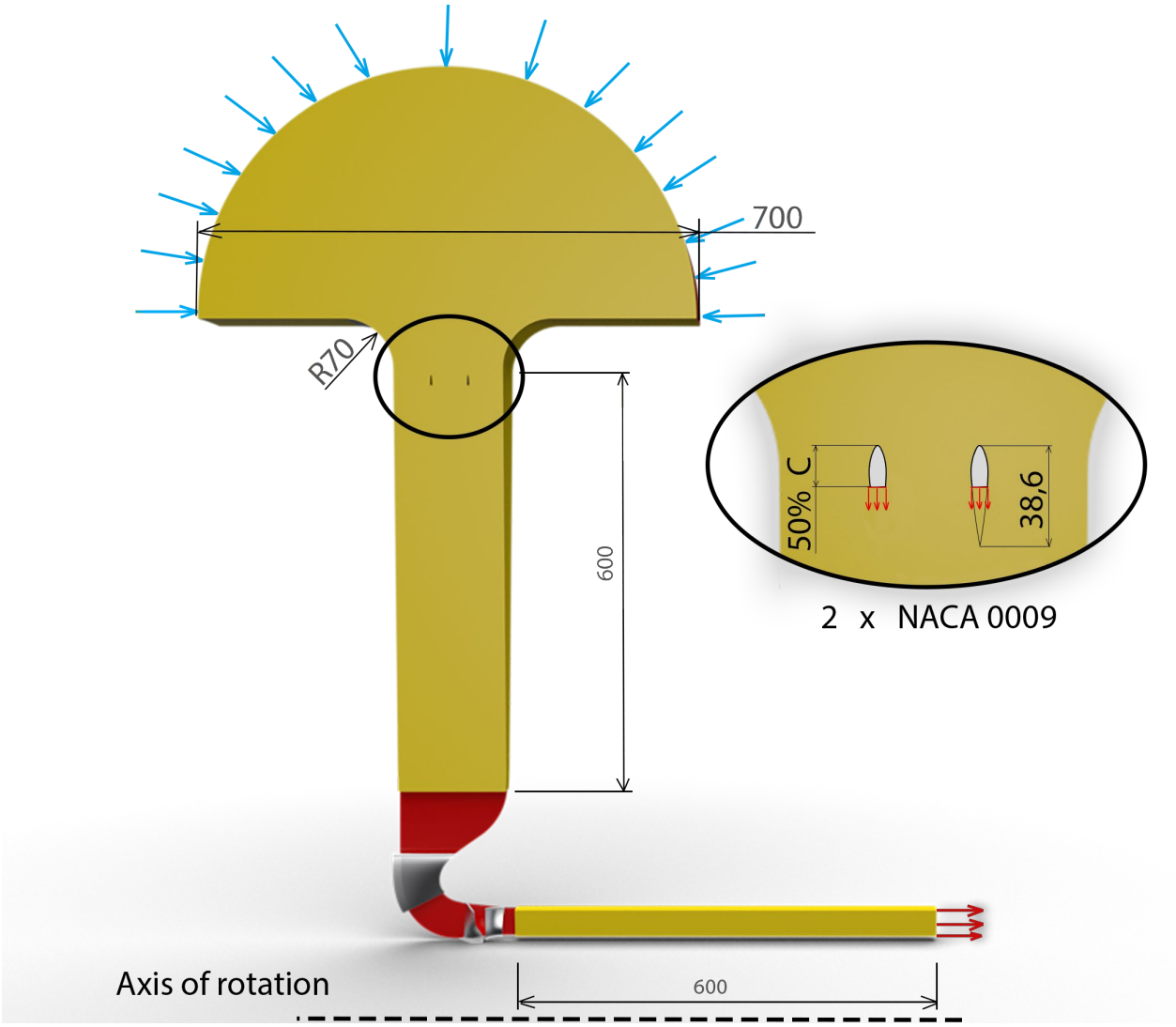

Fig. 3.4: Model setup

Tab. 3.1: Model interface settings

	Inlet device	
Inlet condition	Opening	$p_{1T} = 101\,325\ Pa$ $T_{1T} = 288{,}15\ K$ $Turb.intensity\ I = 5\%$
Wall treatment	Free slip	
Outlet condition	Mixing plane	$Const.Total\ Pressure$
Reference frame	Stationary	

	IGV	
Inlet condition	Mixing plane	$Const. Total\ Pressure$
Wall treatment	No-slip	
Outlet condition	Mixing plane	$Const. Total\ Pressure$
Reference frame	Stationary	
	Rotor	
Inlet condition	Mixing plane	$Const. Total\ Pressure$
Wall treatment	No-slip	
Outlet condition	Mixing plane	$Const. Total\ Pressure$
Reference frame	Rotating	
Rotor tip clearance	Shroud CGI Interface	$0{,}2\ mm$
	Stator	
Inlet condition	Mixing plane	$Const. Total\ Pressure$
Wall treatment	No-slip	
Outlet condition	Mixing plane	$Const. Total\ Pressure$
Reference frame	Stationary	
	Outlet device	
Inlet condition	Mixing plane	$Const. Total\ Pressure$
Wall treatment	Free slip	
Outlet condition	Pressure / Mass flow rate	$Press. profile\ blend\ 0{,}05$
Reference frame	Stationary	

Turbulence intensity value (Tab. 3.1) is according to knowledge of GE Aviation Czech in this particular case not important as long as it stays within reasonable range (around 1% - 5%) due to reasons stated in following paragraph. This thesis deals with airflow that is affected by this value very little, especially close to surge because of high energy levels in flow, unstable airflow and steady-state solver. Flow close to surge is also highly unstable. Not to mention, that there would be complicated engine intake system installed on the engine combined with changing atmospheric conditions, making this value highly variable and different compared to current model configuration. Turbulence intensity is applied to intake bubble that represents atmosphere, which in it self is simplification. Just to be sure, baseline regime was run with values 1%, 2%, 3%, 4% and 5% and there was no difference in obtained values of compression ratio, isentropic efficiency or incidence angle. There is possibility, that if the inlet device was removed and inlet boundary condition would be applied close to strut section, that turbulence intensity could potentially affect the solution, but not in current CFD model.

3.4. Mesh generation

Results from CFD are only an approximation of reality. To capture the shape features mesh is generated while rules for continuum mechanics are applied. Mesh size is important because the smaller the cells are, the better they can capture flow features (in most cases). We are, however, limited by computational resources, that is why only sufficient mesh size was used. For turbomachinery, mesh generating techniques are well established.

2.5.12 Inlet device

The purpose of this device is to guide undisturbed air into the compressor 1st stage without unnecessary numerical errors. Walls in this part do not require prismatic layers, because of the “free slip condition“ settings. Since the direction of flow in all parts of this segment is easily predictable, a structured mesh was used. And since it is not necessary to mesh full 360° part, only 1/90 section was used in the end, because of the mesh size optimalization. The final version of this mesh required significant refining in the connection region with compressor. Low quality mesh increased the residuals within mixing plane. Meshing only one face and revolving it turned up to be the best option for this part, since any other way of meshing a segment like that ended up in a simulation crash. Revoling mesh was the primary reason, why Naca 0009 jets were oriented in a manner as seen in Fig 3.4 (forming 2 rings around the whole compressor), again because it was the only way simulation would not crash after a few iterations.

Tab. 3.2: Inlet device mesh settings

	Mesh settings	
Software	Autodyn	
Mesh type	Revolved & Structured	
Cell type	Hexa	
	Sizing	
Default element size	62	[mm]
Number of edge divisions for segment	20	[-]
Capture proximity	yes	
Capture curvature	yes	
Total number of elements	561 640	[-]
	Face Sizing – mixing plane zone	
Element size	1	[mm]
Growth rate	1,05	[-]
	Face Sizing – Naca 0009 jets	
Element size	0,25	[mm]
Growth rate – Airfoil section	1,2	[-]
Growth rate – Jets section	1,05	[-]

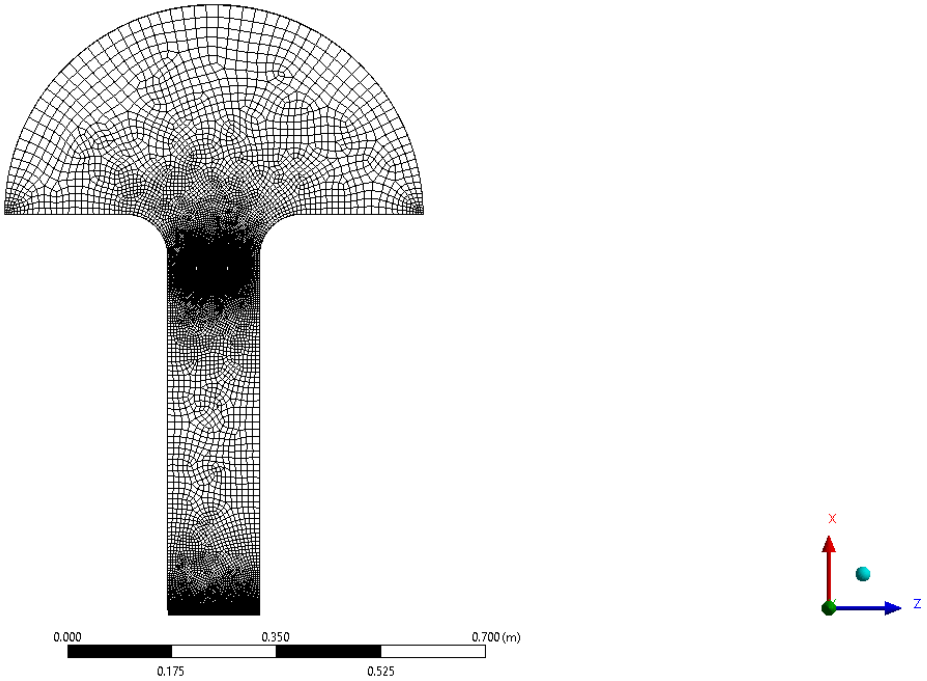

Fig. 3.5: Inlet device mesh cross section

2.5.13 1st compressor stage

It is a common practice to use structured mesh in turbomachinery. Its advantages in performance are significant, a fact that is proved by the creation of Turbogrid software. Its purpose is to quickly create very detailed and perfect turbomachinery mesh without any significant skill. It is still necessary to properly define the prismatic cell layer. Its initial values were estimated by the following equations and then further adjusted iteratively to the final values defined in the table in this section.

Reynolds number $$Re = \frac{\rho \cdot U \cdot L}{\mu} \quad (3.4.1)$$

Target y+ $$\Delta y_1 = \frac{y+ \cdot \mu}{\rho \cdot U_\tau} \quad (3.4.2)$$

Wall shear stress $$\tau_w = \frac{1}{2} \cdot C_f \cdot \rho \cdot U^2 \quad (3.4.3)$$

Frictional velocity $$U_\tau = \sqrt{\frac{\tau_w}{\rho}} \quad (3.4.4)$$

Where $C_f = 0{,}79 \cdot Re^{-0{,}25}$ for turbulent flow [8]

Tab. 3.3: Final 1st rotor stage mesh parameters

	IGV	
Cell type	Hexahedral	
Mesh type	H-grid	
Global Size Factor	2	[-]
First Element Offset	0,006	[mm]
Maximum Expansion Rate	1,3	[-]
Spanwise Blade Distribution Factor	2	[-]
	1st stage rotor	
Cell type	Hexahedral	
Mesh type	H-grid	
Global Size Factor	2,5	[-]
First Element Offset	0,001	[mm]
Maximum Expansion Rate	1,3	[-]
Spanwise Blade Distribution Factor	1,5	[-]
Leading and trailing edge refinement	200	[%]
	1st stage stator	
Cell type	Hexahedral	
Mesh type	H-grid	
Global Size Factor	2,5	[-]
First Element Offset	0,001	[mm]
Maximum Expansion Rate	1,3	[-]
Spanwise Blade Distribution Factor	2	[-]
Leading and trailing edge refinement	200	[%]

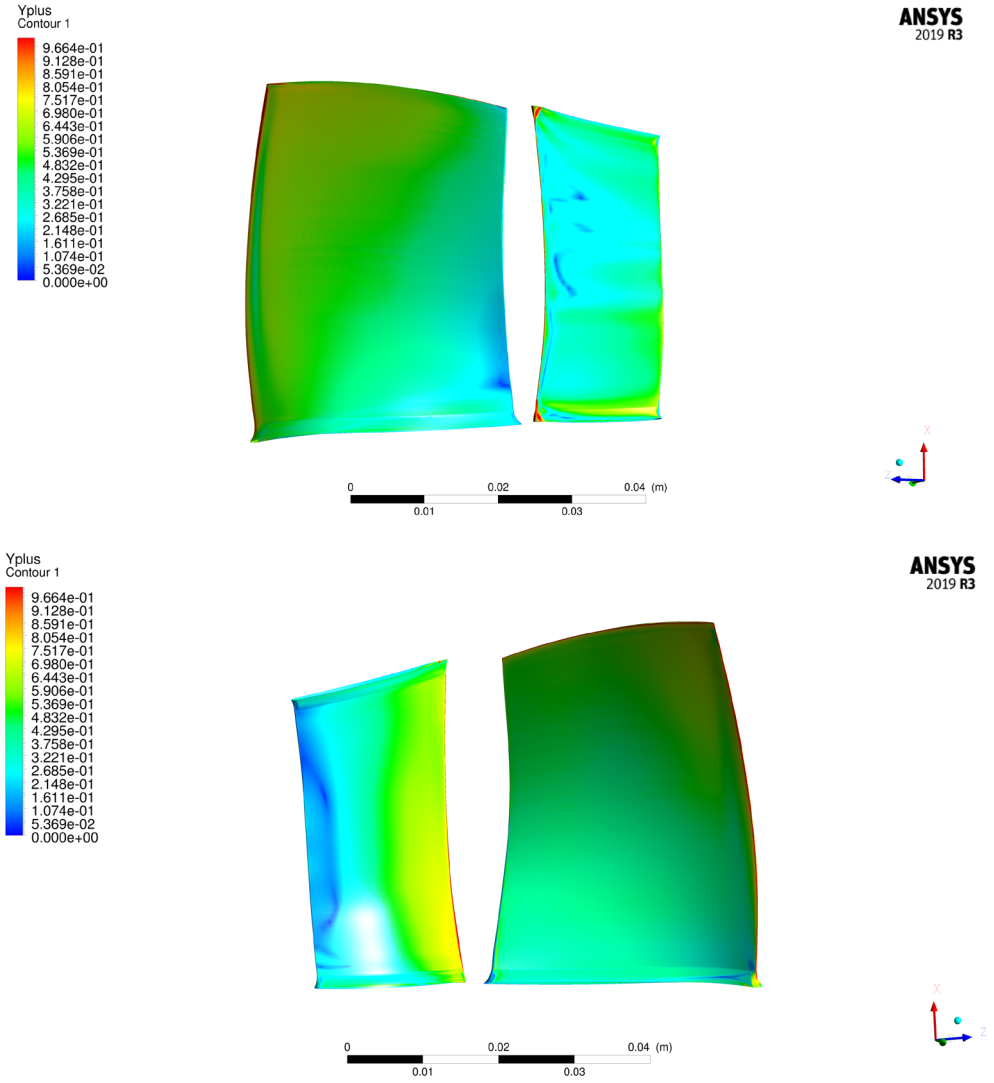

Fig. 3.6 y+

Fig. 3.6 depicts achieved y+ values. Because leading edges were very sharp, in some locations y+ reached values higher than one. However in the most critical places, like suction sides of blades, values were smaller than 1. Velocity values in IGV region were so small that y+ was not an issue in this region.

2.5.14 Outlet device

The purpose of the outlet device is to let the flow structures calm and dissipate before hitting the mass flow rate outlet condition, that would lead to „Fatal overflow in linear solver“. This means that the purpose of this component is simply to improve the numerical stability without altering results. Therefore, the walls on hub and shroud parts of the device should not add pressure losses to the simulation, because that would diminish the simulation precision. For the mesh setup, this means that the boundary layer does not have to be fully resolved with prismatic cells, but because the boundary layer velocity profile will come from stator segment, some prismatic cells were added. It is also not necessary to mesh whole 360° region, because of that only 1/30 of the full circle was meshed, leading to a significant decrease in the mesh size. To improve the numerical stability and decrease the mesh size, only one face of the segment was meshed and revolved around axis. Mesh size was determined so that

the flow structures won't dissipate fast enough to affect flow the in stator section. Because of the length of section, it is unlikely and problematic for flow structure to hit the outlet condition.

Tab. 3.4: Outlet device mesh settings

	Mesh settings	
Software	Autodyn	
Mesh type	Revolved & Structured	
Cell type	Hexa	
	Sizing	
Default element size	1	[mm]
Number of prism layers	5	[-]
First layer height	$5e-5$	[m]
Growth rate	1,2	[-]
Total number of elements	535 800	[-]

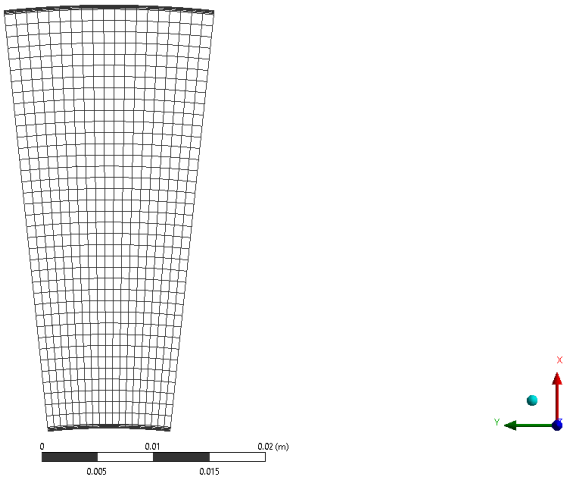

Fig. 3.7: Outlet device mesh cross section

3.5. Solution setup

Physical Timescale estimation was done according to equation 3.5.1. Due to difficulties achieving convergence, used physical timescale was further decreased.

$$Physical\ Timescale\ (100\%\ revolutions) = \frac{1}{\omega} = 2{,}6e-4 \qquad (3.5.1)$$

Tab. 3.5: Numerical settings

	Numerical settings
Advection Scheme	High resolution
Turbulence Numerics	High resolution
Min. Iterations	40
Max. Iterations	1500
	Timestep settings
Physical Timescale	$0{,}0002\ s$
Global dynamic model control	OFF

3.5.1 Judging convergence

First condition was residual target.

Residual type	RMS
Residual target	$1e-6$

The second condition was that the values of all considered parameters within a defined number of iterations must not change too much. For this reason, the convergence criteria were defined by equation 3.5.2.

Number of considered iterations $\boldsymbol{n = 30}$

$$V = \frac{R_{i+n} - R_i}{R_i} \tag{3.5.2}$$

Tab. 3.6: Monitor convergence targets

	Required $V\ [-]$
Mass flow rate – inlet	$0{,}001$
Mass flow rate – outlet	$0{,}001$
Static pressure	$5e-4$
Stagnation pressure	$1e-4$
Static temperature	$5e-5$
Dynamic temperature	$5e-5$

Third condition was that „Mass of rate – inlet“ and „Mass flow rate – outlet“ monitors must give the same absolute value in the following format $xx,xx = -yy,yy$. In other words, the values must be equal to the two decimal places with opposite signs.

The fourth and last condition takes into account shape of residuals as well as property monitors. If the solver suspects transient flow behaviour that might be significant, a monitor or several monitors might show oscilating values. Sometimes the graph might take the shape of sinus function, which usually occurred when using SST model. And other times the graph took the shape of „saw teeth“ as it was in the case when using $RNG\ k-e$ model. This was picked up by the second convergence condition. When such a phenomenon occurred, the point was marked with a triangular shape marker in graph.

3.6 Results validation

3.6.1 Model correlation

Since CFX is a widely used software and the techniques used in this thesis are well established in the turbomachinery industry, one can argue that it is pointless to corellate results with experimental data. Even though it is true to a certain degree, it is always safer to expect bad results from CFD and double check afterwards. Because even the biggest companies don't have unlimited budgets, experimental data are not available for every possible scenario. That is why NASA Rotor 37 was used to corellate CFD model used in this thesis. The value of such comparison is limited, because Rotor 37 is only rotor, without stator or IGV. The geometry is also not identical to the one used in this thesis. It is, however, still beneficial to do it. Data from this experiment are widely available, easy to obtain, and it is far more easier to find correct mesh, numerical and physics settings when working with a simple example.

Mesh settings were similar to those used in the main case.

Tab. 3.7: Rotor 37 settings

	Model properties
Geometry	NASA Rotor 37
Number of passages	36
Rotor tip clearance	$0{,}4\ mm$
Turbulence model	SST
	Material
Material	Air ideal gas
Reference pressure	$1\ atm$
	Physics settings
Reference pressure	0 Pa
Rotational speed	-17 189 RPM
Time settings	Steady - state
	Boundary conditions
Inle total pressure	$101\ 325\ Pa$
Inle total temperature	$288{,}15\ K$
Outlet static pressure	$variable$
Wall	No - Slip

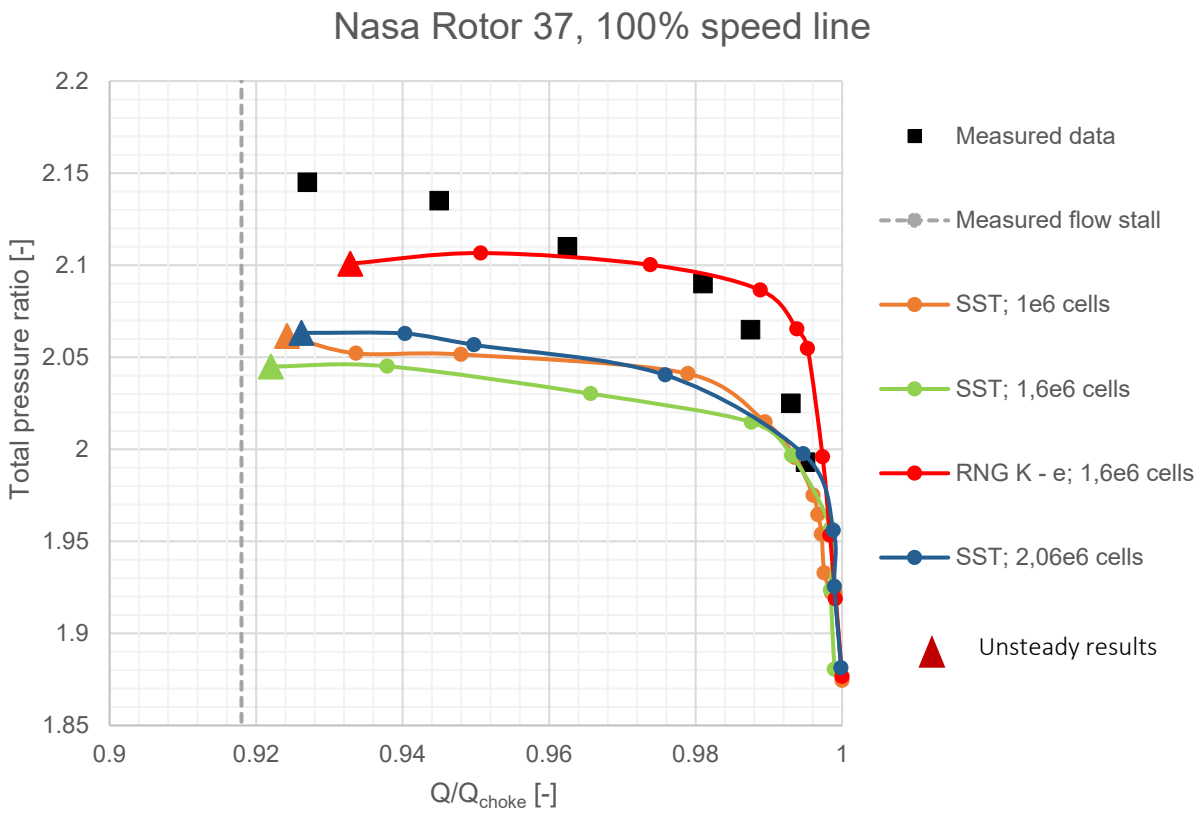

Fig. 3.8: Nasa Rotor 37, 100% speed line

RNG $k-e$ model gives better agreement with experimental data compared to SST. However, in the end, SST model was chosen. The reason is that the first clues of significant flow instability are reasonably well predicted by SST. These transient flow features are small. Whereas RNG $k-e$ model predicted transient flow features far too soon. However, the most important reason is that RNG $k-e$ model predicted huge instability compared to SST. Size and onset of instability was determined by oscilations of CFD monitors.

Even though calculations where significant flow instability could interfere with the results were avoided because of steady-state nature of CFD setup, it is better to choose less accurate model rather than to risk unstable flow features in CFD that will render results not usable.

3.6.2 Mesh depence study

For purpose of this study “First layer thickness“ is multiplied by coeficient which is the same for meshes of IGV, stator and rotor. This approach can be used, because mesh size is dependent on First layer thickness. As for inlet system and outlet systems, mesh settings were left untouched.

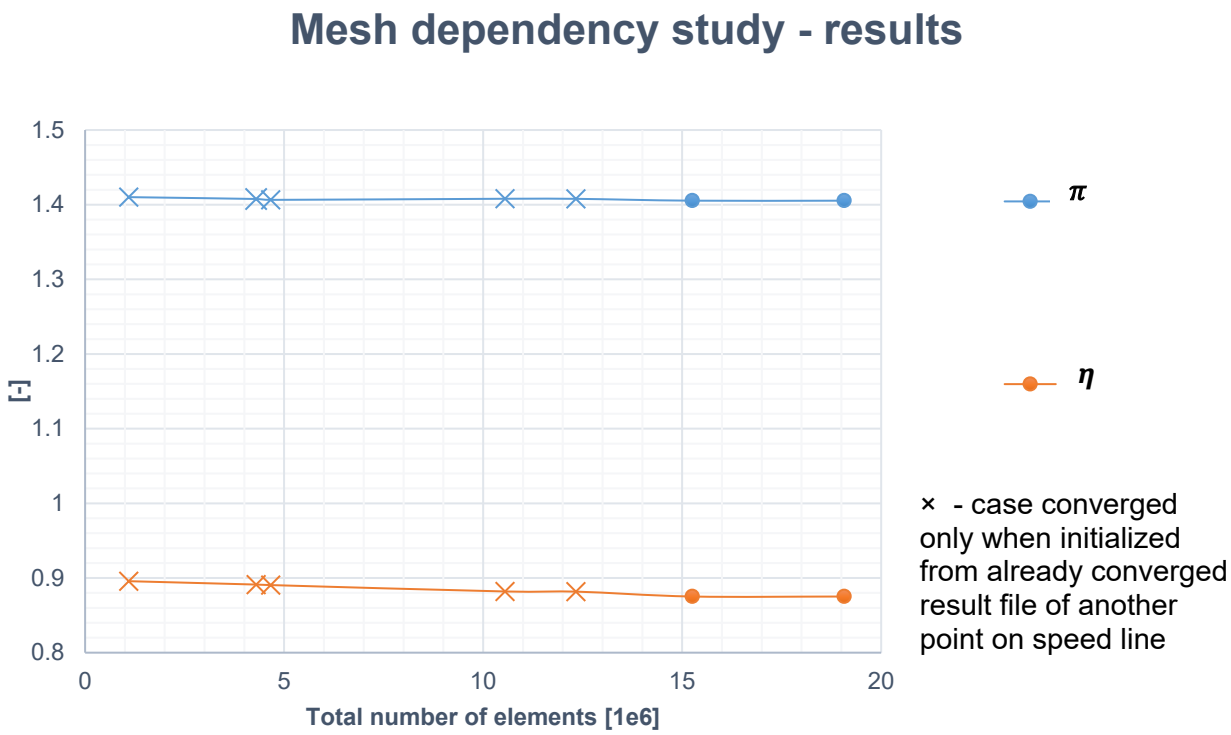

Fig. 3.9: Mesh depedence study – results

As the mesh size and quality drop, eventually errors accumulate and results deteriorate. Still good results can be achieved using a poor quality mesh, if precise initial values are provided. It is, however, impossible to find correct results without initial values with poor mesh, because such cases lead to solution divergence and therefore failure without any results. If, however, good mesh size is used, the solution is not dependent on the mesh quality and size.

3.6. Result quantification

CFD results were analysed using several equations, that are mentioned in the following chapters.

3.6.3 CFD postprocessing

Local incidence angle

$$i = \varphi_1 - \beta_1 \tag{3.6.1}$$

Inlet flow angle

$$\beta_1 = \cos^{-1}\left(\frac{\boxed{w}}{\sqrt{\boxed{w}^2 + \boxed{v}^2}}\right) \tag{3.6.2}$$

Where $\boxed{w}$ represents mass flow averaged axial velocity at given region and $\boxed{v}$ represents mass flow average circumferential velocity at given region. Each region was $1/9$ of total span.

„Integral incidence angle“ represents the average value. Some modifications created local effects and some did not. That is why each modification was judged based on the integral value of incidence angle as well as the distribution of incidence angle along the blade span. Integral value was obtained as showed in Fig 3.10. Because the blade length was normalized to value 1, the integral value represents the average value.

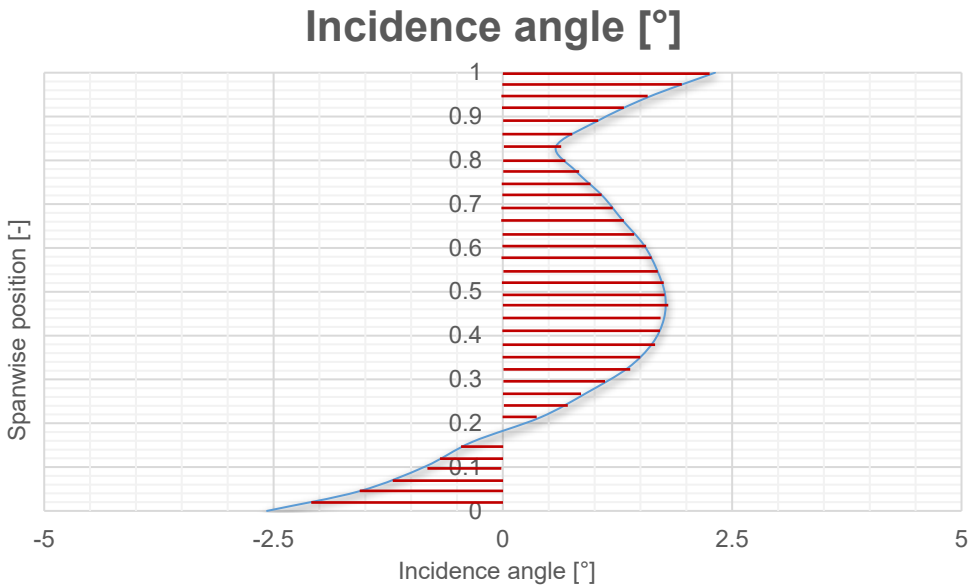

Fig. 3.10: Integral of incidence angle

Incidence angle was evaluated in all cases on the plane with the normal vector (0 0 1). The plane was in strut region, located 2mm from the interface with the rotor (Fig. 3.11).

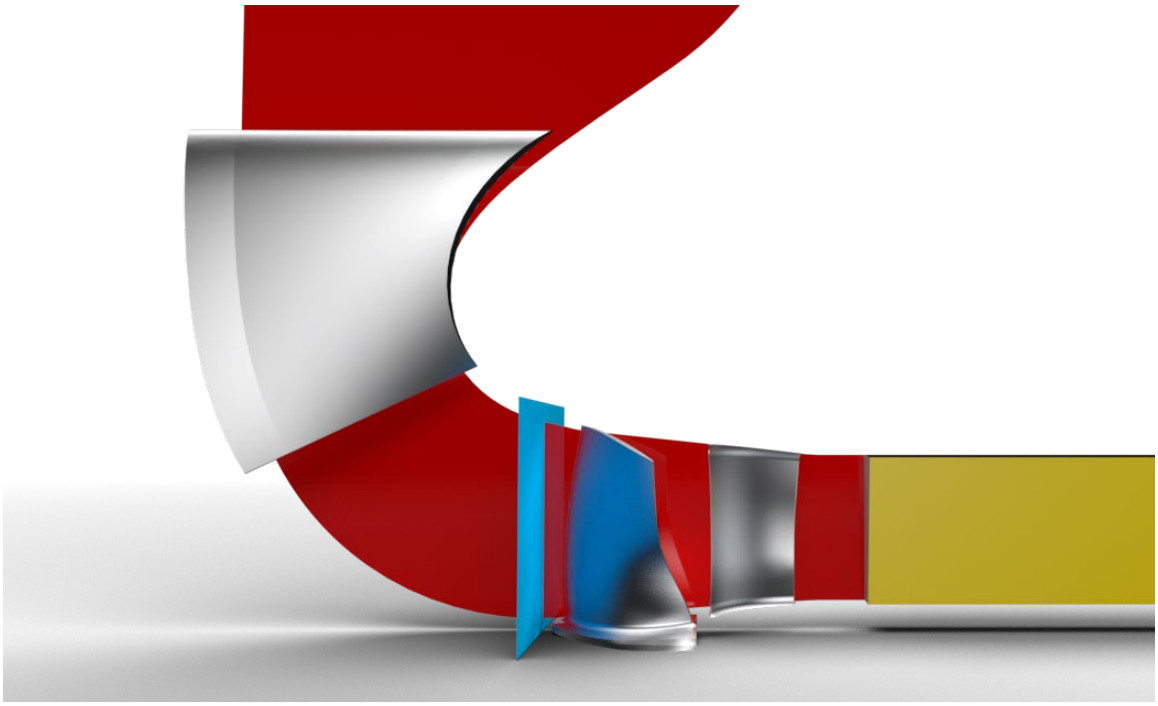

Fig. 3.11 Incidence angle measurement plane - the blue plane

4. Baseline configuration

The first step was to calculate three speed lines. Speed lines are defined by the percentage of reference revolutions per minute. These revolutions are applied to the rotor. Reference revolutions per minute are $36\,660\ RPM$. The first speed line was the design mode which is 97,8% of the reference RPM. The second one was 60% RPM, which is idle mode. These two regimes were chosen because engine is going to operate in region between these two speed lines. The third one is 80%. The 60% one is the most problematic one. However, the main reason why the following data were calculated was the validation of the CFD model and selection of baseline regime. Since the compressor analyzed in this thesis is an existing one, the performance values generated by CFD must stay within the expected limits. Each calculated point must also change its output values relative to other regimes according to the expected logic and therefore must behave like a real compressor.

Surge line (Fig. 4.1) was determined by the last point on each speed line before the simulation crashed. It was expected that the solution monitors would oscilate and based on the oscilation amplitude, the surge line would be determined. This, however, did not happen because of the inlet and outlet devices and that is why crash based approach was used.

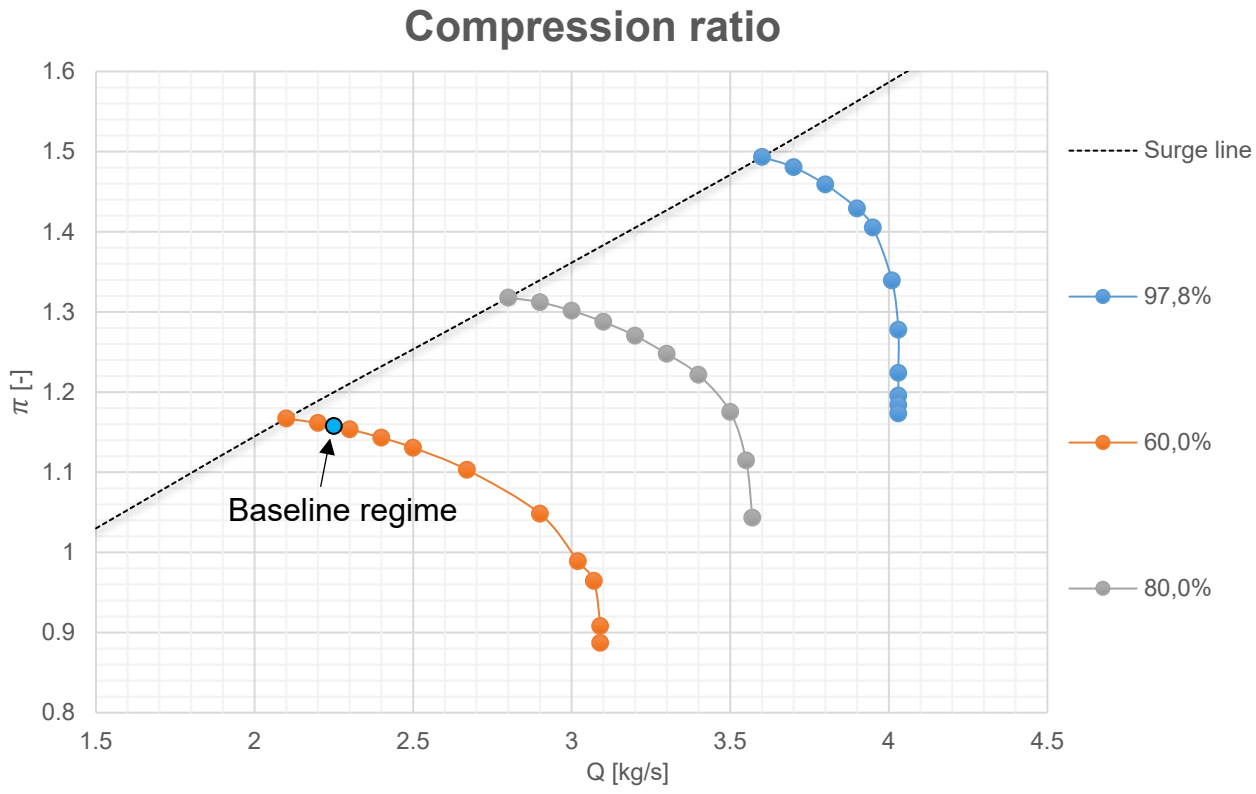

Fig. 4.1: Compression ratio – baseline configuration

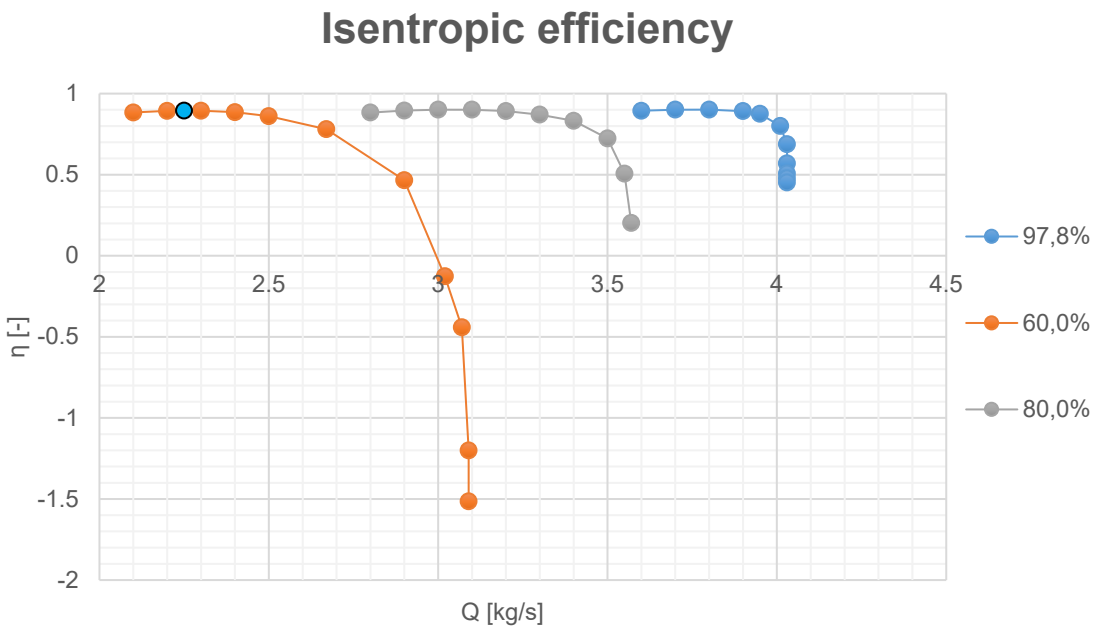

Fig. 4.2: Isentropic efficiency – baseline compressor

Isentropic efficiency is behaving as expected (Fig. 4.2).

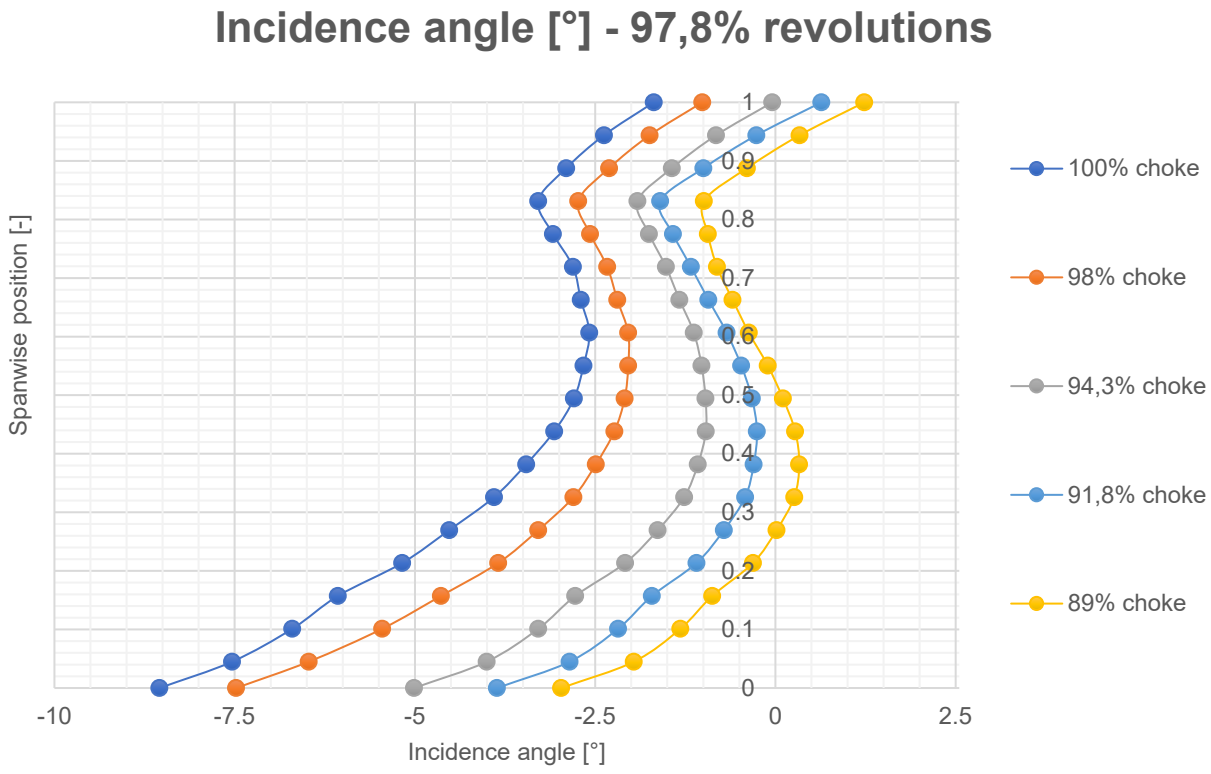

Fig. 4.3: Incidence angle – 97,8% revolutions (100% choke = highest achieved Q_{mr})

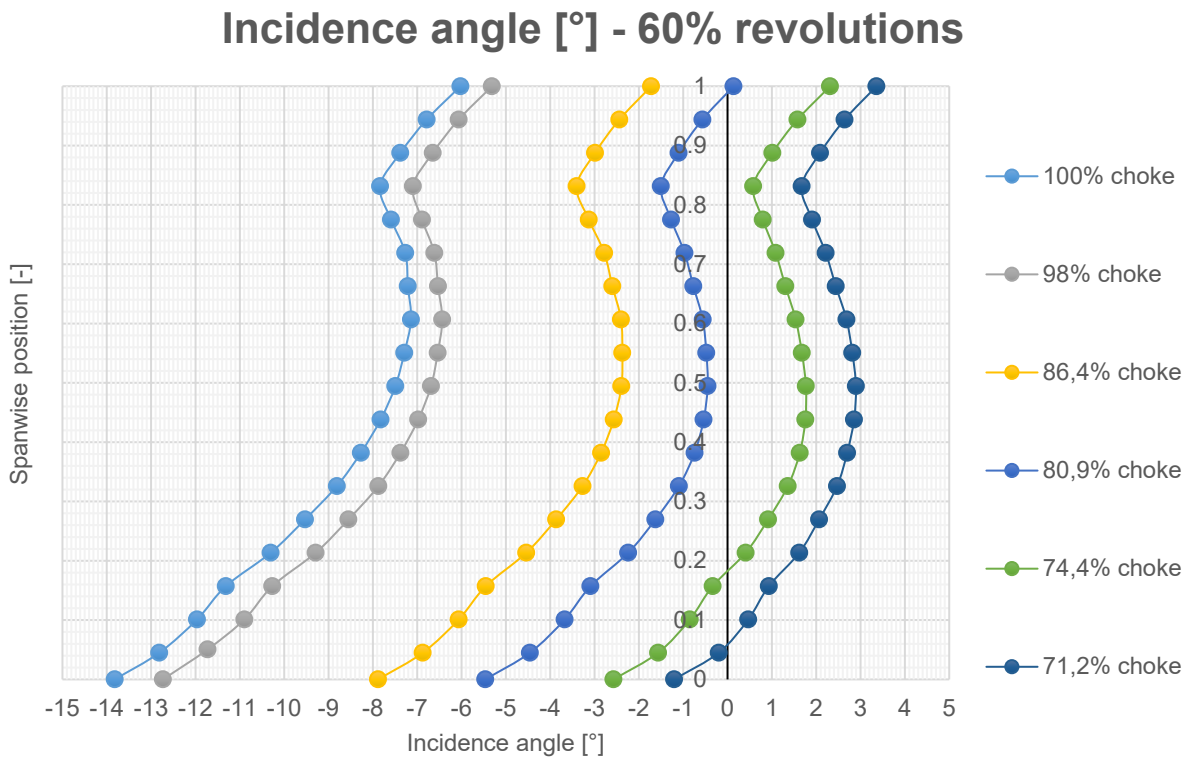

Fig. 4.4: Incidence angle – 60% revolutions (100% choke = highest achieved Q_{mr})

Fig. 4.4 and Fig. 4.3 clearly show, that the further the point from the surge line is, the lower the incidence angle gets. Therefore, lowering incidence angle is a good way of increasing the surge margin. It can also be assumed that incidence angle is a good measure of proximity to the surge line, and therefore calculating the whole speed line and defining the surge line is not necessary for each device and increase in surge margin can be clearly assumed based on decrease in incidence angle.

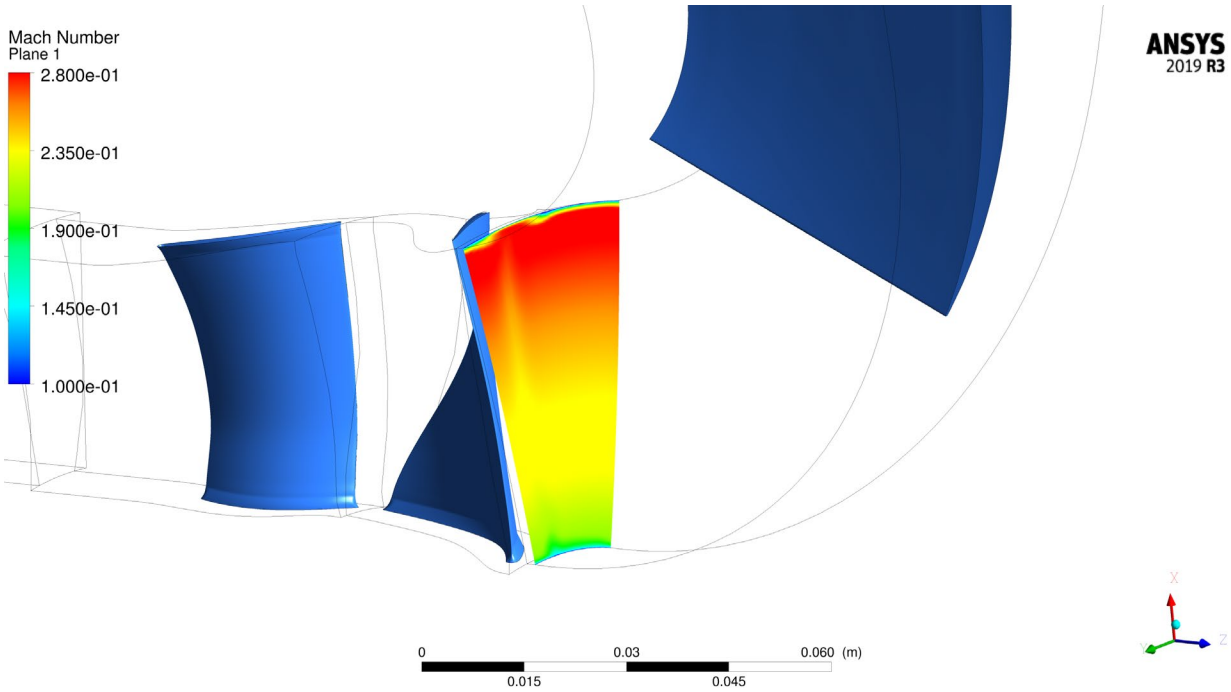

Fig. 4.5 Mach number – Baseline configuration

Analysis of the baseline configuration showed an important issue. Fig. 4.5 shows higher Mach number in front of the rotor in rotor tip region and lower Mach number near the blade root. The cause of this might be a rotor or curve in struts section. This phenomenon is important because some anti-surge devices can be significantly affected by this.

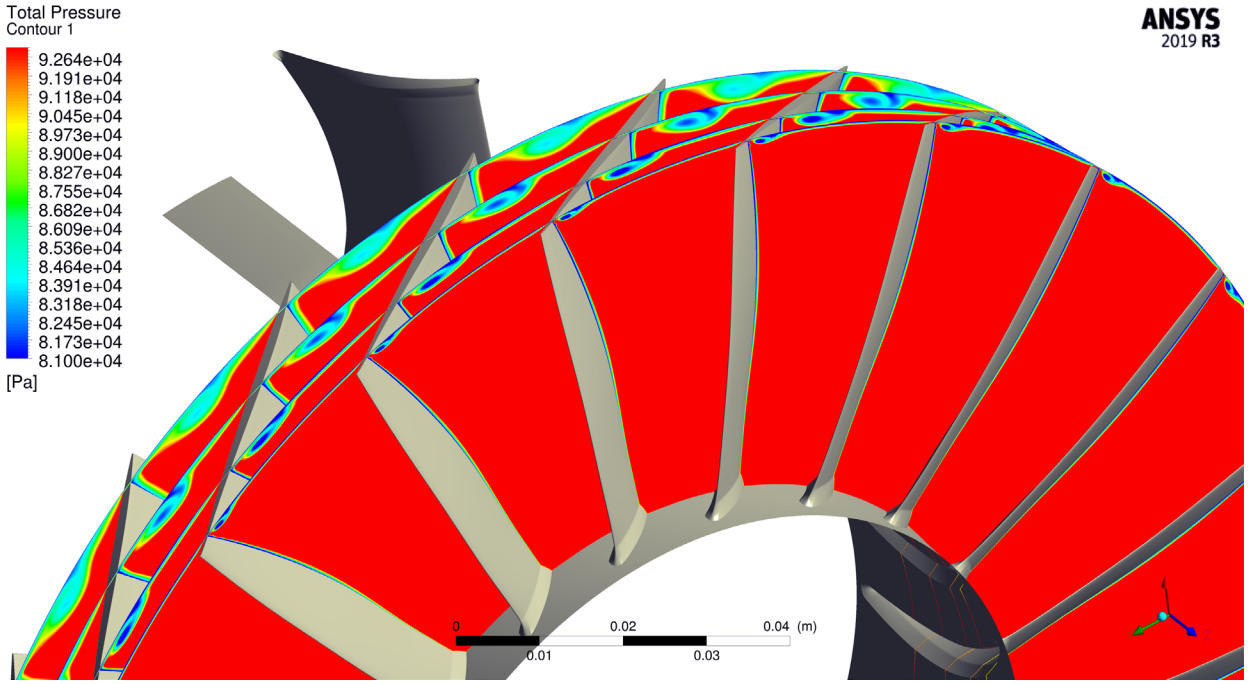

Fig. 4.6 Tip – leakage vortex

Very important flow structure is the tip-leakage vortex. It is shed on suction side of the 1st stage rotor due to rotor tip clearance and rotor leading edge tip. It could cause preliminary flow separation. This vortex is impossible eliminate completely and must be kept in mind when designing anti-surge devices.

5. Anti-surge devices

Each modification was analyzed in the same regime. The selected baseline regime was 60% of revolutions (Fig. 4.1), that means idle revolutions. Inlet boundary conditions were always ISA conditions.

Tab. 5.1: Baseline parameters

Q	2,2515	[kg/s]
Inlet opening stagnation pressure p_{1T}	101,325	[kPa]
Inlet static temperature	288,15	[K]
Outlet stagnation pressure p_{2T}	117,3	[kPa]
Outlet static pressure	110	[kPa]
Outlet static temperature	296,37	[K]
Outlet stagnation temperature T_{2T}	301,89	[K]
π	1,158	[-]
η	0,896	[-]
Q/Q_{choke}	0,729	[-]

Each of the following simulations were done using the outlet average static pressure boundary condition or outlet mass flow rate boundary condition. Tab. 5.1 gives the values for these boundary conditions, especially static pressure or mass flow rate at the outlet and static pressure and temperature at inlet.

5.1. Anti-surge valve

Anti-surge valve was represented in CFD analysis by a hollow cylinder. Only 1/30 was actually used, because the rotational periodic boundary condition allowed the simplification to be done. Boundary condition „Opening“ was applied to the outer wall with ISA parameters. This condition allowed air to leave the domain as well as to enter the domain. Two iterations of the valve with 20mm and 25mm length were simulated (Fig. 5.1). Version where valve was represented by surface boundary outlet condition assigned to outlet device shroud was simulated as well. This version was simulated to make sure, that stability of CFD run was not determined by separation inside valve (Fig. 5.2), but by separations in rotor or stator region.

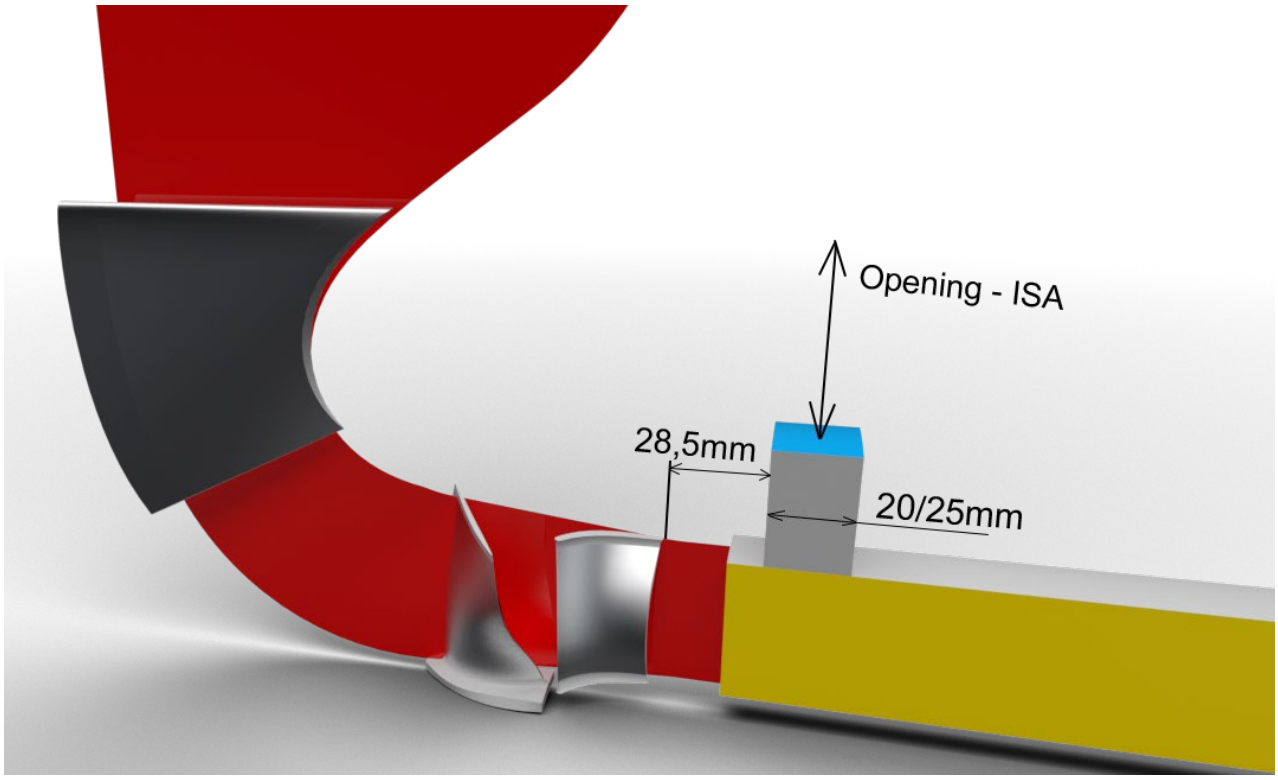

Fig. 5.1: Anti-surge valve – geometry

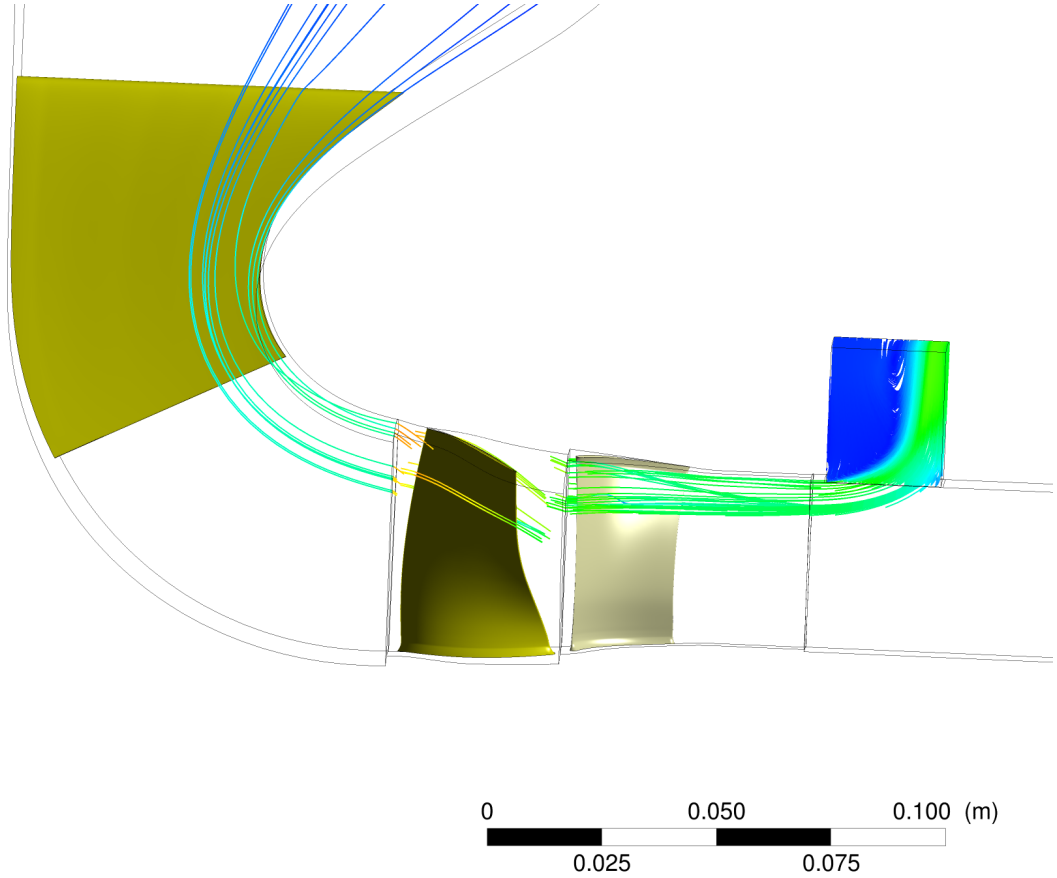

Fig. 5.2: Anti-surge valve – streamlines

Because anti-surge valve was represented by a simple hollow cylinder, the sharp edges caused huge separation inside the valve region (Figure 5.2). This was to be expected and eventhough this would be solved in a real life application by adding small fillets, it is not necessary to do it now because this was just a preliminary analysis.

Tab. 5.2: Anti-surge valve – 60% revolutions, 72,8% choke

	Incidence angle – max [°]	Incidence angle – integral [°]
Baseline	2,78	1,41
Valve 20mm	0,53	-0,82
Valve 25mm	0,18	-1,43

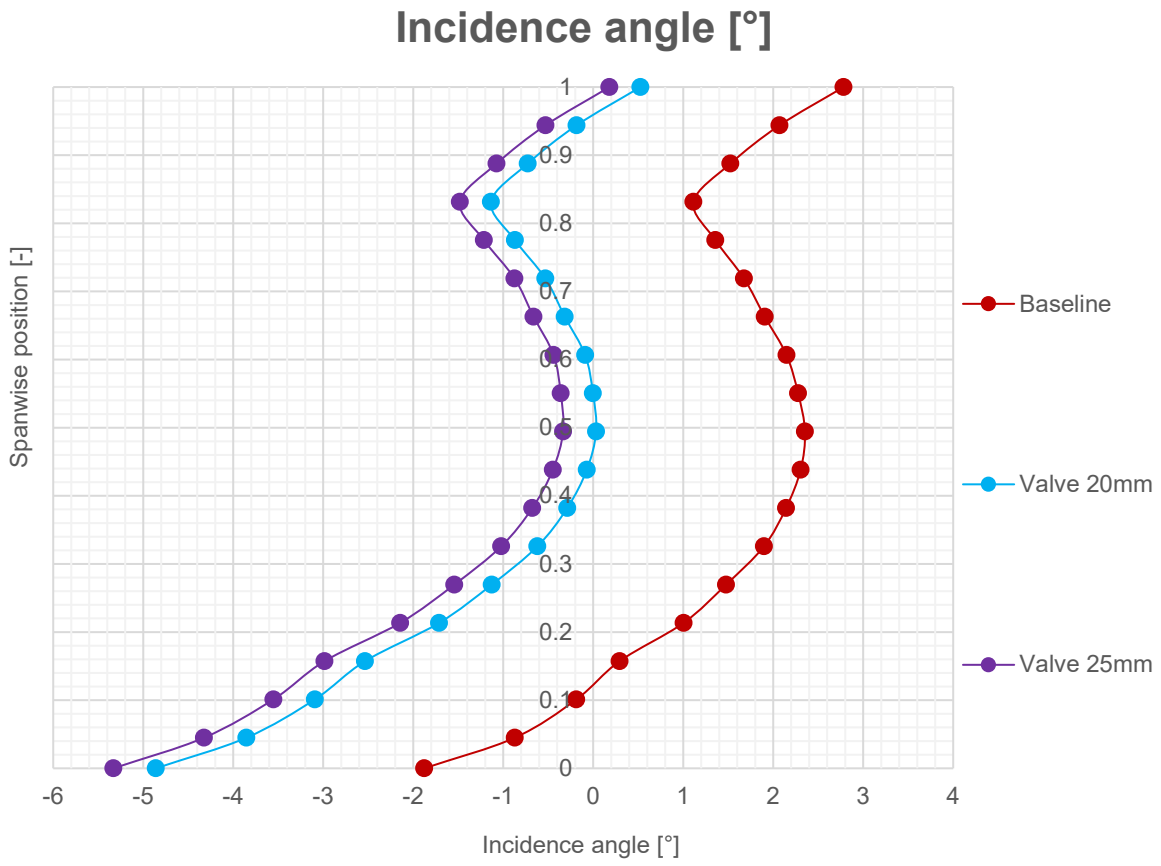

Fig. 5.3: Incidence angle – anti-surge valve – 60% revolutions, 72,8% choke

(100% choke = highest achieved Q_{mr})

The results clearly showed that anti-surge valve is an effective way of decreasing the incidence angle (Tab. 5.2). Valve 20mm in length decreased incidence angle by 2,229° and 25mm valve decreased incidence angle by 2,839°. Because the valve is 28,5mm aft of the 1st stage stator, there is no local effect on incidence angle (Fig. 5.3). Increase in the size of valve further decreased incidence angle, which is to be expected.

5.2. Air preheating

It was assumed that heated air would be taken from anti-surge valve. Therefore it was assumed that 20% of the total mass flow rate at 50 °C would be injected via Naca0009 jets at a significant distance from the struts. This meant that hot air would be at least partially mixed with cold air before entering the compressor areas.

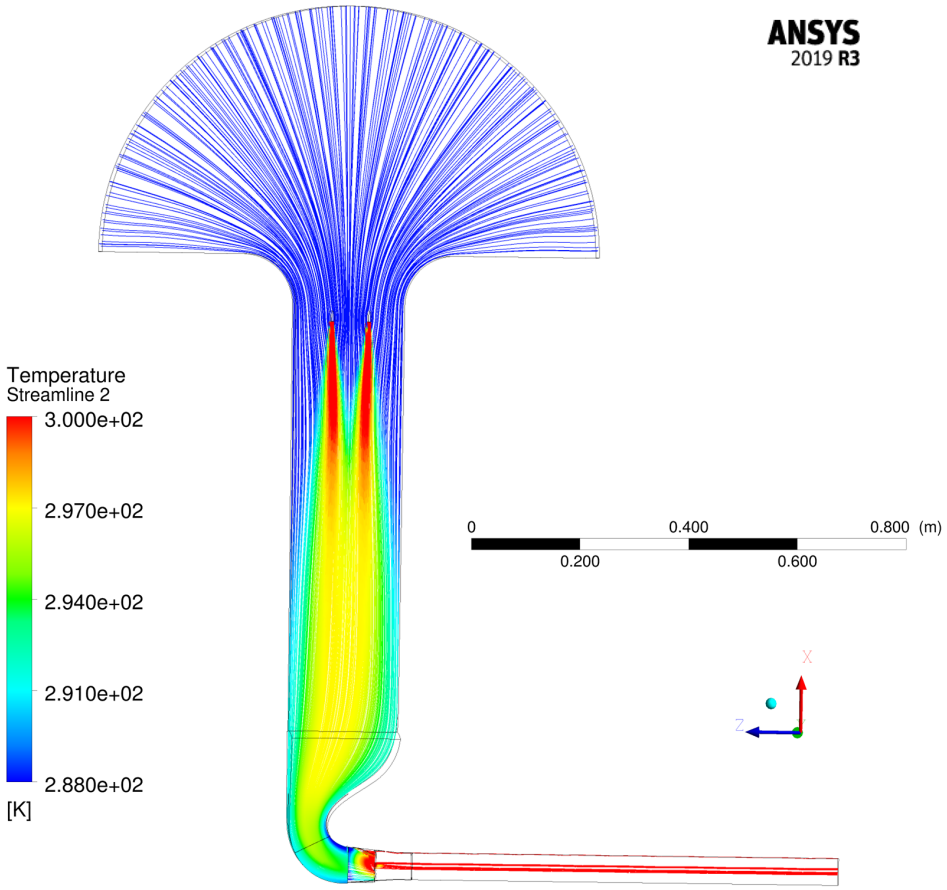

Fig. 5.4: Temperature distribution – Air preheating

Fig. 5.4 shows that temperature was not evenly distributed in struts section. It is still, however, better to use such inlet system, because that allows compressor to suck air from a free atmosphere with the correct parameters.

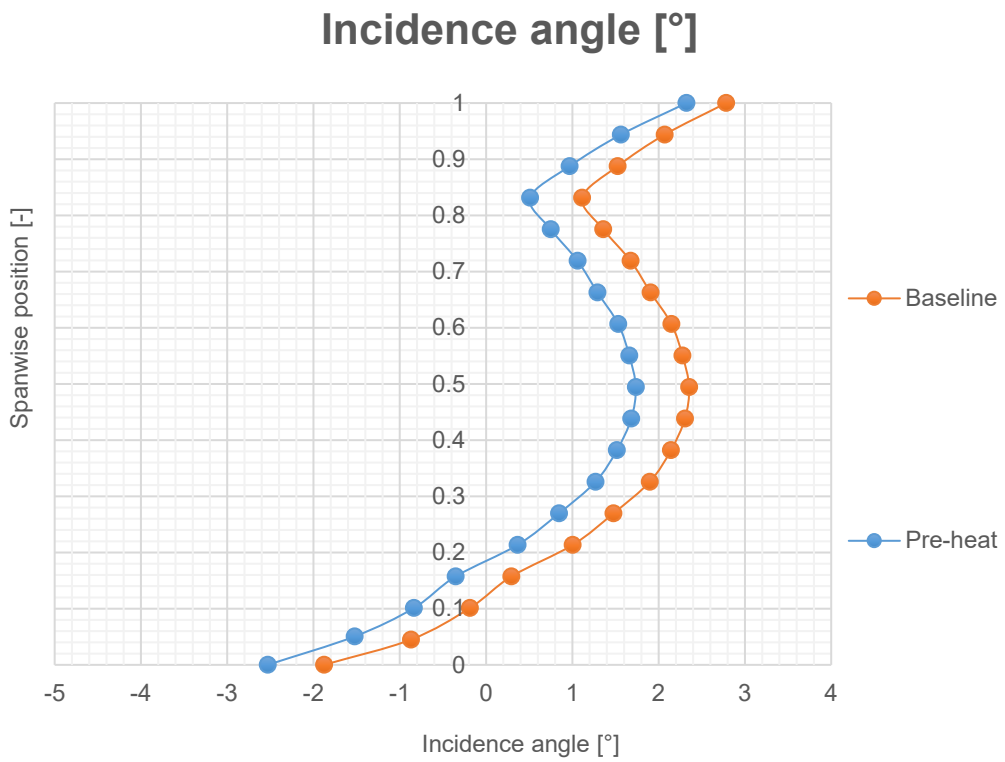

Fig. 5.5: Incidence angle – Preheating

Tab. 5.3: Air preheating – 60% revolutions, 72,8% choke

	Incidence angle – max [°]	Incidence angle – integral [°]
Baseline	2,78	1,41
Preheating	2,32	0,80

As seen in Fig. 5.5 and Tab. 5.3, air preheating yields very small improvement. It can be expected that injecting air with higher temperature will result in a bigger decrease in incidence angle. But that would alter the working cycle and there is still a question where to get air with higher temperature. All of this means that air preheating is a good way of increasing the surge margin, but only when combined with another anti-surge device.

5.3. Inlet guiding vane

IGV is represented by 21 twisted blades with Naca 0009 profile. Blade chord is 19mm, has 10° angle of attack at the root and 26,6° angle of attack at tip. This way of twisting was introduced, because the struts are twisted as well. In this manner, angle of attack should be 10° along the span of IGV.

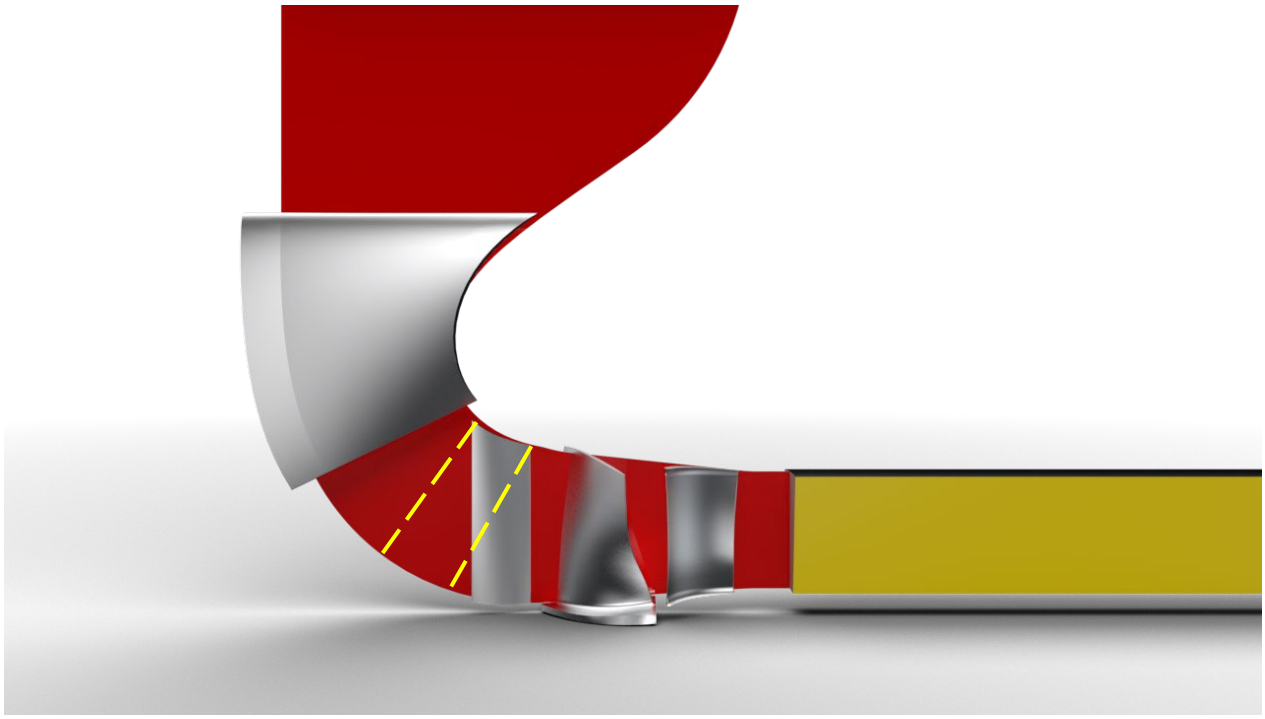

Fig. 5.6 Inlet guiding vane (IGV 10° - close) geometry

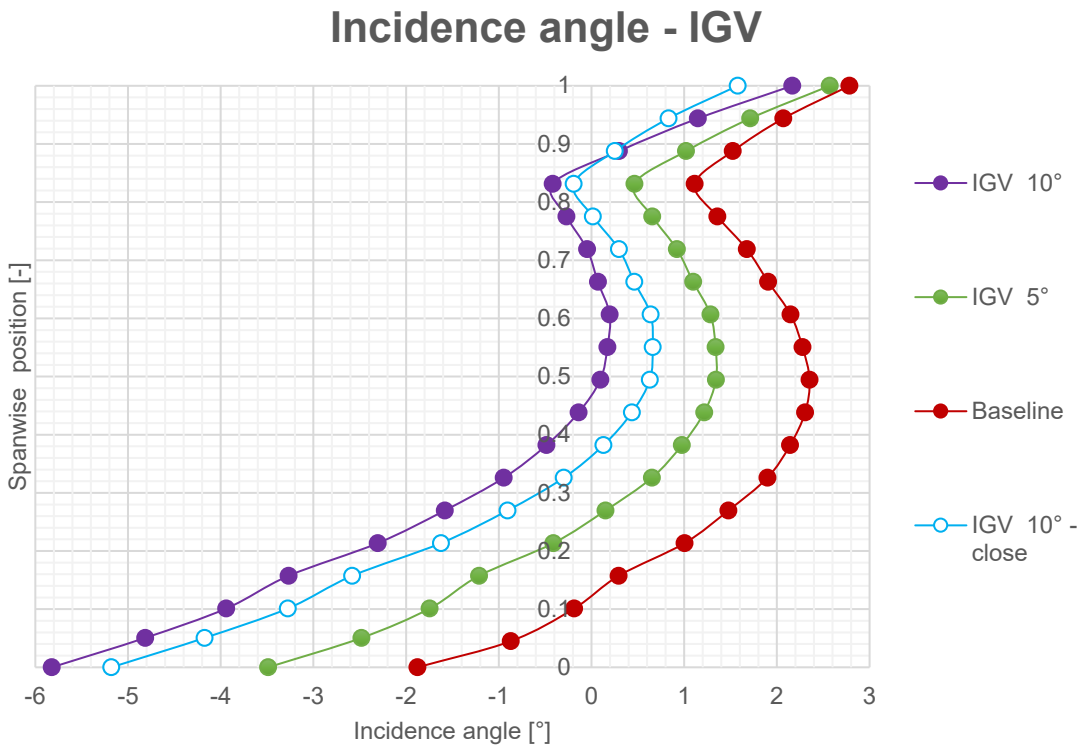

Fig. 5.7 IGV Incidence angle along span

Fig 5.7 depicts incidence angle distribution along the span for the baseline configuration. There are also 3 IGV configurations. IGV 10° and IGV 5° represent IGV in the position marked by the yellow dashed line (Fig. 5.6). As seen in Fig. 5.7, this configuration is effective, but the decrease in incidence angle at the tip is very small. This would function as a weak spot and cause premature separation. It is caused by the uneven distribution of velocity along the span (as seen in Fig. 4.5). That is why IGV was moved as close as possible to the rotor. This led to an increase in the integral

incidence angle (Tab. 5.4), but decrease in maximum incidence angle (Tab. 5.4). For this reason, IGV 10° – close is the best option (depicted in Fig. 5.6).

Tab. 5.4: Inlet guiding vane – 60% revolutions, 72,8% choke

	Incidence angle – max [°]	Incidence angle – integral [°]
Baseline	2,78	1,41
IGV 5°	2,57	-0,39
IGV 10°	2,17	-0,96
IGV 10° – close	1,57	-0,54

5.4. Jetflap

Jetflap was implemented by series of nozzles that blow air at 45° to angle of attack relative to strut. First iterations assumed that the nozzles were placed only on the strut itself.

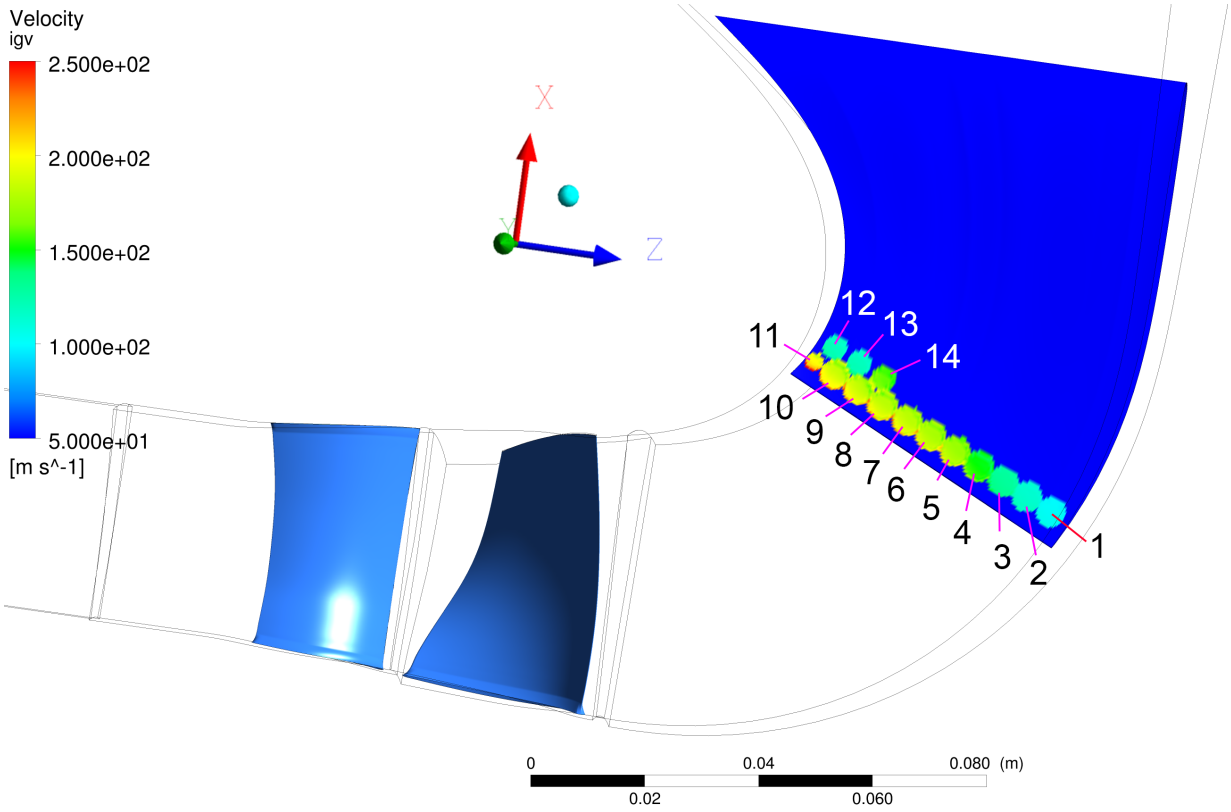

Fig. 5.8 Jet flap nozzles

To each hole, different flow vector was assigned. Following vector was assigned to each injection region $[-10, y, -6{,}8]$, where vector component „y“ was different for each hole so that angle of attack relative to angle of attack of strut was always 45°. All nozzles were 5mm in diameter, except for no. 11, which was 3mm, and nozzles no. 12, 13, and 14, which were 4mm in diameter. Mass flow rate was assigned so that

the whole system would inject 20% of baseline mass flow rate at static temperature 50°C. These conditions were assumed because similar values would be obtained, if this system was coupled with anti-surge valve.

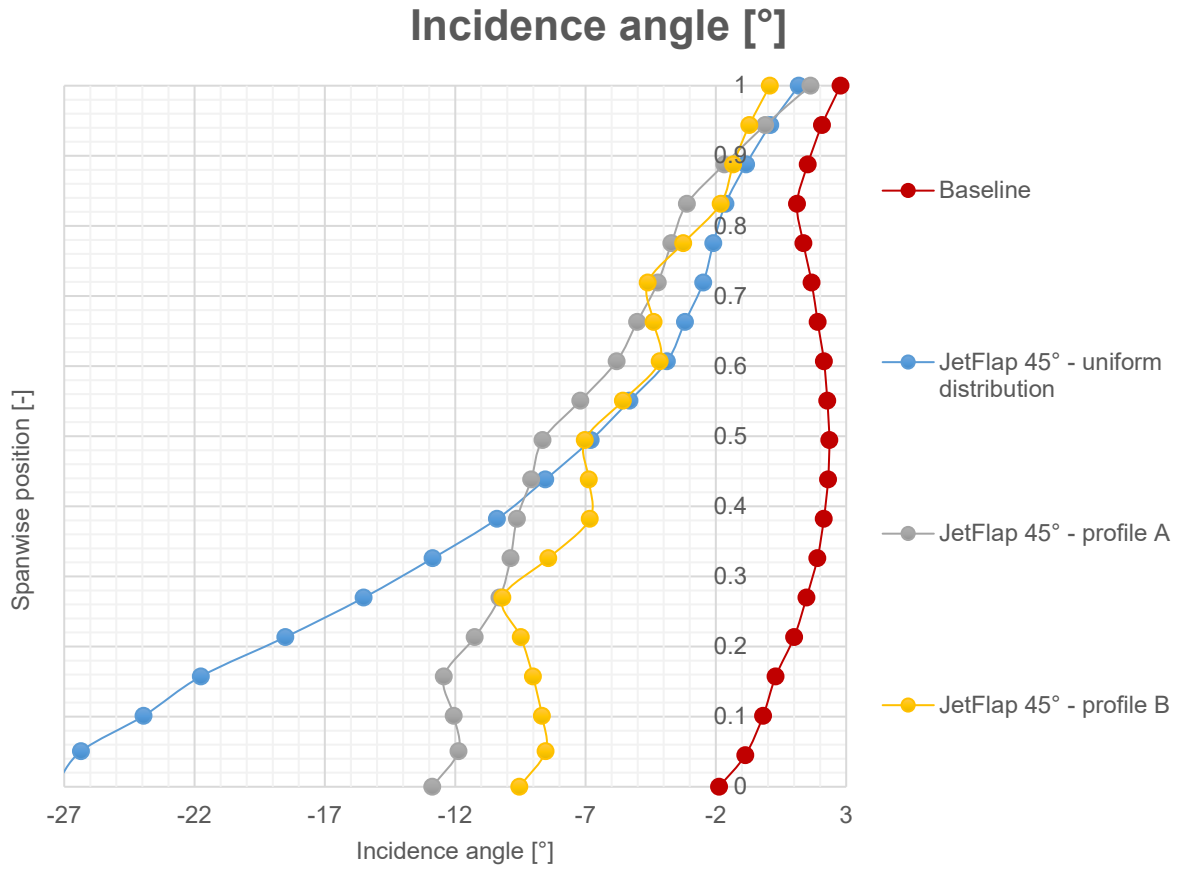

Fig. 5.9 Jetflap – Incidence angle

Fig. 5.9 shows results. The first iteration used nozzles no. 1–10. Mass flow rate was evenly distributed among all nozzles (jetflap 45° - uniform). As seen in Fig. 5.9, incidence angle is dramatically lowered at the root region and by few a degrees at the tip region. This distribution is not good because the decrease at root region is far too big and far too small at the tip. That is why „profile A“ was simulated. Hole no. 11 was activated with the mass flow rate given by Fig. 5.10. This did not help either. That is why nozzles 12, 13, and 14 were activated and assigned significant mass flow rate. This distribution would be likely difficult to achieve in a real application, but the idea was simulated anyway. There were no significant improvements as seen in Fig. 5.9. Fig. 4.5 explains why jetflap alone did not work. High velocity at the tip region dampened any flow vector changes made by jetflap. A different solution had to be devised.

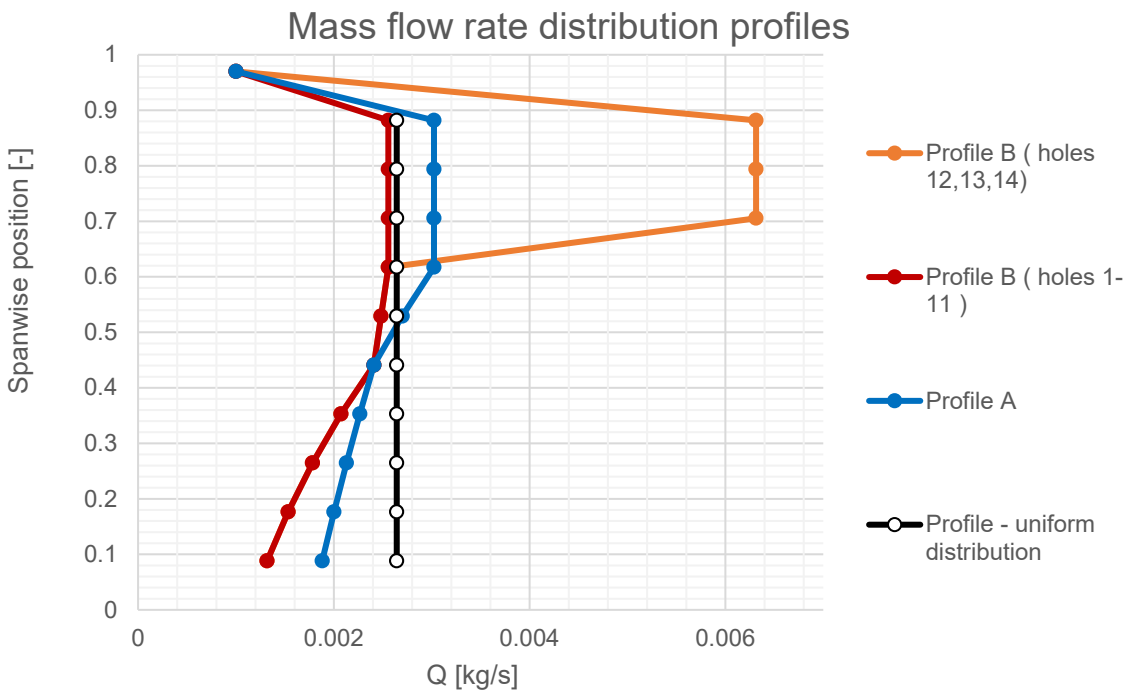

Fig. 5.10 Jetflap – Mass flow distribution

5.4.1 Jetflap & slot

Because the jetflap is very effective at lowering incidence angle at the root region and ineffective at the tip region, a small slot was added to system. It is 2,5mm thick and is 5mm from the edge of strut section. Airflow is blown out at 45° angle relative to the whole assembly coordinate system. To achieve that, the following vector $[-11 \quad 18{,}6 \quad -15]$ was assigned to slot airflow (Fig. 5.11). The slot was also combined with jetflap.

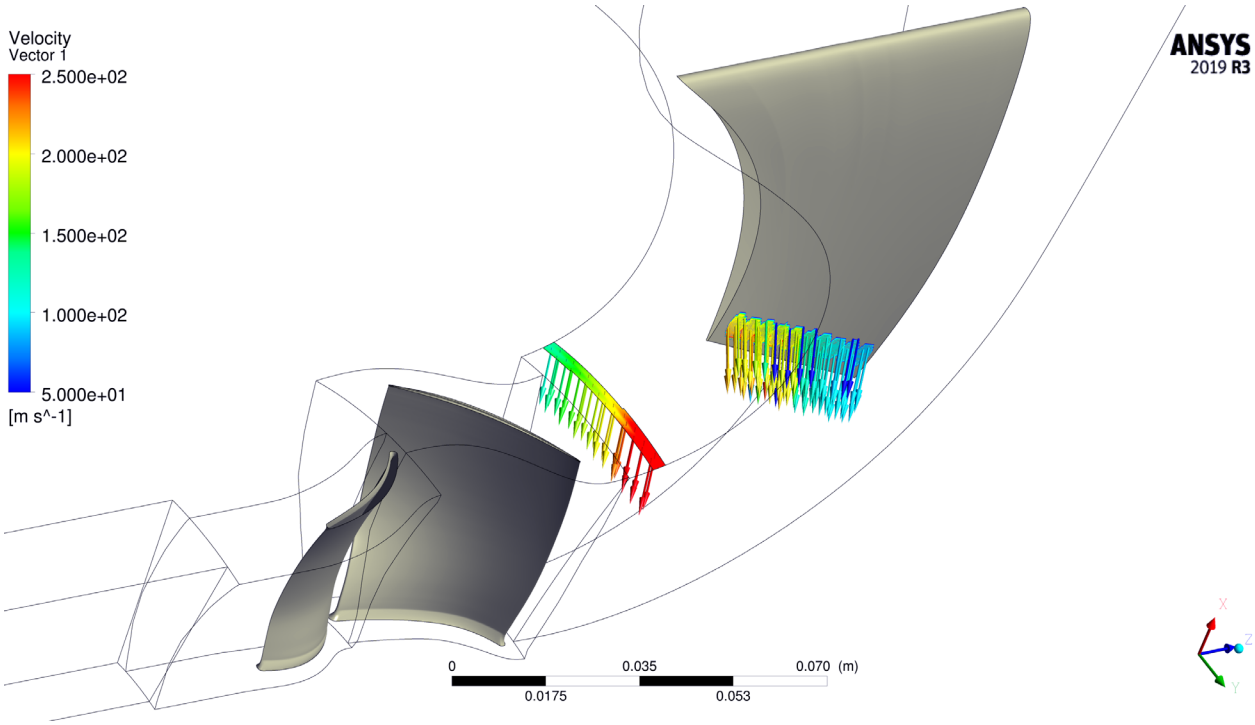

Fig. 5.11 Jetflap & slot – flow vectors

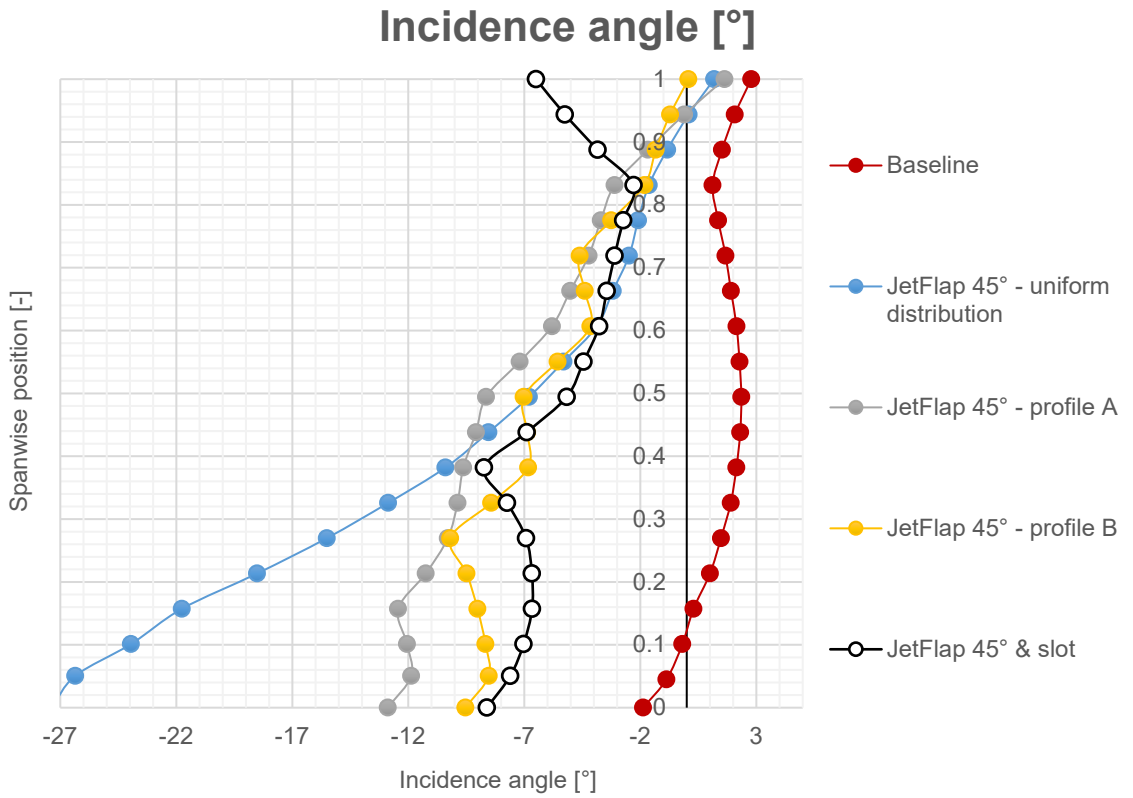

Fig. 5.12 Jetflap & slot - Incidence angle

Tab. 5.5: Jetflap & slot – 60% revolutions, 72,8% choke

	Incidence angle – max [°]	Incidence angle – integral [°]
Baseline	2,78	1,41
Jetflap 45° - uniform	1,18	-9,66
Jetflap 45° - profile A	1,63	-7,27
Jetflap 45° - profile B	0,07	-5,82
Jetflap 45° & slot	-1,51	-5,51

Jetflap significantly lowered incidence angle at the root as well as at the tip region. Fig 5.12 shows how adding the slot altered incidence angle at the tip. This led to significant decrease in the maximum incidence angle compared to using jetflap alone. Integral incidence angle proved not to be the important parameter (Tab 5.5), because it is the maximum value of incidence angle that determines when the separation occours. Since only 20 % of the total mass flow rate could be assigned to blowing, it is necessary to use that energy wisely. Six iterations of mass flow rate distribution among nozzles and slot were simulated before the final version (Fig. 5.13) was achieved. The whole system is relatively sensitive to changes in mass flow rate distribution.

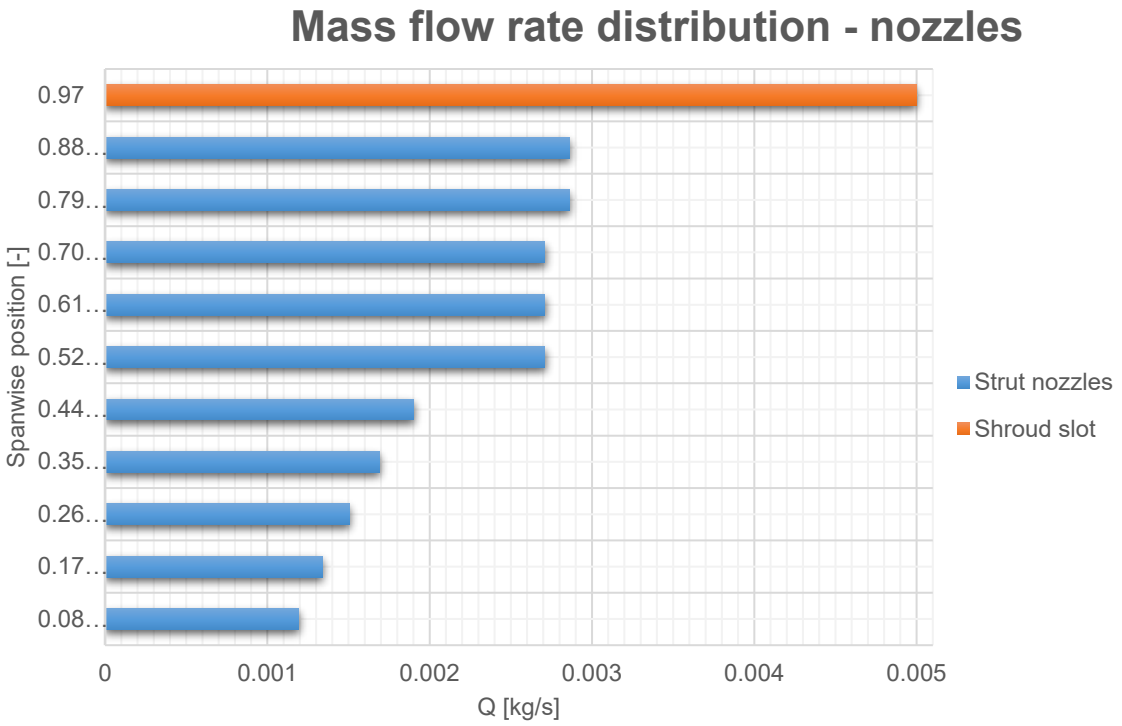

Fig. 5.13 Jetflap & slot – Mass flow rate distribution

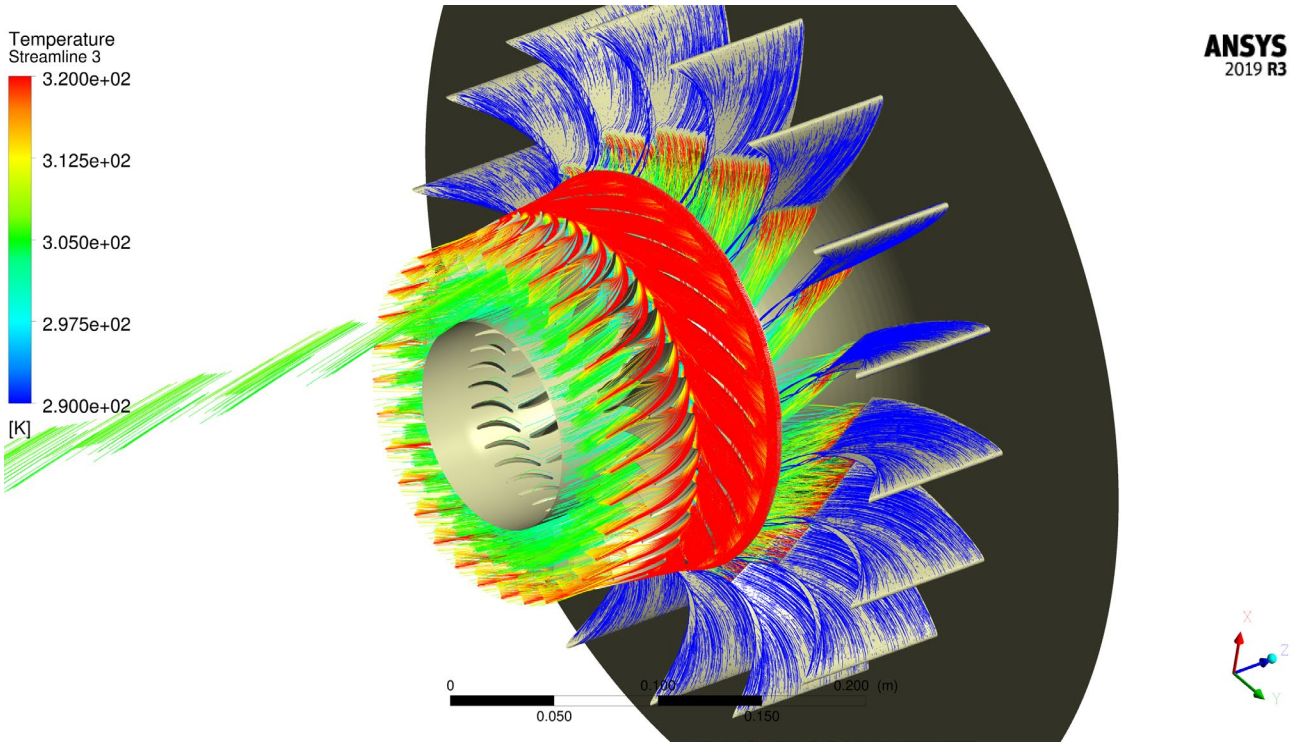

Fig. 5.14 Jetflap & slot – temperature

As depicted in Fig. 5.14, jetflap and slot distribute temperature differently. Jetflap mixes hotter air with cool air from intake causing a uniform temperature distribution fairly quickly. Slot, however, creates a layer of hotter air. This is very effective way to locally lower incidence angle and make sure that tip-leakage vortex does not cause separation and instability (Fig. 4.6).

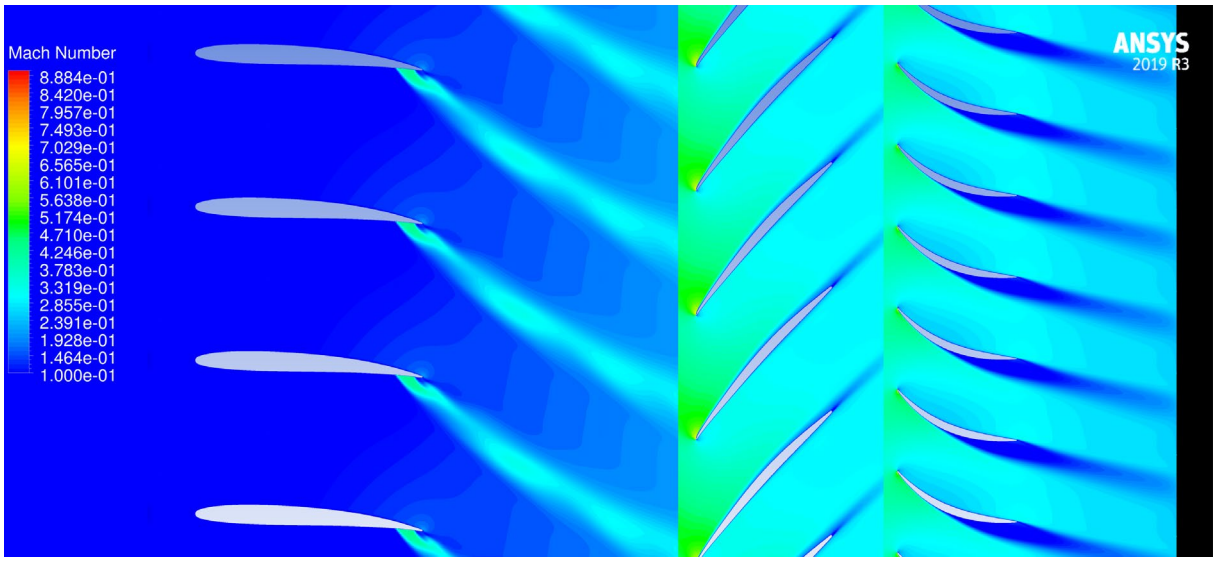

Fig. 5.15 - 60% Span, 60% revolutions – Blade cross section row – last point before surge line

As depicted in Fig. 5.15, the airflow stalls on the suction side of the stator even though the airflow is well attached to the rotor blade. Jetflap and slot affect incidence angle in front of the rotor, but incidence angle behind the rotor is determined by rotor. Therefore, it was concluded that this point is close to the limit of how much jetflap and slot can affect the stall with current configuration.

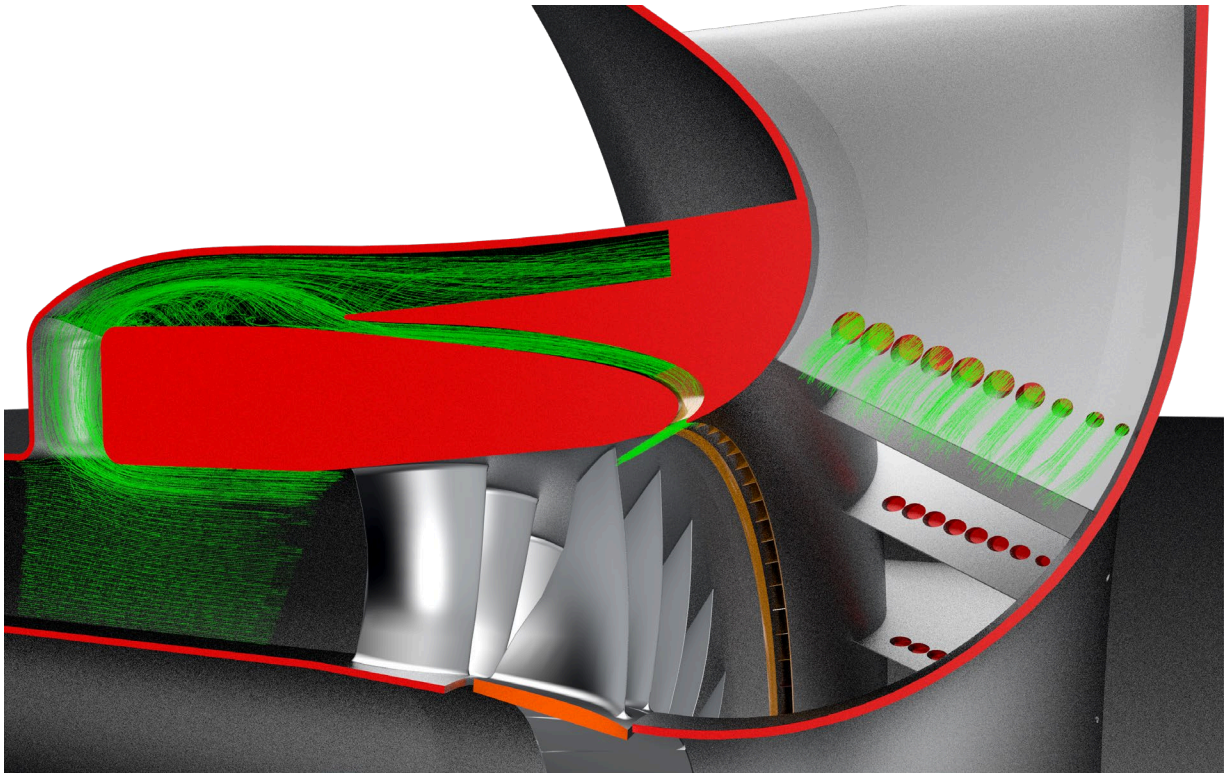

Fig. 5.16 Jetflap & slot combined with anti-surge valve – detailed channel design

Fig. 5.16 depicts how the whole system could be implemented. Air from anti-surge valve would be collected and then fed into the slot and jetflap in correct ratios. Jetflap part of the flow would be collected in the cavity inside struts and then blown of 10 nozzles. The diameter of the nozzles would be determined based on required mass

flow rate out of each hole. The significant portion of air would be blown out through slot and guided by a series of small fins giving air the proper angle of attack.

5.5. Anti-surge devices comparison

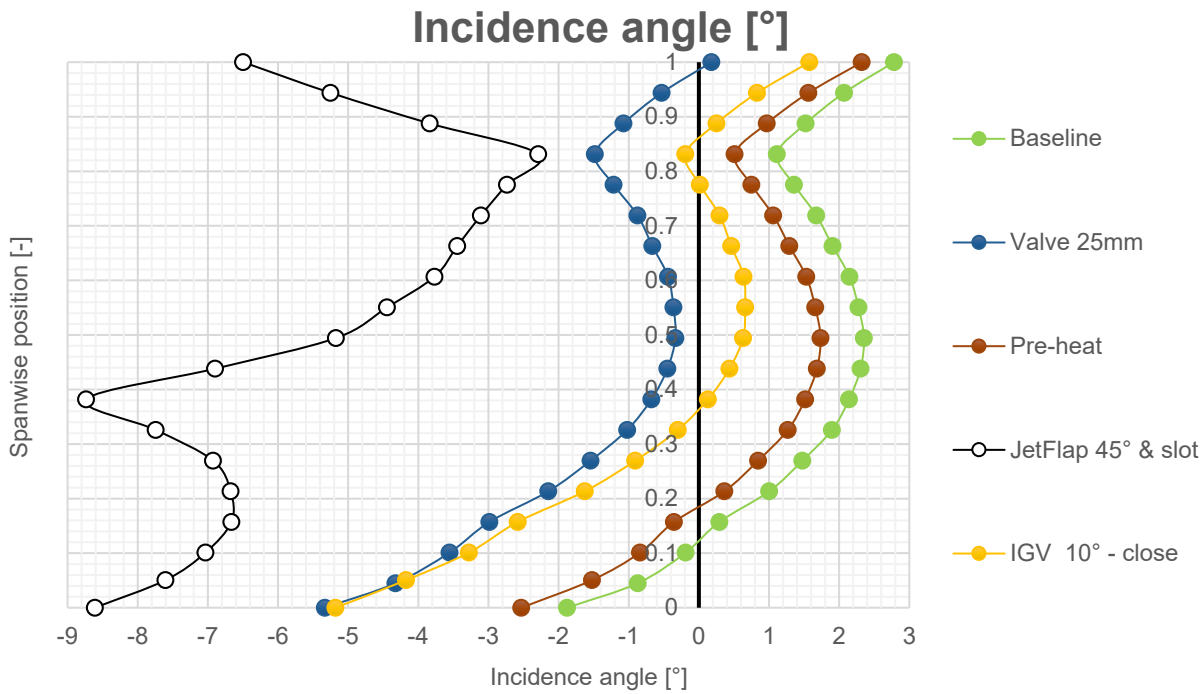

Fig. 5.17 Anti-surge devices – Incidence angle

Pre-heating the air is clearly the least effective option. As seen in Fig. 5.17 and Tab. 6.1, the decrease in incidence angle is very small. IGV 10° - close is a better option than pre-heating. IGV decreased incidence angle but the decrease was proportionaly smaller at the tip. This will lead to premature separation at the rotor tip. Anti-surge valve decreased the incidence angle significantly and the decrease was constant along the span. However, jetflap & slot exhibited the greatest decrease of incidence angle, as depicted in Tab. 5.6.

Tab. 5.6: Anti-surge devices comparison

Anti-surge device	Max. incidence angle [°]	Smallest possible Q_{mr} - 60% revolutions [kg/s]
None (baseline)	2,78	2,1
Pre-heat	2,32	2
IGV	1,57	1,9
Anti-surge valve	0,18	Not comparable
Jetflap & slot	-1,51	1,7

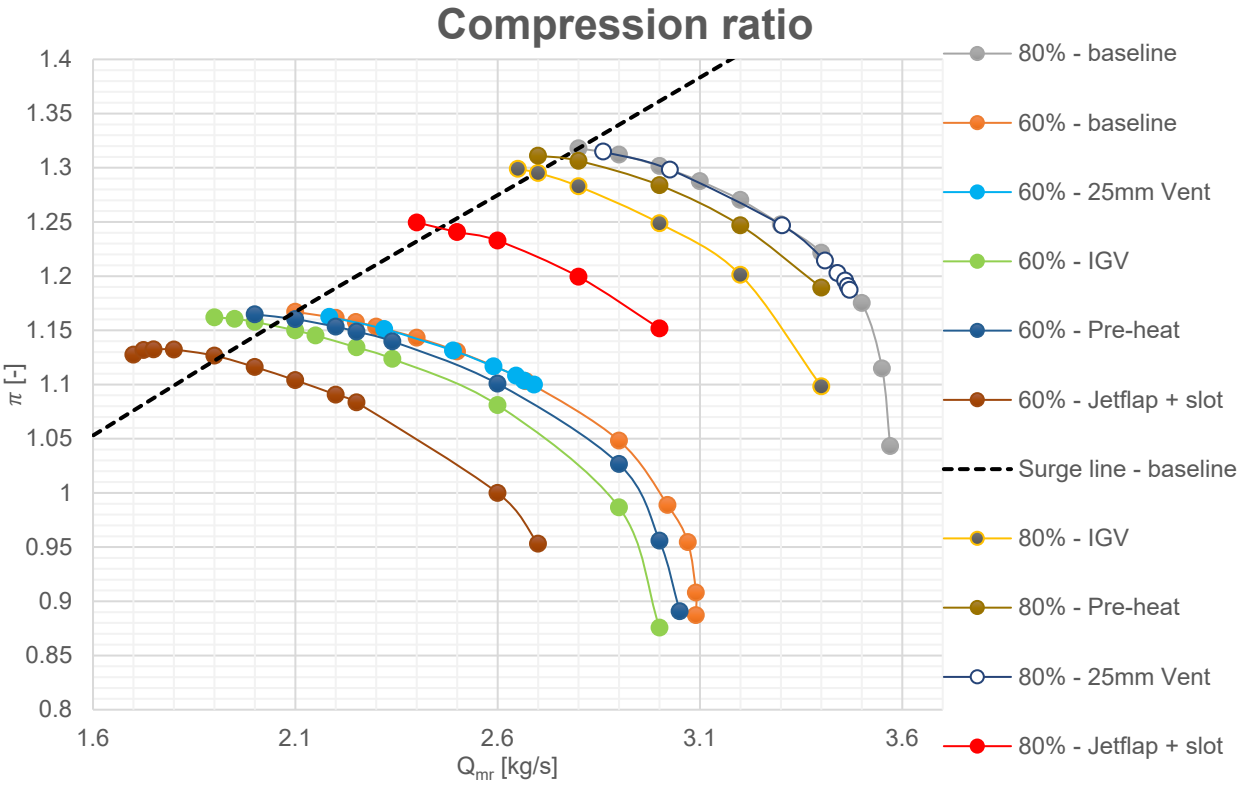

Fig. 5.18 Compressor map – anti-surge devices

As depicted in Fig. 5.18, jetflap & slot increased the surge margin by 0,4 kg/s, which is significant. Unfortunately, increase in the surge margin is not visible for anti-surge valve. This is probably due to steady-state CFD, or the valve shape. Since the anti-surge valve also shifted the working line (which was not analysed) we can not clearly define the increase in the surge margin in Fig. 5.18. Fig 5.19 depicts expected anti-surge valve behaviour and the shift of the working line. However, the decrease in incidence angle gives good indication of effectivity of anti-surge valve. IGV and pre-heating also increased the surge margin, but the increase was 0,2 kg/s and 0,1 kg/s respectively, which is significantly less than jetflap & slot.

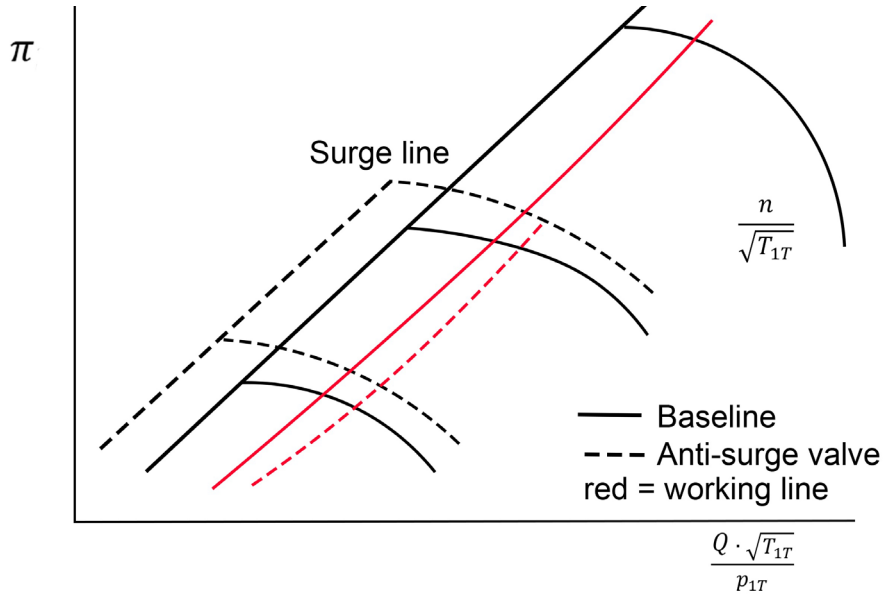

Fig. 5.19 Anti-surge valve – expected compressor map

It is necessary to mention that all devices were simulated in isolation. This approach had the benefit that we could see how much each principle is effective on its own and the data from this thesis can be used even if a different idea to implement them comes later. In reality, they would be combined and their benefits would be most likely superimposed. This thesis dealt with these devices in such a way that IGV is a standalone system that would replace anti-surge valve altogether, but anti-surge valve could be upgraded by recycling the air (air-preheating), and this system could be further upgraded by blowing the recycled air into a specific location to get further benefit (jetflap & slot). It is also necessary to add that the surge margin in this thesis is defined as distance in compressor map between surge line and working line. This is only simplification. To get the full picture of the real surge margin, almost the entire engine would have to be simulated. This is possible, but it would drastically raise the necessary computional resources and level of complexity.

Even though in the assignment of this thesis only detailed design of jetflap is required, broader approach was used after several consultations with GE engineers. Analysis of several anti-surge devices and their comparison provided much more insight at the cost of raising complexity of this analysis. Detailed jetflap design idea was proposed (Fig. 5.16), but more importantly necessary mass flow rate profile was determined (Fig. 5.13). These data can be further utilized if GE decides to invest into further analysis.

According to the results from this thesis, air pre-heating increased surge margin, but this device is not effective enough on its own. Unless a significantly more potent heat source is found, air pre-heating could only be used when coupled with another anti-surge device. IGV increased the surge margin and decreased incidence angle, but these changes were relatively small. Since IGV is expansive a complex device that also comes with the downside of increasing pressure losses in all regimes, it is not recommended in a compressor with similar configuration due to existence of more effective options. Anti-surge valve decreased significantly incidence angle and significant increase in surge margin is expected. This device proved to be a good option. The best device in this case is jetflap & slot. If used with the configuration proposed in this thesis, this device showed the biggest decrease in incidence angle and the biggest increase in surge margin of all devices.

6. Conclusion

This thesis started with creation of knowledge library of compressors, compressor characteristics, unstable work, surge, and rotating stall. Several anti-surge devices were also described. The most important conclusion from this part is that surging can be simplified and the proximity to the surge can be objectively measured by two criteria. The first one is how much each device can decrease the incidence angle. The second one is with how little mass flow can a compressor fitted with anti-surge device operate before CFD simulation crashes, indicating the collapse of compressor characteristics and possibly surge.

CFD model was created in such a way, that all anti-surge devices could be implemented. Mesh dependence study proved that mesh settings is suitable. The model was also applied to NASA Rotor 37. Results were compared to NASA measurements and the results were accurate enough. This undertaking was also used to find suitable model settings.

The first CFD analysis was that of baseline compressor without any anti-surge devices. Results showed expected behaviour indicating correct approach was used. Based on the obtained data, baseline regime was chosen and used in anti-surge device CFD simulations. The most important finding was that the radial intake speeds up the air in front of the rotor tip region, significantly reducing the effectivity of some anti-surge devices. This information was then utilized during optimalization of anti-surge devices.

All anti-surge devices were then analyzed and room for improvement was identified. Several iterations of optimalization for each device were simulated and the most influential are described in this thesis. Once there was no significant room for improvement, the best version of each type of device was chosen. These versions were than compared using two objective criteria. Their complexity and disadvantages were also commented.

Several recommendations for GE can be made from the results. Air pre-heating showed that it works, but increase in surge margin is highly dependant on increase in air temperature. Regenerating air from anti-surge valve in the currently used configuration would provide small benefit and prevent loss of energy. If a sufficient heat source can be found and this change would not ruin engine working cycle, then this device could be promising. Probably the only suitable heat sources are exhaust fumes, but implementation would be very difficult. IGV implemented in the best found configuration works, but the decrease in incidence angle is smaller than in the case of anti-surge valve due to radial air intake. Therefore, it makes no sense to install a device that is much more expensive and less capable than the currently used anti-surge valve. Anti-surge valve showed great results. The only downside is that energy is lost when the valve blows compressed and heated air into the atmosphere, decreasing the efficiency in process. The best solution is jetflap & slot. The only disadvantages of this device are the slight increase in pressure losses in all regimes due to inactive nozzles and slot, and an increase in engine complexity. This solution proved it has the potential to increase significantly the surge margin while removing the disadvantage of anti-surve valve, and therefore it is recommended to invest into the development of this idea using the concept introduced in this thesis.

Bibliography

[1] *ANSYS CFX-Pre User's Guide* [Online]. Release 14.0. U.S.A. 2011 [Accessed 21 February 2021]. Available at: http://150.107.117.36/NPTEL_DISK1/EBOOKS/MECHANICAL/AutoCAD,%20Ansys,%20ProE%20and%20Catia,%20MATLAB/ANSYS%20tutorial/ANSYS%2014.0/CFX-Pre%20User's%20Guide.pdf

[2] *ANSYS CFX-Solver Theory Guide* [Online]. Release 14.0. U.S.A. 2011 [Accessed 22 February 2021].

[3] *Experimental comparison with the law of the wall* [online] [Accessed 19 February 2021]. Available at: https://www.researchgate.net/figure/Experimental-comparison-with-the-law-of-the-wall-Fig-5-Undisturbed-boundary-layer_fig2_228644204

[4] *FREEMAN, C. Axial flow compressors*. Rhode Saint Genèse: von Karman Institute, 1992. ISSN 0377-8312

[5] *GE H80 Turboprop engine by GE AVIATION CZECH* [online] [Accessed 25 February]. Available at: https://pragaglobal.com/ge-h80-turboprop-engine-by-ge-aviation-czech/

[6] HEČL, Pavel. Personal consultation (GE Aviation Czech, s.r.o. , Beranových 65, 19900 Praha 18 - Letňany, 1) 19 December 2020

[7] RŮŽEK, Josef and Petr KMOCH. 1979. *Teorie leteckých motorů I: Kompresory, turbíny a spalovací komory.* Brno: VA, Část I..

[8] *TIPS & TRICKS: ESTIMATING THE FIRST CELL HEIGHT FOR CORRECT Y+* [online] [Accessed 20 February 2021]. Available at: https://www.computationalfluiddynamics.com.au/tips-tricks-cfd-estimate-first-cell-height/

[9] *Turbulence Models In CFD* [online] [Accessed 20 February 2021]. Available at: https://www.idealsimulations.com/resources/turbulence-models-in-cfd/

[10] Wu, C. H. *A general through flow theory of fluid flow with subsonic or supersonic velocities in turbomachines of arbitrary hub and casing shapes.* [online]. Cleveland, Ohio, United States: National Advisory Committee for Aeronautics. Lewis Flight Propulsion Lab., 1951 [Accessed 21 February 2021]. Available at: https://ntrs.nasa.gov/api/citations/19930082962/downloads/19930082962.pdf

List of figures

List of equations

List of tables

Nomenclature & Abbreviation

A	Area	$[m^2]$
C	Absolute velocity in front of IGV	$[m \cdot s^{-1}]$
c_1	Absolute velocity behind IGV	$[m \cdot s^{-1}]$
i	Angle of Indidence	$[°]$
M	Mach number	$[-]$
n	Rotor revolutions	$[RPM]$
n_r	Standardised rotor revolutions	$[RPM]$
p	Static pressure	$[Pa]$
p_{1T}	Total pressure - inlet	$[Pa]$
Q	Mass flow rate	$[kg \cdot s^{-1}]$
Q_m	Corrected mass flow rate	$[kg \cdot s^{-1}]$
Q_{mr}	Standardised corrected mass flow rate	$[kg \cdot s^{-1}]$
Q_{in}	Net heat added	$[J]$
Q_{out}	Net heat rejected	$[J]$
T	Static temperature	$[K]$
T_{1T}	Total temperature - inlet	$[K]$
u_1	Tangential blade speed behind IGV	$[m \cdot s^{-1}]$
V	Volume	$[m^3]$
w_1	Relative velocity behind IGV	$[m \cdot s^{-1}]$
α	Angle of Attack	$[°]$
β_1	Inlet flow angle	$[°]$
β_2	Outlet flow angle	$[°]$
δ	Deviation Angle	$[°]$
η	Isoentropic efficiency	$[-]$
κ	Heat capacity ratio	$[-]$
π	Compression ratio	$[-]$
ρ	Air density	$[kg \cdot m^{-3}]$
φ	Blade pitch angle	$[°]$
φ_1	Inlet metal angle	$[°]$
φ_2	Outlet metal angle	$[°]$
CFD	Computational fluid dynamics	
IGV	Inlet guiding vane	
TBO	Time between overhaul	

Appendices

Speed lines data (underlined are fixed boundary contions)

REVs [%]	MFR [kg/s]	Stagnation pressure [kPa]	Static pressure [kPa]	Static temperature [K]	Total temp [K]	Notes	P_{1c}	T_{1c}	κ	P_{ic}	η	Q/Q_{choke}
60,0	2,1	118,25	111,95	298,17	302,87		101,325	288,15	1,4	1,167	0,88	0,679
60,0	2,2	117,68	110,72	297,02	302,24		101,325	288,15	1,4	1,161	0,89	0,711
60,0	2,25	117,3	109,97	296,39	301,9		101,325	288,15	1,4	1,157	0,89	0,728
60,0	2,3	116,87	109,19	295,73	301,56		101,325	288,15	1,4	1,153	0,89	0,744
60,0	2,4	115,83	107,29	294,28	300,83		101,325	288,15	1,4	1,143	0,88	0,776
60,0	2,5	114,55	104,99	292,66	300,09		101,325	288,15	1,4	1,130	0,86	0,809
60,0	2,67	111,76	100	289,17	298,64		101,325	288,15	1,4	1,102	0,7	0,864
60,0	2,9	106,21	90	282,53	296,53		101,325	288,15	1,4	1,048	0,465	0,938
60,0	3,02	100,2	80	277,06	295,39		101,325	288,15	1,4	0,988	-0,12	0,977
60,0	3,07	97,722	70	271,15	294,87		101,325	288,15	1,4	0,964	-0,44	0,993
60,0	3,09	92,015	65	267,64	294,67	Unsteady oscilations	101,325	288,15	1,4	0,908	-1,20	1
60,0	3,09	89,892	62	265,85	294,55	Unsteady oscilations	101,325	288,15	1,4	0,887	-1,51	1
97,8	3,6	151,32	134,54	316,47	327,28		101,325	288,15	1,4	1,493	0,89	0,893
97,8	3,7	150,02	132,07	314,46	326,11		101,325	288,15	1,4	1,480	0,9	0,918
97,8	3,8	147,83	128,47	311,85	324,59	Flow reversal (S 0,2)	101,325	288,15	1,4	1,458	0,9	0,942
97,8	3,9	144,81	123,59	308,59	322,85	Flow reversal (S 0,1)	101,325	288,15	1,4	1,429	0,89	0,967
97,8	3,95	142,4	120	306,31	321,77		101,325	288,15	1,4	1,405	0,87	0,980
97,8	4,01	135,69	110	300,99	319,5		101,325	288,15	1,4	1,339	0,8	0,995
97,8	4,03	129,47	100	296,18	318,56		101,325	288,15	1,4	1,277	0,68	1
97,8	4,03	124,02	90	291,03	318,22		101,325	288,15	1,4	1,223	0,57	1
97,8	4,03	121,15	85	288,39	317,94	Unsteady oscilations	101,325	288,15	1,4	1,195	0,5	1
97,8	4,03	119,98	83	286,29	318	Unsteady oscilations	101,325	288,15	1,4	1,184	0,47	1
97,8	4,03	118,89	81	285,18	317,98	Unsteady oscilations	101,325	288,15	1,4	1,173	0,45	1
80,0	2,8	133,54	122,89	307,53	314,93		101,325	288,15	1,4	1,317	0,88	0,784
80,0	2,9	132,95	121,44	306,11	314,13		101,325	288,15	1,4	1,312	0,89	0,812
80,0	3	131,88	119,41	304,42	313,17		101,325	288,15	1,4	1,301	0,9	0,840
80,0	3,1	130,47	116,9	302,49	312,12		101,325	288,15	1,4	1,287	0,9	0,868
80,0	3,2	128,71	113,78	300,24	310,99		101,325	288,15	1,4	1,270	0,89	0,896
80,0	3,3	126,42	109,83	297,61	309,76		101,325	288,15	1,4	1,247	0,87	0,924
80,0	3,4	123,78	105,45	294,54	308,53		101,325	288,15	1,4	1,221	0,83	0,952
80,0	3,5	119,08	97,367	289,68	306,95		101,325	288,15	1,4	1,175	0,72	0,980
80,0	3,55	112,95	87,218	284,58	306,09	Unsteady oscilations	101,325	288,15	1,4	1,114	0,5	0,994
80,0	3,57	105,7	72,972	276,32	305,47	Unsteady oscilations	101,325	288,15	1,4	1,043	0,2	1